2017

Effect of Interlayers on Mechanical Properties and Interfacial Stress Transfer of 2D Layered Graphene-Polymer Nanocompsites

Colton C. Roach
University of Kentucky, ccro226@g.uky.edu
Digital Object Identifier: https://doi.org/10.13023/ETD.2017.039

STUDENT AGREEMENT:

I represent that my thesis or dissertation and abstract are my original work. Proper attribution has been given to all outside sources. I understand that I am solely responsible for obtaining any needed copyright permissions. I have obtained needed written permission statement(s) from the owner(s) of each third-party copyrighted matter to be included in my work, allowing electronic distribution (if such use is not permitted by the fair use doctrine) which will be submitted to UKnowledge as Additional File.

I hereby grant to The University of Kentucky and its agents the irrevocable, non-exclusive, and royalty-free license to archive and make accessible my work in whole or in part in all forms of media, now or hereafter known. I agree that the document mentioned above may be made available immediately for worldwide access unless an embargo applies.

I retain all other ownership rights to the copyright of my work. I also retain the right to use in future works (such as articles or books) all or part of my work. I understand that I am free to register the copyright to my work.

REVIEW, APPROVAL AND ACCEPTANCE

The document mentioned above has been reviewed and accepted by the student's advisor, on behalf of the advisory committee, and by the Director of Graduate Studies (DGS), on behalf of the program; we verify that this is the final, approved version of the student's thesis including all changes required by the advisory committee. The undersigned agree to abide by the statements above.

Colton C. Roach, Student

Dr. Y. Charles Lu, Major Professor

Dr. Haluk Karaca, Director of Graduate Studies

EFFECT OF INTERLAYERS ON MECHANICAL PROPERTIES AND INTERFACIAL STRESS TRANSFER OF 2D LAYERED GRAPHENE-POLYMER NANOCOMPOSITES

THESIS

A thesis submitted in partial fulfillment of the
requirements for the degree of Master of Science in Mechanical Engineering
in the College of Engineering
at the University of Kentucky

By

Colton Roach

Lexington, Kentucky

Director: Dr. Y Charles Lu, Associate Professor of Mechanical Engineering
Lexington, Kentucky

2017

ABSTRACT OF THE THESIS

EFFECT OF INTERLAYERS ON MECHANICAL PROPERTIES AND INTERFACIAL STRESS TRANSFER OF 2D LAYERED GRAPHENE-POLYMER NANOCOMPOSITES

Graphene, a monolayer of sp^2-hybridized carbon atoms arranged in a two-dimensional (2D) lattice, is one of the most important 2D nanomaterials and has attracted tremendous attentions due to its unique geometric characteristics and exceptional mechanical properties. One of the most promising applications of this 2D nanomaterial is in polymer nanocomposites, in which the ultra-stiff, ultra-thin graphene layers function as reinforcement fillers. However, two significant questions remain to be answered: (1) whether the mechanical behaviors of 2D graphene reinforced nanocomposites can be analyzed by the convention composite theory, which is developed primarily for one-dimensional (1D) fiber-type of fillers, and (2) what are the effects of the "interlayers" in those 2D, ultra-thin, layered fillers on mechanical properties of the nanocomposites. Composites with both aligned and random-distributed graphene are analyzed using Tandon-Weng and Halpin-Tsai models. For composites reinforced with multi-layered graphene, the presence of soft "interlayers" needs to be considered. These layered graphene are treated as the "effective" reinforcement fillers and the moduli of such structures can be predicted by the Arridge model. Finally, the efficiency of reinforcement by 2D, layered graphene in polymer matrix is examined by using the finite element method. The accuracy of the finite element method is verified with the conventional Shear-Lag theory on a monolayer graphene. The distributions of interfacial shear strain are computed for composites reinforced with various layered graphene.

KEYWORDS: Nanocomposites; Graphene; Interlayers; Stress transfer; Finite element method.

Colton Roach

03/09/2017

EFFECT OF INTERLAYERS ON MECHANICAL PROPERTIES AND INTERFACIAL STRESS TRANSFER OF 2D LAYERED GRAPHENE-POLYMER NANOCOMPOSITES

By

Colton Roach

Dr. Y Charles Lu

Director of Thesis

Dr. Haluk Karaca

Director of Graduate Studies

03/09/2017

Dedicated to my family and friends for always encouraging me to achieve my goals with education.

ACKNOWLEDGEMENTS

I would like to thank my academic advisor Dr. Y. Charles Lu for helping me through my thesis topic and advancing my knowledge in the research community. Dr. Lu also helped in encouraging me to think about higher education where he guided me to success.
I would like to thank Kentucky NASA Space Grant for granting me the possibility to achieve the academic success I desired.

Table of Contents

List of Figures

Page

CHAPTER 1 – INTRODUCTION

Nanocomposites comprised of a polymer matrix and various types of nanosized fillers have remained as one of the most important engineering materials and continue to draw great interest in the research community and industry. One major type of nanosized fillers is the two-dimensional (2D), ultra-thin, layered fillers, the most commonly used being layered graphene [1-10]. The graphene can be in the form of either single-layer (monolayer), few-layer, or multi-layer. Layered graphene are mostly synthetic materials, and each graphene layer consists of a single atomic layer of sp^2 carbon atoms arranged in a honeycomb structure [9].

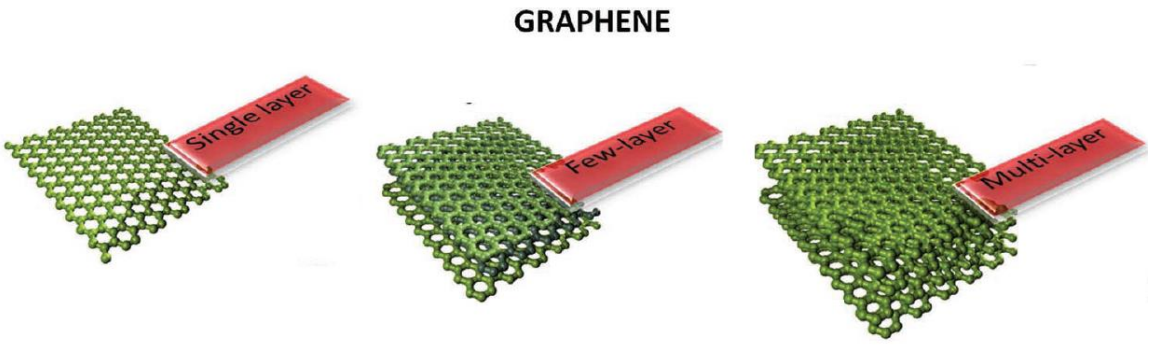

Figure 1.1 Molecular models showing the 2D, ultra-thin, graphene in the form of single-layer, few-layer, and multi-layer (11).

With the unique allotrope carbon structure, graphene is considered to be one of the toughest and most versatile materials ever tested. A monolayer graphene is reported to have a Young's modulus up to 1050 GPa and a tensile strength of around 100 GPa [12, 13]. The material also possesses super electrical conductivity, with the electron mobility of 200,000 cm^2/Vs as compared to silicon having 1400 cm^2/Vs [14]. Graphene is also considered as ultra-capacitors, with a thermal conductivity of 3500 W/mk as compared to 385 W/mk for copper [15, 16]. It is also reported that single layer graphene has exceptional optical properties, capable of absorbing 2.3% of incident light over a broad wavelength range [17]. Due to such exceptional mechanical and physical properties, the 2D, layered graphene has

been considered as the "ideal" reinforcement fillers for making the next generation, high-performance composite materials.

The effectiveness of the 2D, thin, layered fillers in composites can also be explained by one of their unique geometric properties. The thickness of single layer graphene is only about 0.34 nm [18, 14], which yields the extremely high length-to-thickness aspect ratios for this particular type of fillers. In comparison, the aspect ratios for conventional, macroscopic fillers are much lower, typically on the order of tens or hundreds. Based on the classical Halpin-Tsai composite theory, the modulus of the composite is predominated by the aspect ratio (l/t, where l is the length and t is the thickness) of the fillers [19]. Therefore, the layered fillers have exceptionally higher reinforcing efficiency than the conventional, macroscopic fillers. As a result, the content of reinforcement fillers used in nanocomposites is typically only 0.05-5% [20], far less than what is required in conventional composites (20-60%).

The effectiveness of the 2D, thin, layered fillers in composites is further due to their large surface area and surface energy. As the size of the filler decreases, the specific surface area of the filler increases drastically. In addition, at the nanoscale, the fillers have the dimensions that are close to the size of atoms or molecules. As a result, the surface energy of the nanosized filler is substantially higher compared to that of the bulk [21, 22]. Therefore, with the greater surface area and surface energy, the nanolayered fillers dispersed in a polymer matrix would form much larger and stronger "interfaces" than the micro-scale fillers, which can lead to significant improvements in mechanical properties of the composites.

Although extensive work has been conducted on composites reinforced by layered graphene and layered graphene sheets, there is a lack of thorough study on the analytical modeling of nanocomposites reinforced by 2D, ultra-thin, graphene fillers. The 2D, layered graphene is extremely thin (0.34 nm for monolayer graphene and a few nanometers for layered graphene), sheet-like platelets that possess very high aspect ratios. In addition, the graphene fillers have an exceptionally high modulus in comparison with most polymers

and even many other fillers. Therefore, when dispersed in a polymer matrix, the graphene may have the ability to significantly alter the properties of the polymer matrix. Thus, one significant question is whether the graphene reinforced nanocomposites can be modeled by conventional composite theory. Another important issue is the roles of interlayers in those two-dimensional, ultra-thin, layered fillers. The so-called "interlayer" or the "gallery layer" is the materials that lie between individual graphene sheets. These special materials may be either the surfactants that are used to modify the fillers, or the polymer matrix chains that have penetrated into the spaces between the layers during various stages of synthesis and processing, or a mixture of both surfactants and polymer chains [5, 9, 22]. The mechanical properties of the interlayer materials are often unknown and may be difficult to be determined to a greater accuracy. The sizes of the interlayers (interlayer spacing) in the layered fillers can be also unknown, since they depend upon the crystal structure of the specific graphene or graphene layer and also the amount of polymer chains that penetrate into the inter-layers as results of various processing conditions [5].

The main objective of this thesis is to comprehensively examine the mechanical properties of layered graphene-polymer nanocomposites through analytical modeling. Chapter 2 presents the analytical modeling on mechanical properties of polymer nanocomposites reinforced with a monolayer graphene. Chapter 3 presents the analytical modeling on mechanical properties of polymer nanocomposites reinforced with a multi-layer graphene. In both chapters, the conventional composite theories of Tandon-Weng and Halpin–Tsai are used to evaluate the effects of filler geometry, stiffness, and volume fraction. Chapter 4 investigates the effect of interlayer in a graphene stack on mechanical properties of the graphene nanocomposites. Chapter 5 investigates the effect of interlayer in a graphene stack on interfacial stress transfer of the graphene nanocomposites. Chapter 6 provides a summary on the results of the present studies and also highlights the possible future work.

CHAPTER 2 - ANALYTICAL MODELS FOR NANOCOMPOSITES REINFORCED WITH 2D FILLERS: MONOLAYER GRAPHENE

2.1 Introduction

The interest of nanocomposites has grown exponentially over the past decade. Reinforcing fillers such as graphene show great potential for producing stiffer composites. Several analytical models have been produced to predict different characteristics for one-dimensional (1D) filler reinforced composites. The Halpin-Tsai and the Tandon-Weng models are very popular and both give reasonable predictions for unidirectional and randomly aligned fillers in composites. Halpin-Tsai equations are popular for their easy to use characteristics while the Tandon-Weng models are predicted to give better results. Both of these models have the same basic assumptions for a composite. The filler and matrix are linearly elastic [23,24,25]. The matrix is isotropic while the filler is either isotropic or transversely isotropic [23,24,25]. Also, these models do not account for filler-matrix debonding or micro-cracking [23]. These analytical models depend on multiple aspects from the filler and the matrix such as, Young's modulus, shear modulus and Poisson's ratio from the matrix and filler, the aspect ratio of the filler and the volume fraction contributions in the composite. The models have been refined even further based on the geometry of the filler, whether the filler is an elongated tube or spheroidal in shape.

Unlike the conventional 1D fillers, graphene is two-dimensional (2D) in shape and has the capability of very high aspect ratios. The Halpin-Tsai and Tandon-Weng models are intended for 1D short fiber composites. In this chapter, the Tandon-Weng and Halpin-Tsai models are used to model the 2D, ultra-thin graphene reinforced composites. In particular, the graphene filler is assumed to be a monolayer.

2.2 Tandon-Weng Models

The early works for composite models came from the work of Eshelby. Eshelby solved for a dilute composite model which was a single ellipsoidal inclusion in an infinite matrix [24]. Therefore, Eshebly's solution only applies to composites with very low volume fractions and appears to be accurate. The difficult problem is to include fillers at high volume fractions. Mori and Tanaka proposed a non-dilute composite model from the work of Eshelby [24]. Tandon and Weng took Mori and Tanaka's approach and developed a complete set of elastic constants for 2-D short fiber composites. The key assumption to Tandon-Weng's model is that the average strain in the filler is related to the average strain in the matrix by a fourth order tensor. This fourth order tensor gives the relation between the uniform strain in the filler embedded in all matrix material. Also, the material is subjected to uniform strain at infinity. The fourth order tensor that relates the average strain in the filler to the average strain in the matrix is the Eshelby tensor. The elastic constants Tandon and Weng proposed are represented for two types of filler orientations. They developed one complete set for aligned fillers and a separate set that applies to randomly aligned fillers.

2.2.1 Nanocomposites reinforced with aligned graphene fillers

The composite shown in Figure 2.1 has an elliptical fiber aligned in the 1 direction embedded in an infinite matrix. The concept originally introduced by Mori and Tanaka was that the average stress from the fiber to the matrix was related to the average strain from the fiber to the matrix [26]. Tandon and Weng used Mori and Tanaka's average stress theory and combined it with Eshelby's solution for an ellipsoidal fiber inclusion. The Eshelby tensor has components that depend on aspect ratio and matrix modulus. Rearranging terms for stress and strain allows the prediction for the effective modulus for the composite.

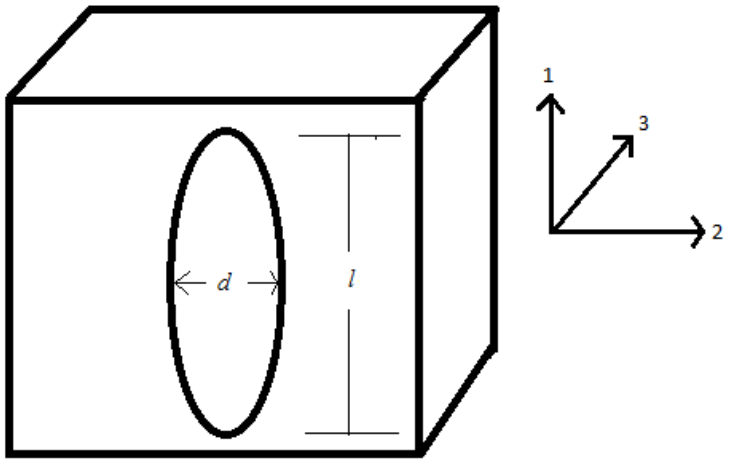

Figure 2.1 Elliptical fiber embedded in an infinite matrix

When elliptical fibers are oriented in a matrix to form a composite the composite is treated as transversely isotropic. This assumption allowed Tandon and Weng to develop equations to solve for the five elastic constants associated with the composite. Equations 2.1 and 2.2 are Tandon and Weng's derived equations with the fiber aligned in the 1 direction. The focus is on the longitudinal and transverse modulus and the other 3 elastic constants are not listed. *c* is the volume fraction contribution of the fiber in the composite and v_o is the Poission's ratio of the matrix.

$$E_1 = \frac{E_o}{1 + c(A_1 + 2\nu_o A_2)/A} \tag{2.1}$$

$$E_2 = \frac{E_o}{1 + c[-2\nu_o A_3 + (1-\nu_o)A_4 + (1+\nu_o)A_5 A]/2A} \tag{2.2}$$

Equations 2.1 and 2.2 are simplified from the tensor matrix with constants *A,B,D* and S_{ijkl} where *i,j,k,* and *l* vary from 1 to 3.

$$A_1 = D_1(B_4 + B_5) - 2B_2 \tag{2.3a}$$

$$A_2 = (1+D_1)B_2 - (B_4 + B_5) \tag{2.3b}$$

$$A_3 = B_1 - D_1 B_3 \tag{2.3c}$$

$$A_4 = (1+D_1)B_1 - 2B_3 \tag{2.3d}$$

$$A_5 = \frac{(1-D_1)}{(B_4 - B_5)} \tag{2.3e}$$

$$A = 2B_2 B_3 - B_1(B_4 + B_5) \tag{2.3f}$$

$$D_1 = 1 + \frac{2(\mu_1 - \mu_o)}{(\lambda_1 - \lambda_o)} \tag{2.3g}$$

$$D_2 = \frac{(\lambda_o + 2\mu_o)}{(\lambda_1 - \lambda_o)} \tag{2.3h}$$

$$D_3 = \frac{\lambda_o}{(\lambda_1 - \lambda_o)} \tag{2.3i}$$

$$B_1 = cD_1 + D_2 + (1-c)(D_1 S_{1111} + 2S_{2222}) \tag{2.3j}$$

$$B_2 = c + D_3 + (1-c)(D_1 S_{1122} + S_{2222} + S_{2233}) \tag{2.3k}$$

$$B_3 = c + D_3 + (1-c)[S_{1111} + (1+D_1)S_{2211}] \tag{2.3l}$$

$$B_4 = cD_1 + D_2 + (1-c)(S_{1122} + D_1 S_{2222} + S_{2233}) \tag{2.3m}$$

$$B_5 = c + D_3 + (1-c)(S_{1122} + S_{2222} + D_1 S_{2233}) \tag{2.3n}$$

α is the aspect ratio of the fiber $(= l/d)$

$$S_{1111} = \frac{1}{2(1-\nu_o)}\{1 - 2\nu_o + \frac{3\alpha^2 - 1}{\alpha^2 - 1} - [1 - 2\nu_o + \frac{3\alpha^2}{\alpha^2 - 1}]g\} \tag{2.3p}$$

$$S_{2222} = S_{3333} = \frac{3}{8(1-\nu_o)}\frac{\alpha^2}{\alpha^2 - 1} + \frac{1}{4(1-\nu_o)}[1 - 2\nu_o - \frac{9}{4(\alpha^2 - 1)}]g \tag{2.3q}$$

$$S_{2233} = S_{3322} = \frac{1}{4(1-\nu_o)}\{\frac{\alpha^2}{2(\alpha^2 - 1)} - [1 - 2\nu_o + \frac{3}{4(\alpha^2 - 1)}]g\} \tag{2.3r}$$

$$S_{2211} = S_{3311} = -\frac{1}{2(1-\nu_o)}\frac{\alpha^2}{\alpha^2-1} + \frac{1}{4(1-\nu_o)}\{\frac{3\alpha^2}{\alpha^2-1} - (1-2\nu_o)\}g \quad (2.3s)$$

$$S_{2323} = S_{3232} = \frac{1}{4(1-\nu_o)}\{\frac{\alpha^2}{2(\alpha^2-1)} + [1-2\nu_o - \frac{3}{4(\alpha^2-1)}]g\} \quad (2.3t)$$

$$S_{1212} = S_{1313} = \frac{1}{4(1-\nu_o)}\{1-2\nu_o - \frac{\alpha^2+1}{2(\alpha^2-1)} - \frac{1}{2}[1-2\nu_o - \frac{3(\alpha^2+1)}{\alpha^2-1}]g\} \quad (2.3u)$$

$$g = \frac{\alpha}{(\alpha^{2`}-1)^{2/3}}\{\alpha(\alpha^2-1)^{1/2} - \cosh^{-1}\alpha\} \quad (2.3v)$$

One important note to have in mind is that S_{ijkl} and g represent spheroidal fibers and S_{ijkl} and g will be different for disk shaped spheroidal fibers. λ_o, μ_o and λ_1, μ_1 are the lame' constants of the matrix and the fiber respectively.

$$\lambda = \frac{\nu E}{(1+\nu)(1-2\nu)} \quad (2.4)$$

$$\mu = 2G \quad (2.5)$$

2.2.2 Nanocomposites reinforced with random graphene fillers

When the spheroidal fibers are randomly oriented in the 1-2 plane the composite as a whole is transversely isotropic. This assumption allowed Tandon and Weng to arrive at a new set of equations to evaluate the five elastic constants associated with the composite. In this composite all of the fibers are dispersed in the matrix at random, due to this the longitudinal and transverse modulus are evaluated from the same equation. Equation 2.6 is Tandon and Weng's prediction for the longitudinal and transverse modulus of randomly oriented fibers.

$$E_1 = \frac{E_o}{1 + c\,p_{11}} \tag{2.6}$$

where p11 is defined as

$$p_{11} = \frac{1+\nu_o}{1+c(b_1-b_2)}\{\frac{2(a_1+a_2-a_3)+a_4+a_5 a}{16a} - \frac{1}{4[2S_{1212}+\mu_o/(\mu_1-\mu_o)}\}$$

$$-\frac{(1-\nu_o)(1+c\,b_5)+2c\,\nu_o\,b_3}{2c^2 b_3 b_4-(1+c\,b_5)[1+c(b_1+b_2)]}\frac{2(a_1-a_2+a_3)+a_4+a_5 a}{8a}$$

$$+\frac{(1-\nu_o)c\,b_4+\nu_o[1+c(b_1+b_2)]}{2c^2 b_3 b_4-(1+c\,b_5)[1+c(b_1+b_2)]}\frac{-2a_2+a_4-a_5 a}{4a} \tag{2.6a}$$

a and *b* are the new derived constants from the tensor matrix. k_1 and k_o are the plane strain bulk modulus of the fiber and the matrix. The components of the Eshelby tensor S_{ijkl} and g where stated previously for a spheroidal fiber.

$$a_1 = 6(k_1-k_o)(\mu_1-\mu_o)(S_{2222}+S_{2233}-1)-2(k_o\mu_1-k_1\mu_o)+6k_1(\mu_1-\mu_o) \tag{2.7a}$$

$$a_2 = 6(k_1-k_o)(\mu_1-\mu_o)S_{1133}+2(k_o\mu_1-k_1\mu_o) \tag{2.7b}$$

$$a_3 = -6(k_1-k_o)(\mu_1-\mu_o)S_{3311}-2(k_o\mu_1-k_1\mu_o) \tag{2.7c}$$

$$a_4 = 6(k_1-k_o)(\mu_1-\mu_o)(S_{1111}-1)+2(k_o\mu_1-k_1\mu_o)+6\mu_1(k_1-k_o) \tag{2.7d}$$

$$a_5 = \frac{1}{[S_{3322}-S_{3333}+1-\mu_1/(\mu_1-\mu_o)]} \tag{2.7e}$$

$$\begin{aligned} a = {} & 6(k_1-k_o)(\mu_1-\mu_o)[2S_{1133}S_{3311}-(S_{1111}-1)(S_{3322}+S_{3333}-1)] \\ & +2(k_o\mu_1-k_1\mu_o)[2(S_{1133}+S_{3311})+(S_{1111}-S_{3322}-S_{3333})] \\ & -6k_1(\mu_1-\mu_o)(S_{1111}-1)-6\mu_1(k_1-k_o)(S_{2222}+S_{2233}-1)-6k_1\mu_1 \end{aligned} \tag{2.7f}$$

$$b_1 = (1/16a)\{2a_3(6S_{1122} + S_{2222} + S_{2233} - 1) + a_4[3(S_{2222} + S_{2233} - 1) + 2S_{1122}] + 3a_5 a(S_{2222} - S_{2233} - 1) + 2a_1[3(S_{1111} - 1) + S_{2211}] - 2a_2(S_{1111} + 3S_{2211} - 1) - 4a(2S_{1212} - 1)/[2S_{1212} + \mu_o/(\mu_1 - \mu_o)]\} \quad (2.7g)$$

$$b_2 = (1/16a)\{2a_3[2S_{1122} + 3(S_{2222} + S_{2233} - 1)] + a_4(6S_{1122} + S_{2222} + S_{2233} - 1) + a_5 a(S_{2222} - S_{2233} - 1) + 2a_1(S_{1111} + 3S_{2211} - 1) - 2a_2[S_{2211} + 3S_{1111} - 1)] + 4a(2S_{1212} - 1)/[2S_{1212} + \mu_o/(\mu_1 - \mu_o)]\} \quad (2.7h)$$

$$b_3 = (1/4a)\{-2a_2(S_{1111} + S_{2211} - 1) + a_4(2S_{1122} + S_{2222} + S_{2233} - 1) - a_5 a(S_{2222} - S_{2233} - 1)\} \quad (2.7i)$$

$$b_4 = (1/4a)\{2(a_1 - a_2)S_{2211} + (2a_3 + a_4)(S_{2222} + S_{2233} - 1) - a_5 a(S_{2222} - S_{2233} - 1)\} \quad (2.7j)$$

$$b_5 = (1/2a)\{-2a_2 S_{2211} + a_4(S_{2222} + S_{2233} - 1) + a_5 a(S_{2222} - S_{2233} - 1)\} \quad (2.7k)$$

2.3 The Halpin-Tsai Models

The micromechanics employed in the development of the Halpin-Tsai equations is based upon the "self-consistent" method developed by Hill [25]. Hill modeled the composite as a single fiber, encased in a cylinder of matrix with both embedded in an unbounded homogeneous medium which is macroscopically indistinguishable from the composite [25]. Herman employed this model to obtain a solution in terms of Hill's "reduced moduli". Halpin and Tsai have reduced Herman's results to a simpler analytical form and extended

its use to a wide variety of reinforcement geometries [23]. Halpin and Tsai's elastic constant predictions apply to aligned and randomly aligned filler composites.

2.3.1 Nanocomposites reinforced with aligned graphene fillers

The Halpin-Tsai equations have been popular for many people to predict properties for short-fiber composites. One important aspect for Halpin-Tsai's equations is that they are good for short fiber composites and for predicting the longitudinal modulus for 1D fibers. Halpin and Tsai's original intent was to create models for continuous fiber composites and was derived from the previous work of Hermans and Hill [23]. Halpin and Tsai expressed three of Hermans equations in a common form, as shown in Equation 2.9, where P represents a generic property that relates to elastic constants, c is the volume fraction contribution of the fiber in the composite, η is a constant defined by fiber properties and ξ is a measure of reinforcement geometry which depends on loading conditions.

$$\frac{P}{P_m} = \frac{(1+\zeta c\eta)}{(1-c\eta)} \tag{2.9}$$

where the constant η is defined as

$$\eta = \frac{(\frac{P_f}{P_m} - 1)}{(\frac{P_f}{P_m} + \zeta)} \tag{2.10}$$

From Equation 2.9, the longitudinal modulus and transverse modulus can be expressed as follows

$$E_1 = \frac{(1+2(l/t)\eta_1 c)E_0}{1-c\eta_1} \tag{2.11a}$$

$$E_2 = \frac{(1+2\eta_2 c)E_0}{1-c\eta_2} \tag{2.11b}$$

where $\eta_1 = \frac{E_f/E_0 - 1}{E_f/E_0 + 2(l/t)}$ and $\eta_2 = \frac{E_f/E_0 - 1}{E_f/E_0 + 2}$. E_f and E_0 are modulus of the filler and matrix, respectively; l is the length, t is the thickness and c is the volume fraction contribution of the fillers in the composite.

2.3.2 Nanocomposites reinforced with random graphene fillers

Accurate predictions for randomly aligned fillers in composites have been attempted by several people and most predictions fall closely together for simple composites. The equations that predict these elastic constants can be very complicated like the predictions from Tandon and Weng. Halpin and Tsai took a simple approach for the solution to this. Equation 2.12 gives an estimate for randomly aligned filler composites.

$$E = \frac{3}{8}E_1 + \frac{5}{8}E_2 \tag{2.12}$$

2.4 Comparisons of Tandon-Weng model and Halpin-Tsai model: nanocomposite reinforced with aligned graphene fillers

2.4.1 Longitudinal modulus effect of volume fractions and aspect ratios

Halpin-Tsai and Tandon-Weng have produced several models to predict the five major elastic constants from a composite. The focus for the comparisons of Halpin-Tsai and Tandon-Weng are the longitudinal and transverse modulus elastic constants. These models where initially used for short fiber inclusions at moderate volume fractions and results from

these predictions are when the fiber has a low aspect ratio. One major problem when wanting to use graphene as a filler is that graphene has the capability of very high aspect ratios. It is unclear how a large aspect ratio filler will affect the accuracy of Halpin-Tsai and Tandon-Weng's predictions.

A test for composite predictions from analytical calculations of Tandon-Weng and Halpin-Tsai uses the same base material properties for all representative graphs. The elastic modulus for the matrix and filler are 5 Gpa and 1050 Gpa respectively and the Poisson's ratios are .35 and .19 respectively. Out of the five major elastic constants that can be calculated from the analytical models only the longitudinal modulus and the transverse modulus are represented. Figure 2.2 shows the comparison between Tandon-Weng and Halpin-Tsai for a low aspect ratio filler.

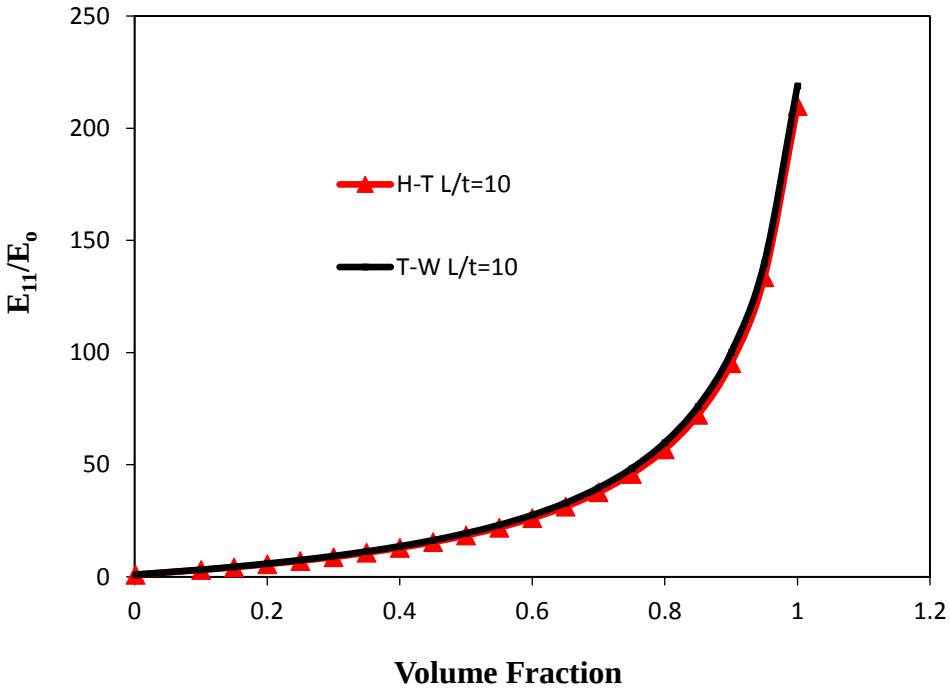

Figure 2.2 Longitudinal modulus ratios vs volume fractions at an aspect ratio of 10.

Figure 2.2 shows that at low aspect ratios with increasing volume fraction Tandon-Weng and Halpin-Tsai both give close estimations for the composite. The low aspect ratio of 10 shows good approximation for the analytical models that where intended for short fiber

composites. Also, if inspected closely it is noticed that Tandon-Weng's model very slightly over predicts the Halpin-Tsai model. Figure 2.3 shows the estimation like Figure 2.2 only now the aspect ratio has increased to 1000.

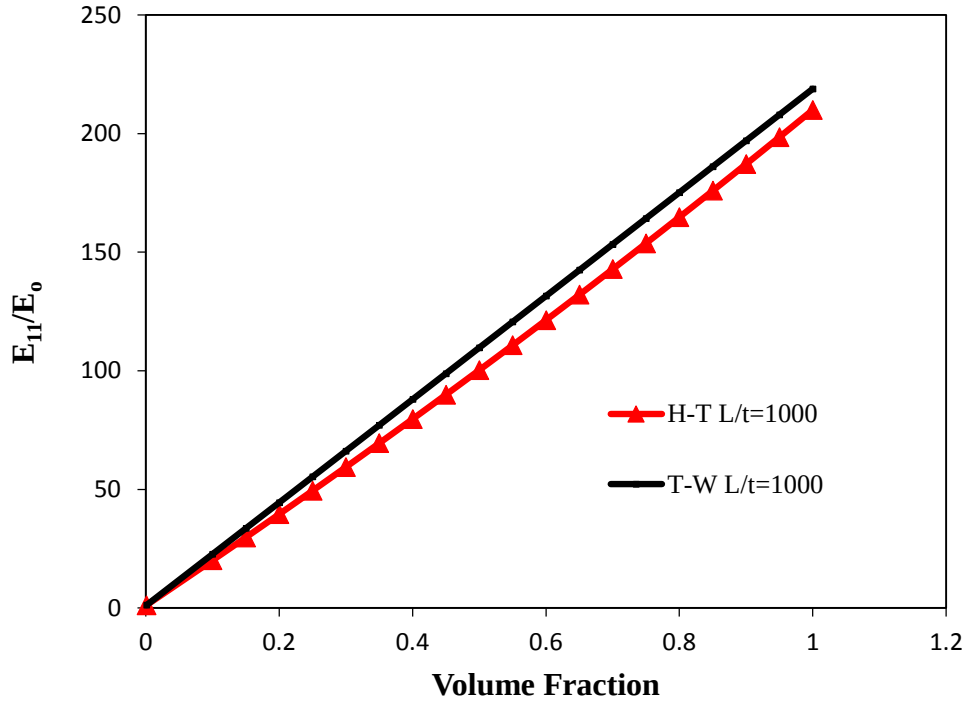

Figure 2.3 Longitudinal modulus ratios vs volume fractions at an aspect ratio of 1000.

Figure 2.3 shows that Tandon-Weng over predicts Halpin-Tsai at high aspect ratio fillers. The high aspect ratio of 1000 shows the analytical models predicting linear modulus ratio estimations. The reason the models predict a linear modulus ratio is due to the effects of the aspect ratio being very high. After the aspect ratio reaches a certain value the models treat the composite as a continuous fiber composite. One important aspect of the comparison between Figure 2.2 and Figure 2.3 is the effect of high aspect ratio fillers can produce higher composite moduli at moderate volume fractions. In the interest for composite modeling, volume fractions may not exceed 50 percent. Figure 2.4 and Figure 2.5 show the effects of low volume fractions and moderate volume fractions with increasing aspect ratios respectively.

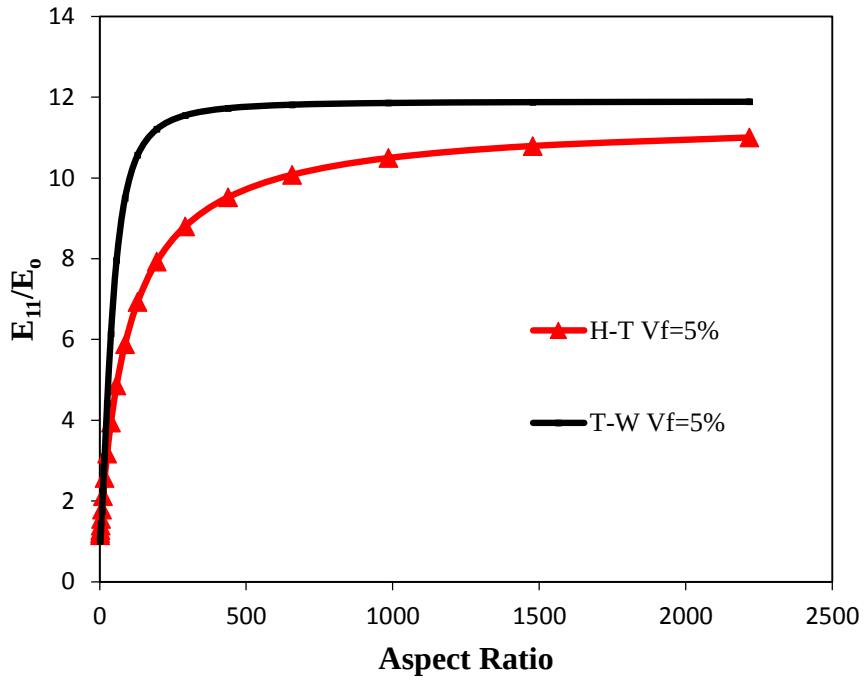

Figure 2.4 Longitudinal modulus ratios vs aspect ratios with constant volume fractions of 5%.

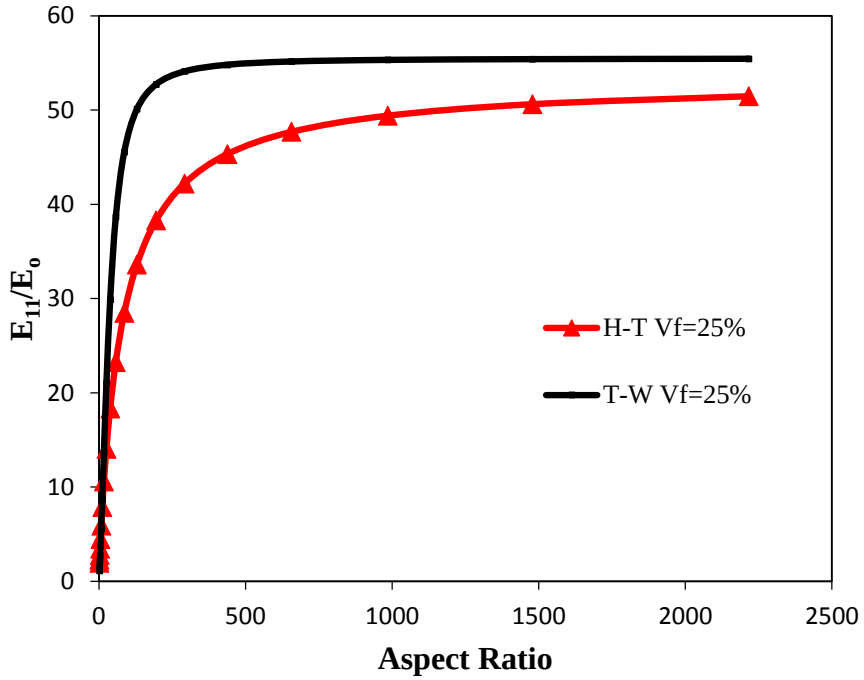

Figure 2.5 Longitudinal modulus ratios vs aspect ratios with constant volume fractions of 25%.

Figure 2.4 and 2.5 show at low and moderate volume fractions with increasing aspect ratios the Tandon-Weng model over predicts Halpin-Tsai's model. The trend from both models is the longitudinal modulus ratio does not change based on volume fraction. Figure 2.4 and Figure 2.5 both predict at aspect ratios above 300 the longitudinal modulus ratio no longer increases. From Figures 2.2-2.5 it is easy to see that increasing the aspect ratio above 500 will not increase the longitudinal modulus ratio, however, increasing the volume fraction will continue to increase the longitudinal modulus ratio.

2.4.2 Transverse modulus effects of volume fraction and aspect ratios

The transverse modulus ratio is another composite elastic constant of interest when modeling. Figure 2.6 and Figure 2.7 show the effects of volume fraction on the transverse modulus.

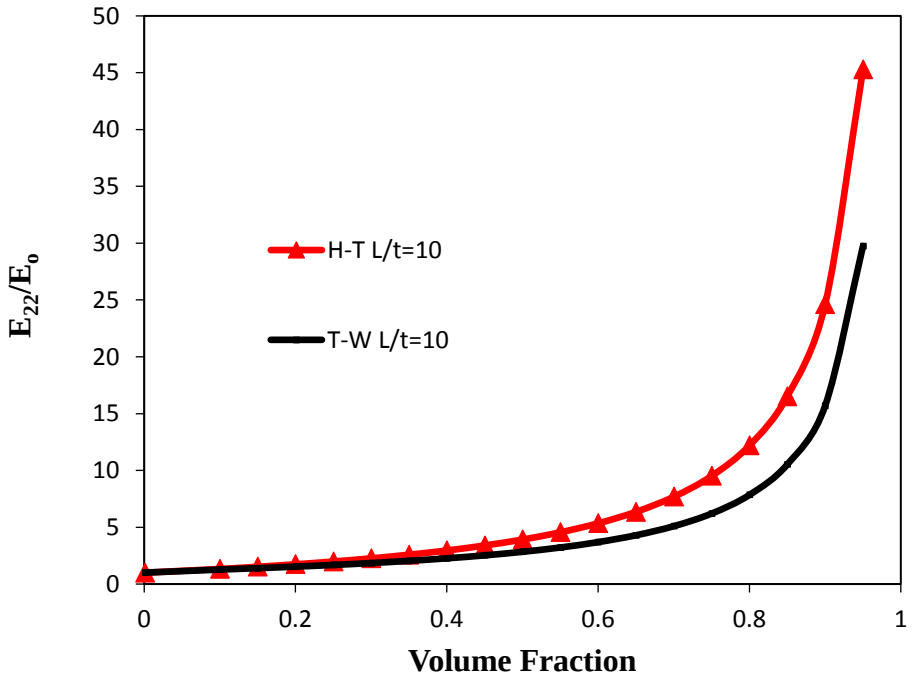

Figure 2.6 Transverse modulus ratios vs volume fractions with an aspect ratio of 10.

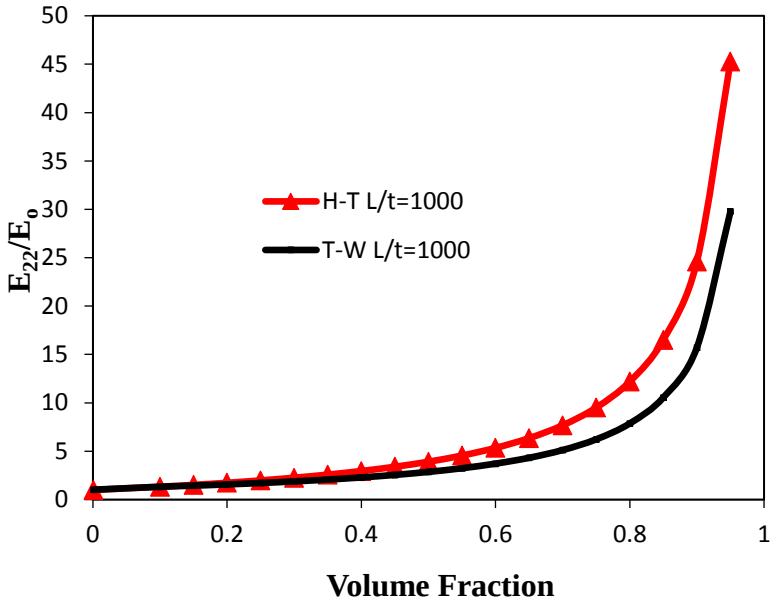

Figure 2.7 Transverse modulus ratios vs volume fraction with an aspect ratio of 1000.

Figure 2.6 and Figure 2.7 show the value of the aspect ratio having little effect on the transverse modulus with increasing volume fraction. To investigate the effects of aspect ratio and volume fraction Figure 2.8 and Figure 2.9 show the effects of constant volume fractions with increasing aspect ratio.

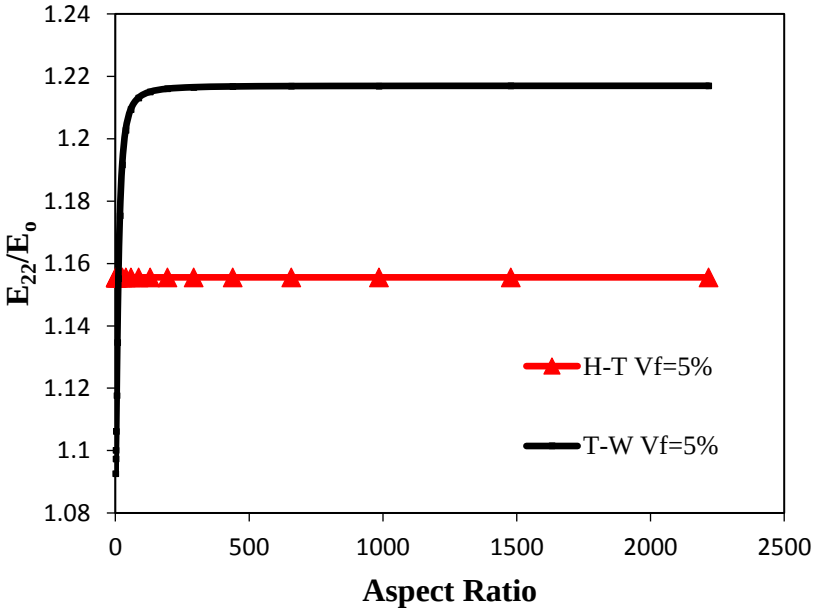

Figure 2.8 Transverse modulus ratios vs aspect ratios with a volume fraction at 5%.

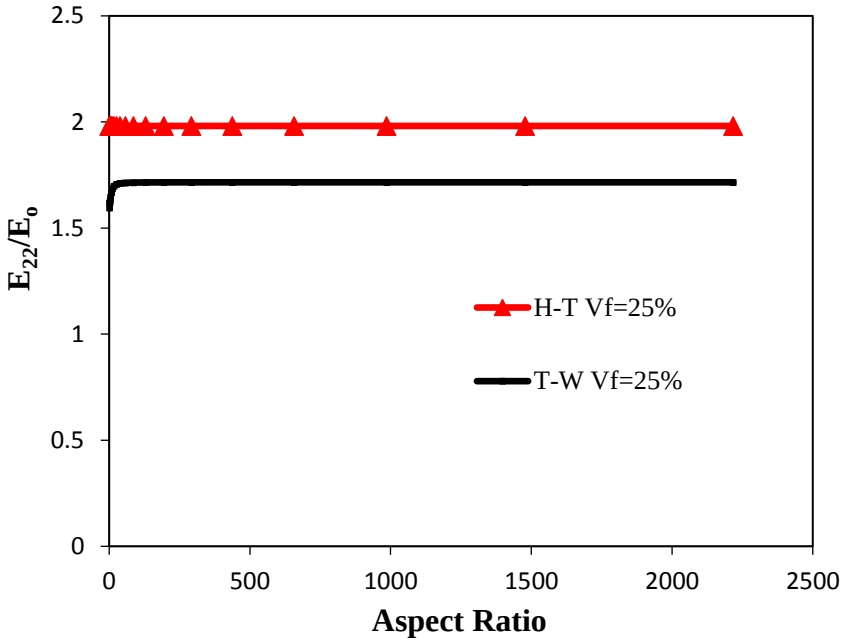

Figure 2.9 Transverse modulus ratios vs aspect ratios with a volume fraction at 25%.

Figure 2.8 shows Tandon-Weng predicting higher transverse modulus ratios than Halpin-Tsai at a volume fraction of 5%. The opposite happens in Figure 2.9 where the volume fraction is 25%. The Halpin-Tsai model from Figures 2.8 and 2.9 show the transverse modulus ratio is insensitive to aspect ratio. The Tandon-Weng model in Figure 2.8 shows at low volume fractions and low aspect ratios the transverse modulus is affected by the aspect ratio, but only at low aspect ratios. The reason the Halpin-Tsai model is not affected by the aspect ratio is due to the zeta term in the equation that relates the fiber geometry parameter.

2.4.3 Effect of filler/matrix modulus ratios

Previous representative graphs have held the fiber and matrix material properties constant. Now the modulus for the fiber will vary while the modulus for the matrix will remain constant. The Young's modulus for the fiber will vary from 0-600 Gpa with a Poisson's ratio of .19. The matrix Young's modulus and Poisson's ratio will be 1 Gpa and .35

respectively. Changing the fiber's Young's modulus will allow for a modulus ratio comparison using the same volume fractions of 5% and 25% and the same aspect ratios of 10 and 1000. Modular ratio representative graphs help aid in the process for modeling novel nanocomposites of extreme variables and are particularly useful for deciding on a certain type of matrix material that can be used with the fiber of choice. Figure 2.10 shows the effects on the longitudinal modulus by varying the modulus ratio with an aspect ratio held to 10 and two different volume fractions of 5% and 25%.

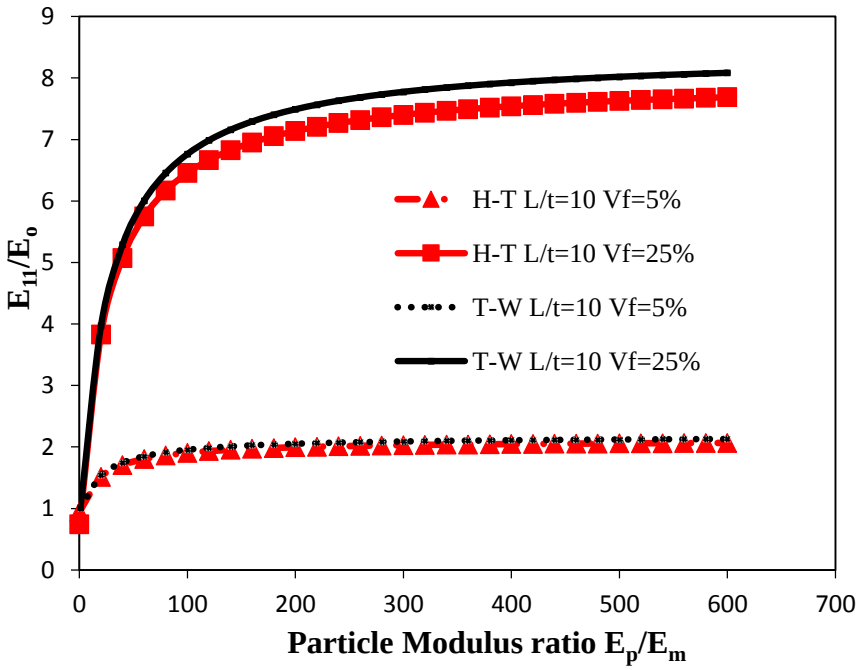

Figure 2.10 Longitudinal modulus ratios vs particle modulus ratios with an aspect ratio held at 10 and volume fraction varying from 5% and 25%.

Figure 2.10 shows at low volume fractions and low aspect ratios Tandon-Weng and Halpin-Tsai have relatively the same prediction with Tandon-Weng being slightly above Halpin-Tsai. Increasing the volume fraction to 25% shows Tandon-Weng predicting a noticeably higher longitudinal modulus ratio than Halpin-Tsai with a varied modular ratio. Figure 2.11 shows the effects of the longitudinal modulus ratio to the particle modulus ratio with an increased aspect ratio of 1000 and having the same varied volume fractions of 5% and 25%.

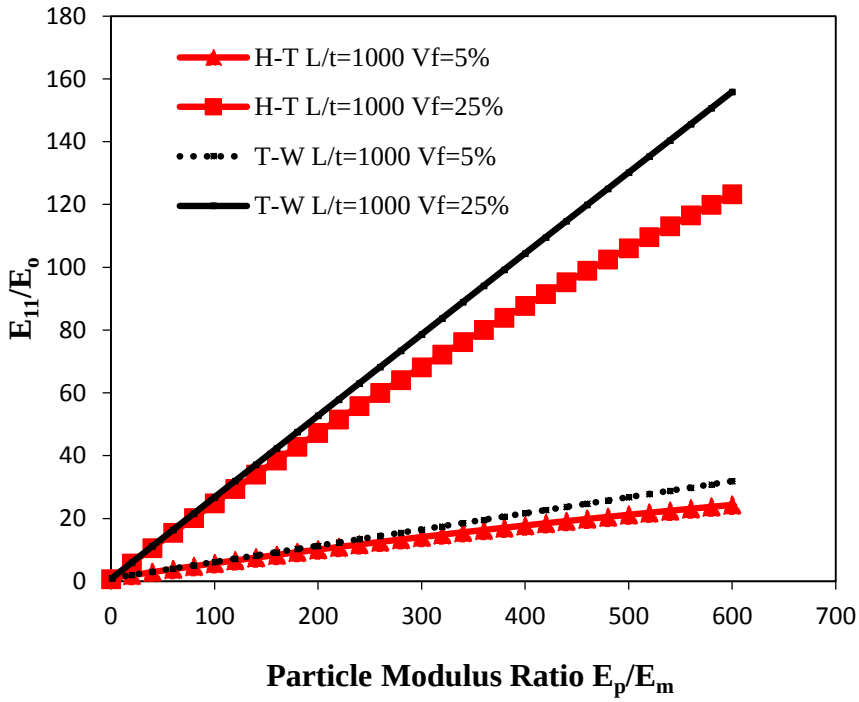

Figure 2.11 Longitudinal modulus ratios vs particle modulus ratios with an aspect ratio held at 1000 and volume fraction varying from 5% and 25%.

From Figure 2.11 Tandon-Weng has higher predictions than Halpin-Tsai at 5% volume fractions and at 25% volume fractions. At 5% volume fraction Tandon-Weng slightly predicts a higher longitudinal modulus ratio than Halpin-Tsai. At 25% volume fraction Tandon-Weng has much higher predictions to the longitudinal modulus ratio than Halpin-Tsai.

Transverse modulus ratios are another important analytical prediction necessary for novel nanocomposites when selecting matrix modulus values. Figure 2.12 shows the effects of transverse modulus ratios by again varying the particle modulus ratio. The volume fractions will also vary from 5% and 25% while holding the aspect ratio constant at 10.

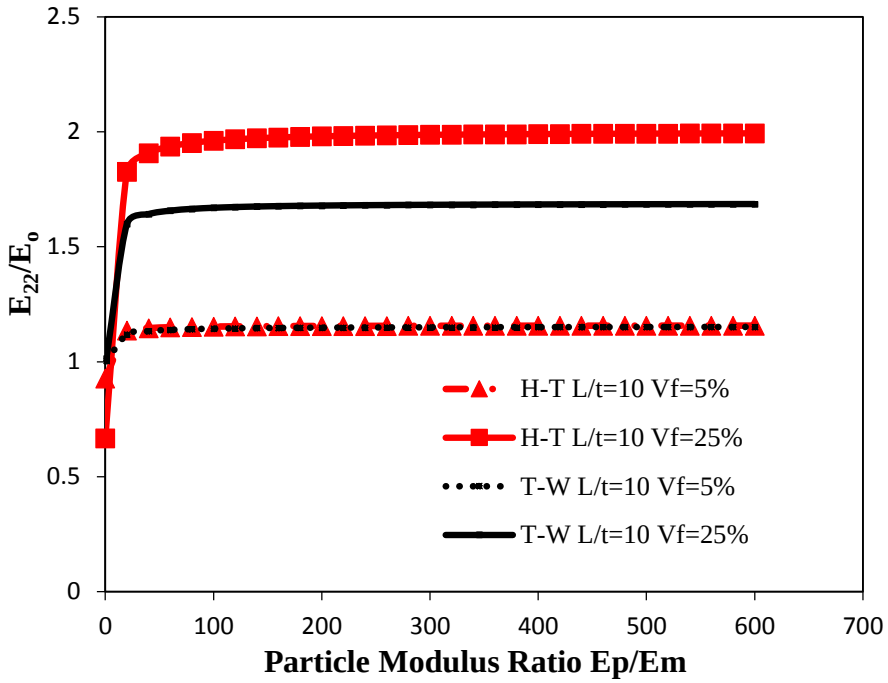

Figure 2.12 Transverse modulus ratios vs particle modulus ratios with an aspect ratio held at 10 and volume fraction varying from 5% and 25%.

Figure 2.12 shows at 5% volume fraction with an aspect ratio of 10 Tandon-Weng slightly predicts higher transverse modulus ratios than Halpin-Tsai. When the volume fraction is increased to 25% with the same aspect ratio of 10, Halpin-Tsai predicts much higher results than Tandon-Weng. Figure 2.13 shows the same transverse modulus ratio and varying particle modulus ratio, but the aspect ratio is now increased to 1000.

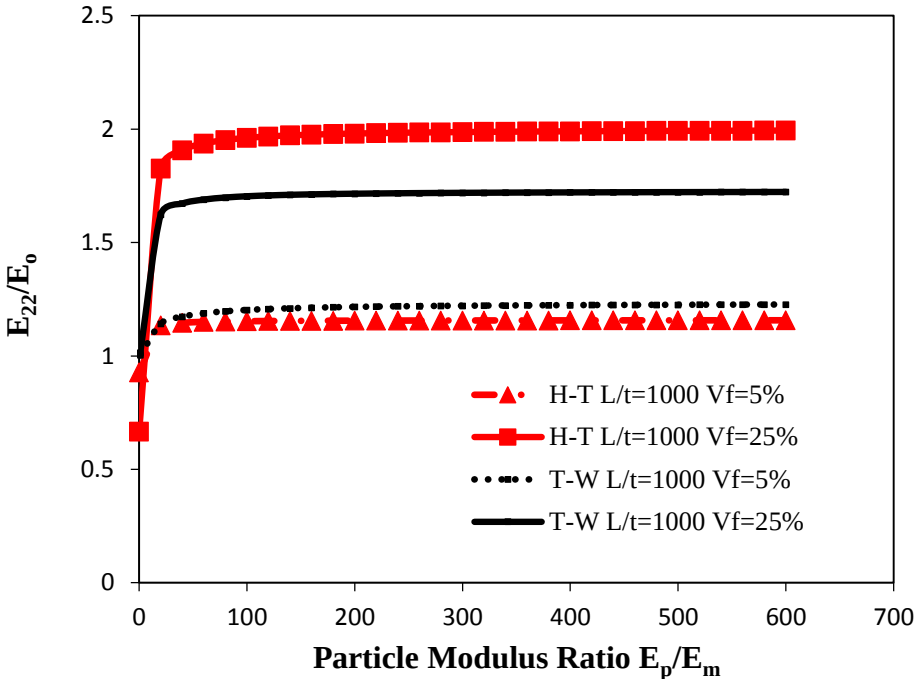

Figure 2.13 Transverse modulus ratios vs particle modulus ratios with aspect ratio held at 1000 and volume fraction varying from 5% and 25%.

At 5% volume fraction with an aspect ratio of 1000 Tandon-Weng predicts higher transverse modulus ratios than Halpin-Tsai. When increasing the volume fraction to 25% Halpin-Tsai predicts higher transverse modulus ratios than Tandon-Weng. The change in predictions is Halpin-Tsai's independence of aspect ratio in the transverse modulus analytical calculations. This explanation applies to Figure 2.12 and Figure 2.13.

2.5 Comparisons of Tandon-Weng model and Halpin-Tsai model: nanocomposite reinforced with randomly aligned graphene fillers

2.5.1 Effect of volume fractions

The complexities for nanocomposites are well known and it is not entirely accurate to predict elastic constants for a composite when the fibers are aligned in the same direction. The fibers will be randomly aligned when dispersed into a matrix to form a composite. The material properties through the next set of representative graphs illustrate the random orientation of fibers and the graphs will remain with the fiber Young's modulus and Poisson's ratio at 1050 Gpa and .19 respectively. The matrix Young's modulus and Poisson's ratio are at 5 Gpa and .35 respectively. Figure 2.14 shows the randomly aligned fiber predictions for the longitudinal modulus ratio and transverse modulus ratio by varying the volume fraction with a constant aspect ratio of 10.

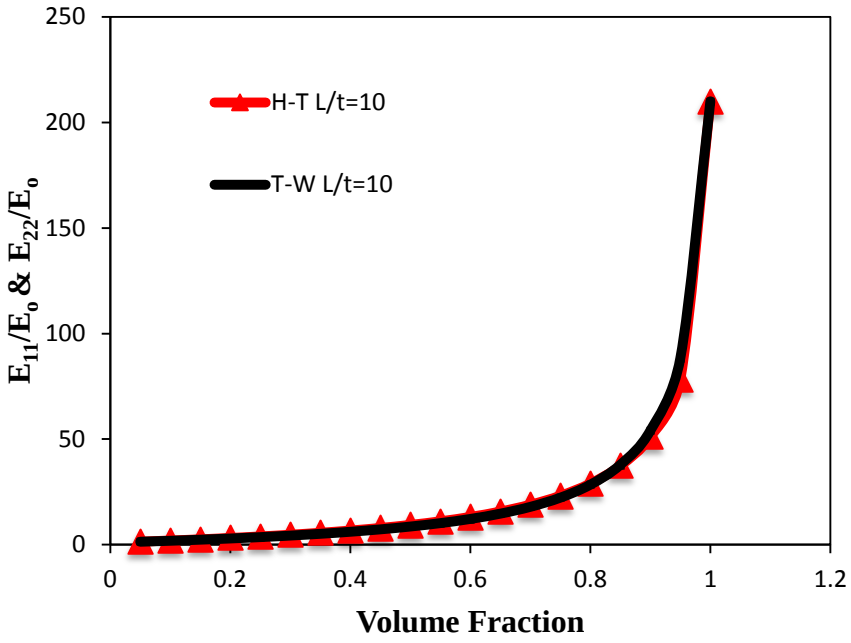

Figure 2.14 Longitudinal and transverse modulus ratios vs volume fraction with an aspect ratio of 10.

Figure 2.14 shows Tandon-Weng and Halpin-Tsai have very close predictions at an aspect ratio of 10 while varying the volume fraction. Figure 2.15 shows effects like Figure 2.14 only now the aspect ratio has been increased to 1000.

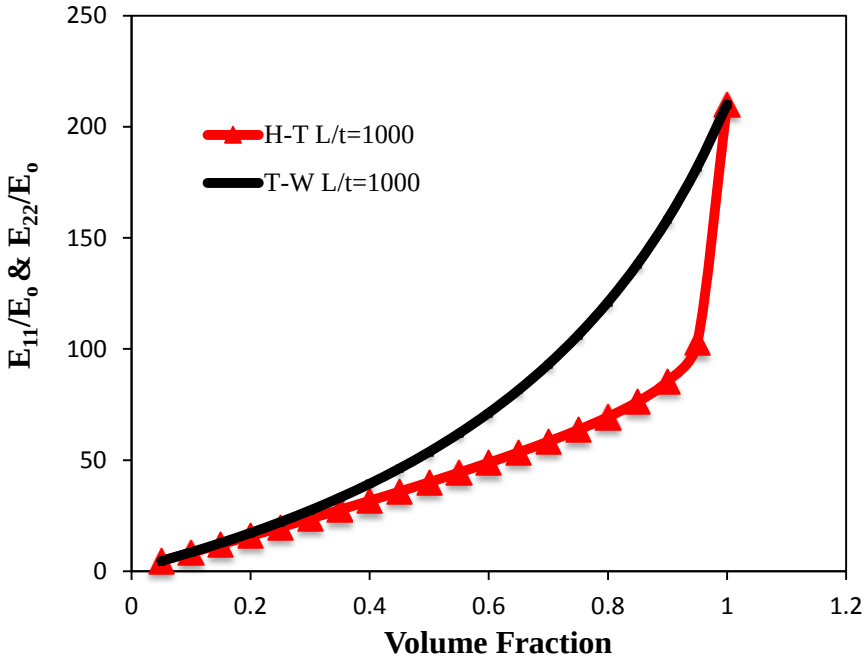

Figure 2.15 Longitudinal and transverse modulus ratios vs volume fraction with an aspect ratio of 1000.

The increased aspect ratio had a large effect to Tandon-Weng's prediction when compared to Halpin-Tsai's. Halpin-Tsai's prediction doesn't show a consistent trend like Tandon-Weng's prediction. Halpin-Tsai predicts a linear increase to modulus values until 80% volume fraction. Then Halpin-Tsai's predictions between 95% and 100% volume fraction doubles. Although a composite will not have volumes fractions as high as 95% what is noticed is the accuracy for predictions with aspect ratios as high as 1000 may not be effective when using Halpin-Tsai. However, there are significant changes to the trends for Tandon-Weng's predictions. When the aspect ratio is increased from 10 to 1000 Tandon-Weng predicts much higher modulus values through the middle range of volume fractions.

2.5.2 Effect of aspect ratios

The variation between low and high aspect ratio has been well established. The proceeding graphs will represent varying the aspect ratio with randomly aligned fibers of graphene.

Figure 2.16 shows the effects to the longitudinal and transverse modulus by varying the aspect ratio with a constant volume fraction of 5%.

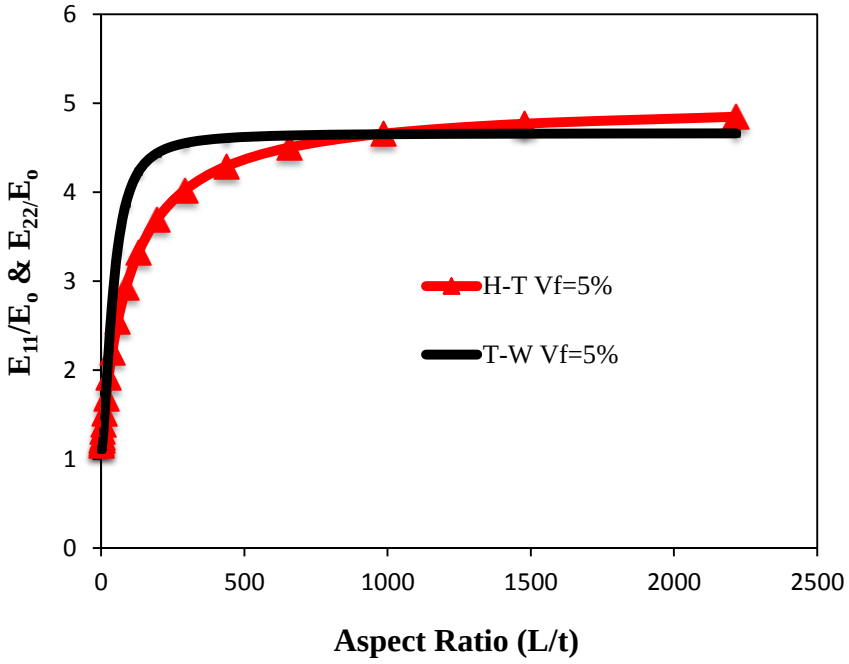

Figure 2.16 Longitudinal and transverse modulus ratios vs aspect ratios with a volume fraction of 5%.

Tandon-Weng has higher predictions than Halpin-Tsai until the aspect ratio reaches 1000. After the aspect ratio reaches 1000 Halpin-Tsai has a higher prediction than Tandon-Weng. Tandon-Weng predicts at aspect ratios above 300 will only have a small effect to the longitudinal and transverse modulus ratios, whereas, Halpin-Tsai has a steady increase to the modular ratios with increasing aspect ratio. Figure 2.17 has the same representative graphs as Figure 2.16, but now the volume fraction has been increased to 25%.

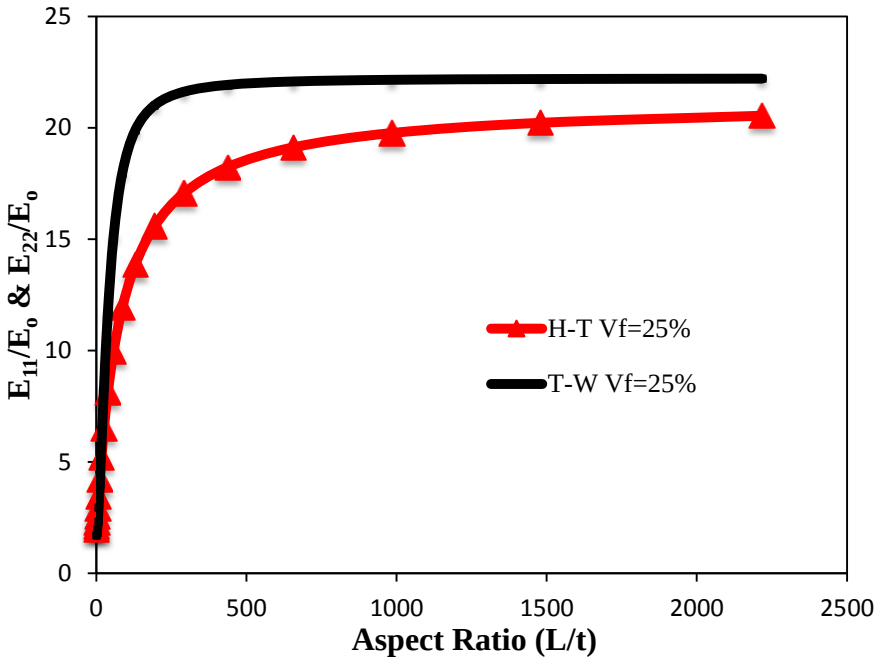

Figure 2.17 Composite modulus vs aspect ratio with a volume fraction of 25%.

Increasing the volume fraction to 25% did not change the trends of the two models predictions only the values of the predicted modular ratios. Again Tandon-Weng's prediction to the modular ratio has little effect after the aspect ratio is increased to 300 while Halpin-Tsai's prediction continues to increase with increasing aspect ratio. For Figure 2.17 Tandon-Weng predicts higher modular ratios than Halpin-Tsai until the predictions for the model stops.

2.5.3 Effect of filler/matrix modulus ratios

The particle modulus ratio representative graphs will have the same analytical calculating parameters as before with the aligned case. The Young's modulus for the fiber will vary from 0-600 Gpa with a Poisson's ratio of .19. The matrix Young's modulus and Poisson's ratio will be 1 Gpa and .35 respectively. Changing the fiber's Young's modulus will allow for a modulus ratio comparison using the same volume fractions of 5% and 25% and the same aspect ratios of 10 and 1000. Figure 2.18 shows the longitudinal and transverse

modulus predictions with varying particle modulus ratios. For this case the volume fraction will also vary from 5% and 25% while the aspect ratio will remain constant at 10.

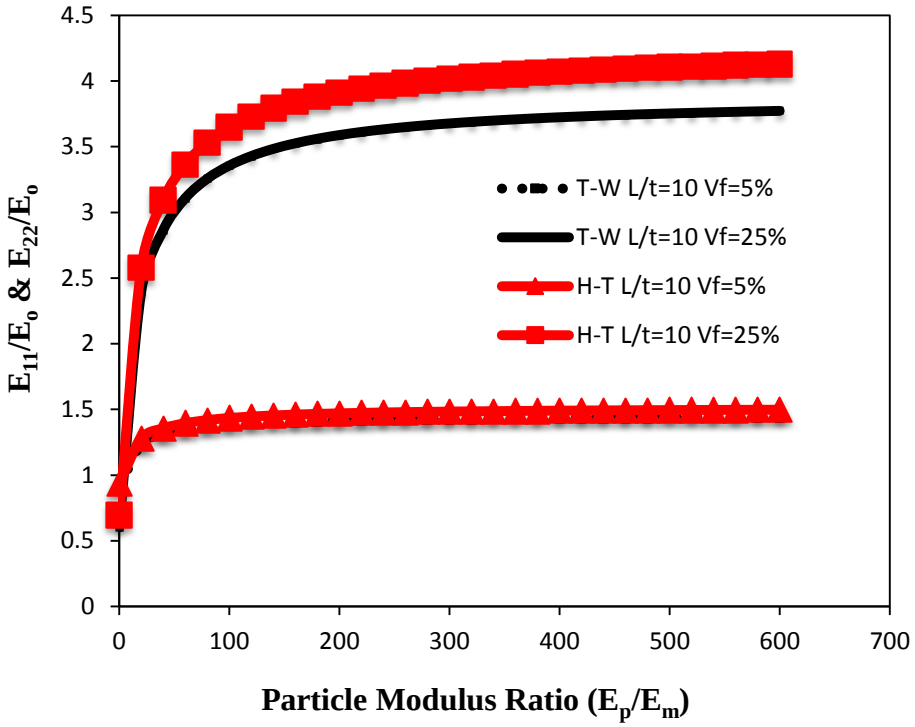

Figure 2.18 Composite modulus ratios vs particle modulus ratios with an aspect ratio held at 10 and volume fraction varying from 5% to 25%.

Figure 2.18 shows Halpin-Tsai predicts higher longitudinal and transverse modulus ratios than Tandon-Weng for both cases of volume fractions of 5% and 25% with a constant aspect ratio of 10. Figure 2.19 shows the same representative graph as Figure 2.18, but the aspect ratio is increased to 1000.

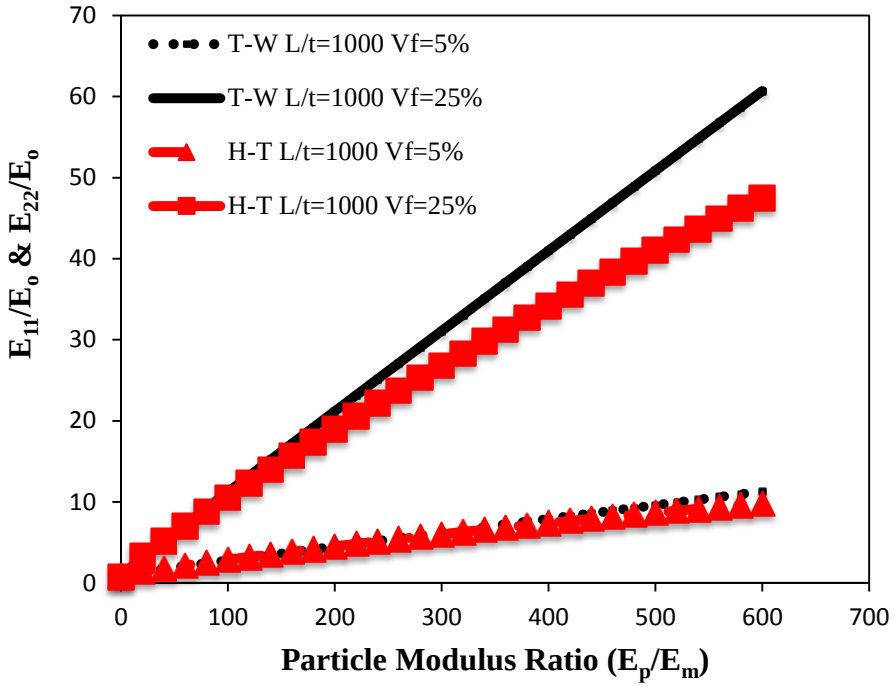

Figure 2.19 Longitudinal and transverse modulus ratios vs particle modulus ratio were aspect ratio is held at 1000 and volume fraction varies from 5% to 25%.

When the aspect ratio is increased to 1000 the predictions for Tandon-Weng and Halpin-Tsai are opposite to that of the aspect ratio of 10. Now Tandon-Weng predicts higher longitudinal and transverse modulus ratios than Halpin-Tsai. Due to Halpin-Tsai's analytical predictions for randomly aligned modulus ratios it can be expected to vary in comparison to Tandon-Weng. From equation 2.5 the transverse modulus provides a larger portion to the prediction than the longitudinal modulus portion. This leaves the dependence to aspect ratio only being accounted for in the E_1 term of the equation.

2.6 Conclusions

Although several theoretical frameworks have been developed for predicting properties of composite materials reinforced with one-dimensional (1D) fillers, they have yet been

proven to be suitable for 2D, ultra-thin, high aspect graphene fillers. This chapter has comprehensively examined the existing composite models (Halpin-Tsai model and the Tandon-Weng model) in the modeling of graphene-polymer composites. The graphene is assumed to be a monolayer, isotropic material. The composites have been considered for the cases of both aligned fillers and randomly distributed fillers.

As expected, Halpin-Tsai model and Tandon-Weng model show consistent predictions for composites with fillers at lower aspect ratio (L/t=10). However, there are consistent discrepancies between these two models in predicting the behavior of composites with fillers at high aspect ratios (L/t>1000), which represent the actual 2D graphene fillers: the Halpin-Tasi model gives lower predictions for all conditions, i.e., aspect ratio, volume fraction, filler/matrix modulus ratio, and filler orientations (aligned and random distributions). In particular, Halpin-Tsai shows poor predictions for the transverse modulus (E_{22}).

The primary reasons for the inadequacy of using Halpin–Tsai model for 2D graphene fillers may be the followings. First, the Halpin-Tsai model treats a filler as a 1D fiber. Secondly, The Halpin–Tsai equations are independent of the Poisson's ratio of the filler or the matrix, which would inherently cause errors in calculating axial strain and modulus. Thirdly, the Halpin–Tsai equation for transverse modulus (E_2) lacks of consideration for aspect ratio (L/t). In contrast, the Tandon-Weng's predictions are more consistent through the range of varying aspect ratios, volume fractions, particle modular ratios, and filler orientations (aligned and randomly distributed).

CHAPTER 3 - ANALYTICAL MODELS FOR NANOCOMPOSITES REINFORCED WITH 2D FILLERS: MULTILAYER GRAPHENE

3.1 Introduction

The two-dimensional (2D), ultra-thin graphene fillers used in nanocomposites are mostly in the form of multi-layers. Layered graphenes can be produced by simple mechanical peeling of natural graphite [27], or by sophisticate methods such as liquid-phase exfoliation of bulk graphite [28], chemical vapor deposition of carbon on metal substrates [29], and oxidization of graphite crystals [30], etc. One important issue in layered graphene fillers is the presence of "interlayers" between individual graphene. These special materials may be either the chemicals and/or solvents that are used to exfoliate the fillers, or the polymer chains that penetrate into the spaces between graphene layers during preparations of the composites, or a mixture of both [31]. The mechanical properties of the interlayer materials are often unknown and the sizes of the interlayers (interlayer spacing) may also be subjected to continuous changes, depending upon the structures of the specific graphene layer and the polymer chains.

The previous chapter (Chapter 2) examined the analytical models that may be used for 2D, graphene polymer nanocomposites, in which the graphene is in the form of monolayer. A monolayer graphene does not contain an "interlayer" and thus can be treated as a homogeneous material. In this chapter, the Tandon-Weng and Halpin-Tsai models are used to model the nanocomposites reinforced with layered graphene, where the "interlayers" are presented.

3.2 Predictions of elastic moduli of polymer-layered graphene composites

3.2.1 Analysis of effective elastic moduli of layered graphene

The two-dimensional, layered graphene filler consists of alternating layers (graphene layers and interlayers) having different physical and mechanical properties. When those layered fillers are dispersed into a polymer matrix, the polymer chains will intercalate into the interlayers and thus increase the spacing of the interlayers (If the amount of layered graphene fillers is kept to be very small, i.e., <1%, the layered graphenes may be partially or completely exfoliated into the polymer matrix [30, 31]). These layered graphene stacks are considered to be the "effective" reinforcement fillers and the moduli of such structures may be estimated by using the Arridge model, which was originally developed for two-dimensional, layered copolymer lamella [32].

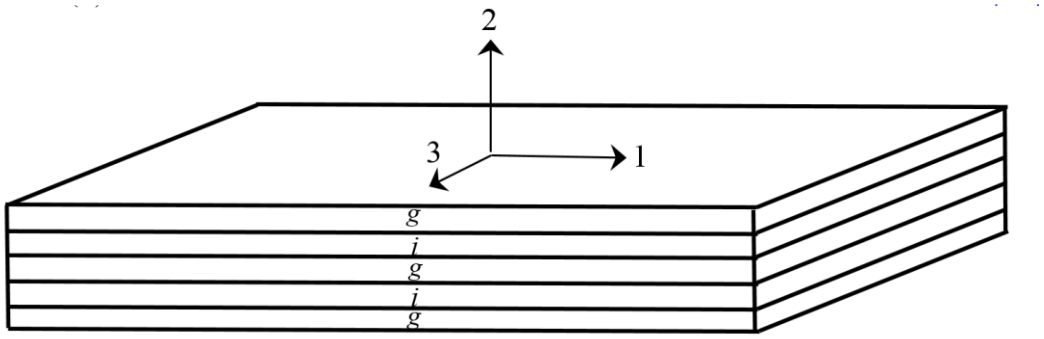

Figure 3.1 Model for the "effective" layered graphene filler.

From Figure 3.1 the "g" stands for graphene layer and "i" stands for interlayer.

Take the 1-axis as parallel to the planes of the layered graphenes and the 2-axis as perpendicular to the planes of the layered graphenes. By assuming uniform stress and uniform strain in each layer upon loading, the effective elastic moduli (E_{L1} and E_{L2}) of a layered graphene filler can be computed as

$$E_{L1} = V_g E_g + V_i E_i - \frac{V_g V_i E_g E_i (\mu_i - \mu_g)^2}{V_g E_g (\mu_i^2 - 1) + V_i E_i (\mu_g^2 - 1)} \quad (3.1)$$

$$\frac{1}{E_{L2}} = \frac{V_g}{E_g} + \frac{V_i}{E_i} - \frac{2V_g V_i (\mu_g E_i - \mu_i E_g)^2}{E_g E_i [V_g E_g (1-\mu_i) + V_i E_i (1-\mu_g)]} \quad (3.2)$$

where "g" stands for graphene layer and "i" stands for interlayer. "V" stands for volume fraction within the layered stack and "μ" stands for Poisson's ratio for the materials within the layered stack.

In both equations, the second terms are responsible for the lateral deformations in the two-dimensional, layered fillers. For one-dimensional fillers, such as fibers, the lateral deformations can be ignored (μ=0), then the Arridge's lamella model is reduced to the simple "rule-of-mixtures" model [13]: $E_{L1} = V_s E_s + V_i E_i$ and $1/E_{L2} = V_s/E_s + V_i/E_i$.

3.2.2 Analysis of effective elastic moduli of polymer-layered graphene composites

When dispersed into a polymer matrix, the layered graphene stacks remain as the "effective" fillers. The mechanical properties of the layered graphenes-polymer composites may be estimated through conventional composite theories. Although several theoretical frameworks exist for predicting the properties of reinforced composites, the Tandon-Weng and Halpin–Tsai theories were chosen in this work because of their effectiveness in predicting the stiffness of various types of nanocomposites and their adaptability for "plate-type" filler geometries [33,34].

3.2.3 The Tandon-Weng Solutions

The Tandon-Weng equations are a set of analytical solutions to the combined Eshelby's and Mori-Tanaka's theories of inclusion [35-37]. Those expressions allow the predictions of the properties of a composite in terms of properties of the polymer matrix and reinforcing fillers together with their proportions and geometry. The effective moduli of composites with aligned fillers are:

$$E_1 = \frac{E_o}{1 + c(A_1 + 2\nu_o A_2)/A} \tag{3.3}$$

$$E_2 = \frac{E_o}{1 + c[-2\nu_o A_3 + (1-\nu_o)A_4 + (1+\nu_o)A_5 A]/2A} \tag{3.4}$$

where E_1 and E_2 are the modulus of the composite in 1-axis and 2-axis, respectively. c is the volume fraction of the inclusion in the composite. E_0 and ν_0 are the modulus and Poisson's ratio of the matrix, respectively. A and A_1-A_5 are constants that are defined by

$$A_1 = D_1(B_4 + B_5) - 2B_2 \tag{3.5a}$$

$$A_2 = (1 + D_1)B_2 - (B_4 + B_5) \tag{3.5b}$$

$$A_3 = B_1 - D_1 B_3 \tag{3.5c}$$

$$A_4 = (1 + D_1)B_1 - 2B_3 \tag{3.5d}$$

$$A_5 = \frac{(1 - D_1)}{(B_4 - B_5)} \tag{3.5e}$$

$$A = 2B_2 B_3 - B_1(B_4 + B_5) \tag{3.5f}$$

where B_1-B_5 and D_1 are constants that can be directly computed from material and geometrical properties of the filler and the matrix [37].

Tandon and Weng further develop the solutions for the effective modulus of composites with randomly distributed fillers [38]

$$E = \frac{E_o}{1 + c\,p_{11}} \tag{3.6}$$

where p_{11} is given as follows

$$p_{11} = \frac{1+\nu_o}{1+c(b_1-b_2)}\left\{\frac{2(a_1+a_2-a_3)+a_4+a_5 a}{16a} - \frac{1}{4[2S_{1212}+\mu_o/(\mu_1-\mu_o)}\right\}$$

$$-\frac{(1-\nu_o)(1+c\,b_5)+2c\,\nu_o\,b_3}{2c^2 b_3 b_4-(1+c\,b_5)[1+c(b_1+b_2)]}\,\frac{2(a_1-a_2+a_3)+a_4+a_5 a}{8a}$$

$$+\frac{(1-\nu_o)c\,b_4+\nu_o[1+c(b_1+b_2)]}{2c^2 b_3 b_4-(1+c\,b_5)[1+c(b_1+b_2)]}\,\frac{-2a_2+a_4-a_5 a}{4a} \tag{3.7}$$

where a, a_1-a_5 and b_1-b_5 are constants that can be directly computed from material and geometrical properties of the filler and the matrix. S_{1212} is one of the components of the Eshelby tensor, ν_0 is the Poisson's ratio of the matrix, and μ_0 and μ_1 are Lame's constants of matrix and filler, respectively.

3.2.4 The Halpin-Tsai Solutions

The Halpin-Tsai equations are a set of empirical solutions which have been widely used to estimate the properties of a composite in terms of properties of the matrix and reinforcing phases together with their proportions and geometry [30-32]. The effective moduli of a composite with aligned fillers are:

$$E_1 = \frac{(1+2(l/t)\eta_1 c)E_0}{1-c\eta_1} \tag{3.8}$$

$$E_2 = \frac{(1+2\eta_2 c)E_0}{1-c\eta_2} \tag{3.9}$$

where $\eta_1 = \frac{E_f/E_0 - 1}{E_f/E_0 + 2(l/t)}$ and $\eta_2 = \frac{E_f/E_0 - 1}{E_f/E_0 + 2}$. E_f and E_0 are modulus of the filler and matrix, respectively; l and t are the length and thickness of the filler, respectively. c is the volume fraction contribution of the fillers in the composite

The effective modulus of composites with randomly distributed fillers is approximated as

$$E = \frac{3}{8}E_1 + \frac{5}{8}E_2 \tag{3.10}$$

where E_1 and E_2 are the longitudinal and transverse moduli of the composite, as defined in Eqs. (3.8) and (3.9) [39-41].

3.3 Results and discussions

3.3.1 Effective elastic moduli of 2D layered graphenes

The macroscopic properties of composites are determined by the reinforcement "filler" and the polymer "matrix". The conventional "fillers", such as most 1D fillers and the 2D monolayer graphene, are homogeneous materials with distinctly defined properties. However, in the case of ultra-thin, "layered fillers", such as and the layered graphene, the stiffening layers are separated by the complex interlayer materials with varying sizes and

properties. Therefore, the effective moduli of the "layered fillers" are dependent upon the properties of interlayers.

Figures 3.2 – 3.4 show the effective moduli of layered graphene stacks as computed by using Arridge's lamella model (Eqs. (3.1)-(3.2)). These solutions are derived based on the deformations of a two-dimensional, thin plates, as opposed to the simple "rule-of-mixtures" solutions which are derived based on the uniaxial deformation only. Figure 3.2 shows the effects of Poisson's ratio in the interlayers.

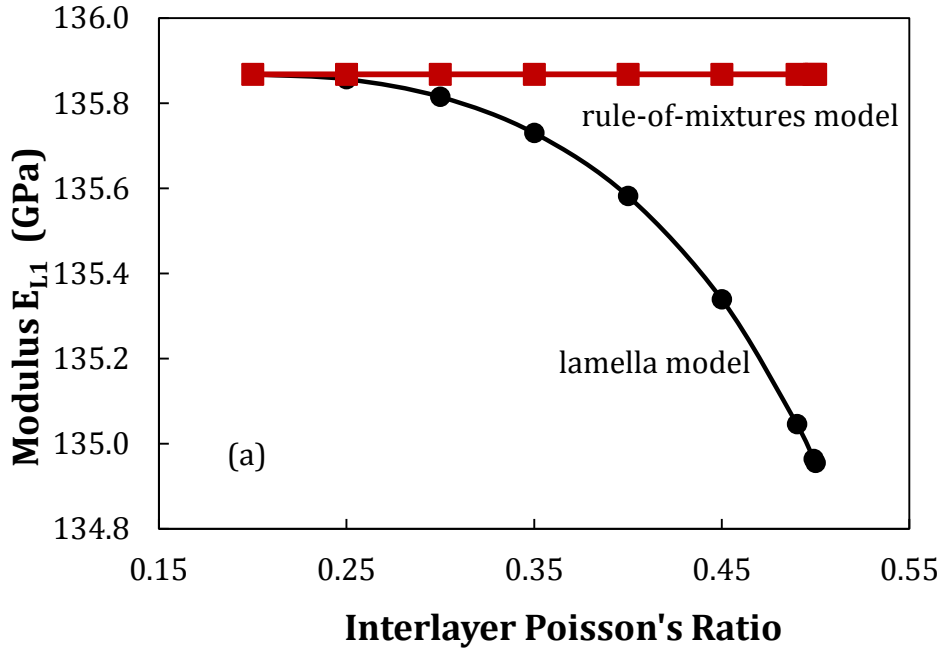

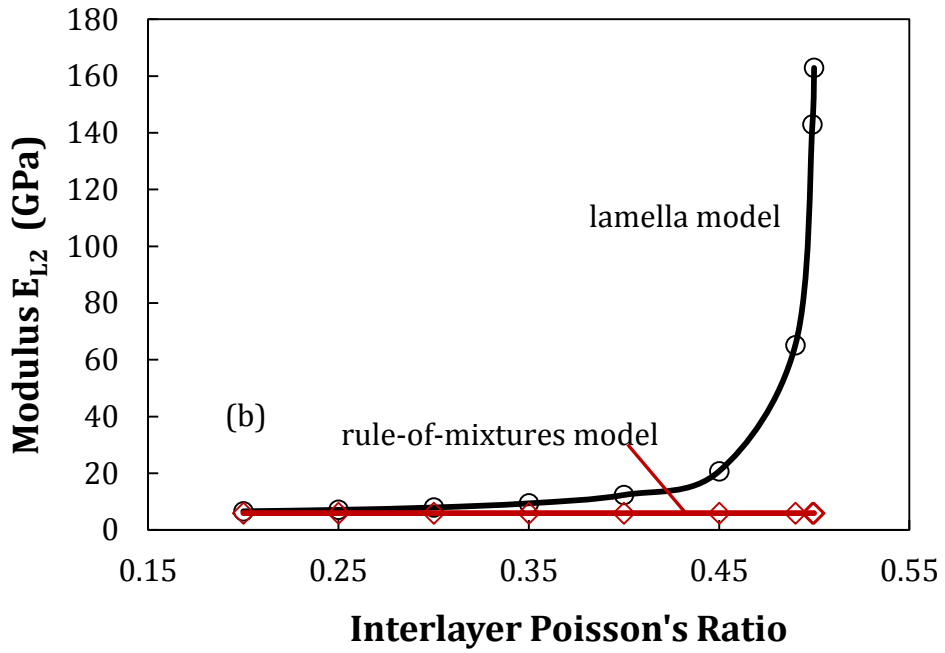

Figure 3.2 Effect of interlayer Poisson's ratio on the moduli of layered graphenes: a) In-plane modulus E_{L1} and b) Out-of-plane modulus E_{L2}.

As shown in Figure. 3.2, the simple "rule-of-mixtures" do not take into account of the lateral deflections (as governed by the Poisson's ratios) and thus predict the constant moduli. In contrast, the Arridge's lamella model predicts that, as the Poisson's ratio of the interlayer increases, the in-plane modulus (E_{L1}) of the layered graphenes will decrease and the out-of-plane modulus (E_{L2}) of the layered graphenes will increase. Figure 3.3 shows the effects of the interlayer modulus.

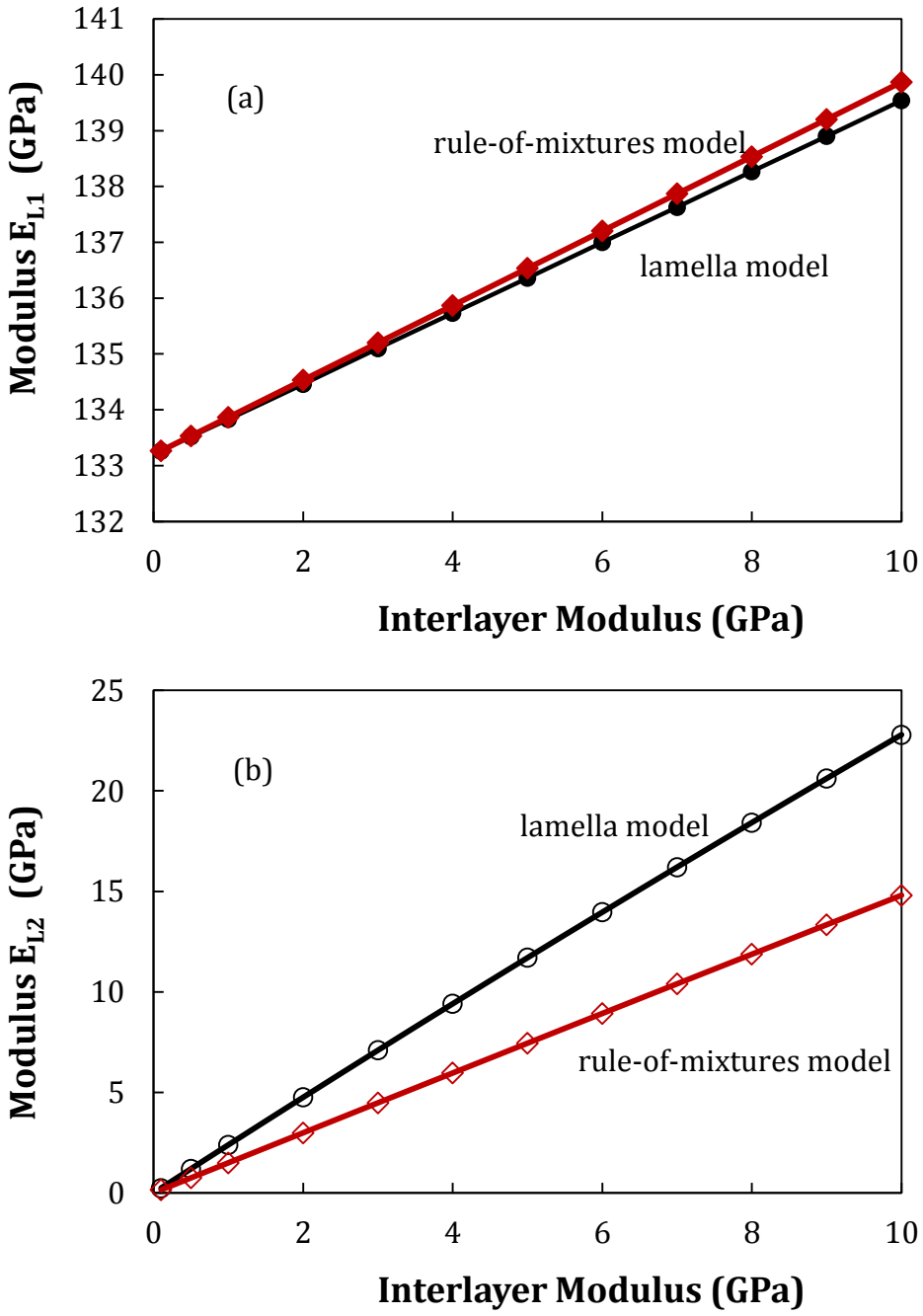

Figure 3.3 Effect of interlayer modulus on the moduli of layered graphenes: a) In-plane modulus E_{L1} and b) Out-of-plane modulus E_{L2}.

Figure. 3.3 shows the effective moduli of the layered graphenes as a function of interlayer modulus. Due to the complex structure (a mixed surfactant modifier molecules and polymer chains), the exact properties of the interlayer are always uncertain. In this study,

the modulus of the interlayer was varied in the range of 0.1GPa-10 GPa, which are typical values for polymeric materials. It is seen that as the interlayer modulus increases, both in-plane modulus and out-of-plane modulus increase. In case (a) the "rule of mixtures" slightly over estimates the in-plane modulus (E_{L1}) as compared to the 2D Arridge lamella model. In case (b) the simple "rule-of-mixtures" solutions underestimate the elastic properties of the out-of-plane modulus (E_{L2}), of the layered graphene stacks as compared to the 2D Arridge lamella model. Figure 3.4 shows the effective moduli of the layered graphenes as a function of interlayer content (interlayer spacing).

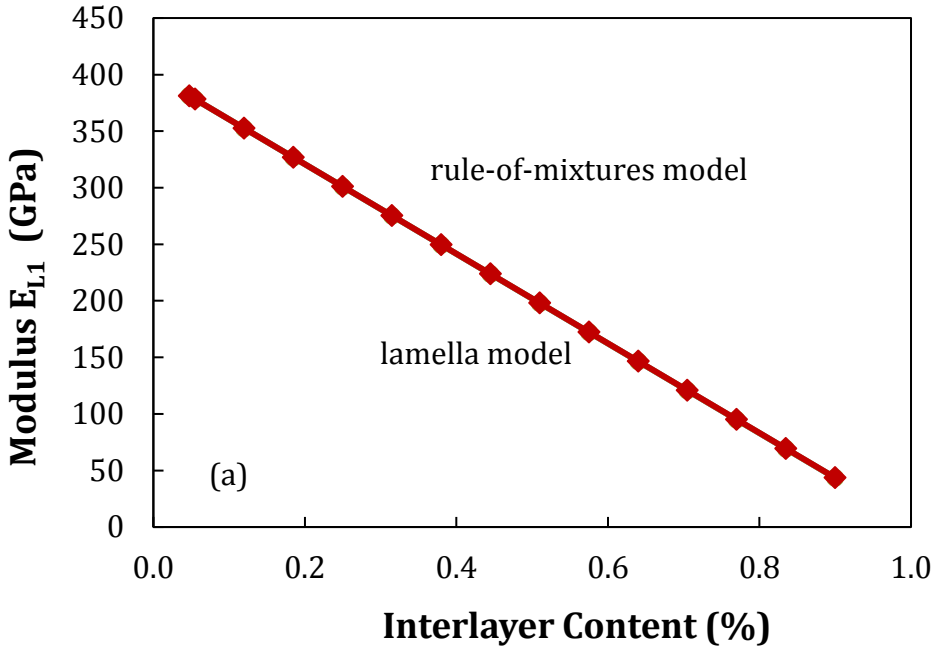

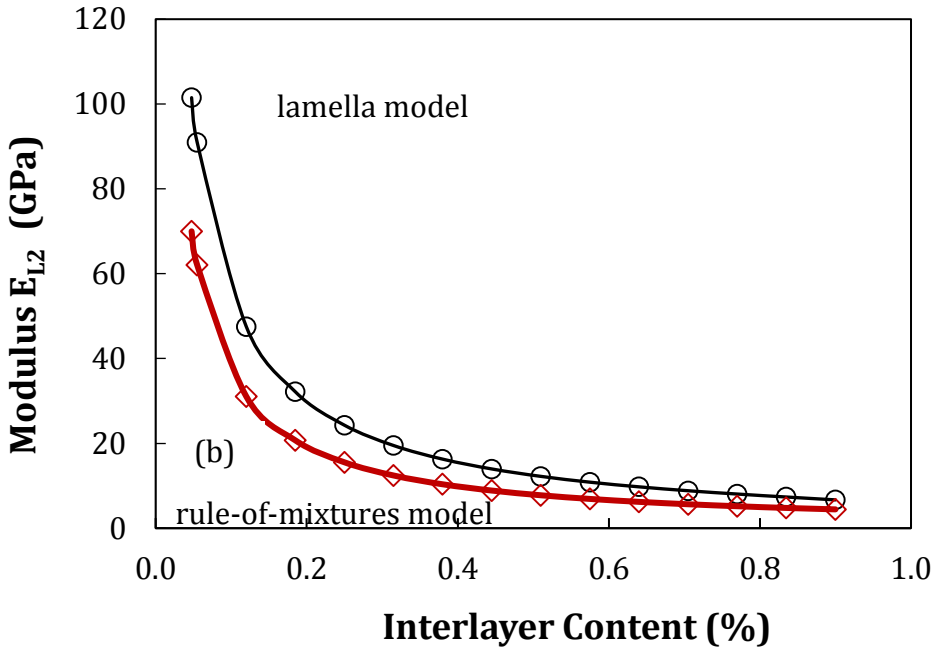

Figure 3.4 Effect of interlayer content on the moduli of layered graphenes: a) In-plane modulus E_{L1} and b) Out-of-plane modulus E_{L2}.

From figure 3.4 it is shown that with the increase of interlayer content between the graphene layers, both in-plane modulus and out-of-plane modulus decrease. Specifically, the in-plane modulus decreases linearly with respect to the interlayer content while the out-of-plane modulus decreases in a more drastic fashion. Again, the simple "rule-of-mixtures" solution has underestimated the out-of-plane modulus (E_{L2}) as compared to the 2D Arridge's lamella model.

3.3.2 Effective elastic moduli of composite with aligned layered graphene

Due to their nano-scale thickness and large surface areas, the 2D, layered fillers often remain in the "intercalated" form in the polymer matrix during the mixing (Even as the filler content is kept very small, a completely exfoliated morphology is still difficult to achieve [20, 30, 31]). These intercalated fillers, as shown in Figure 3.5, act as "effective fillers" in reinforcing the polymer matrix.

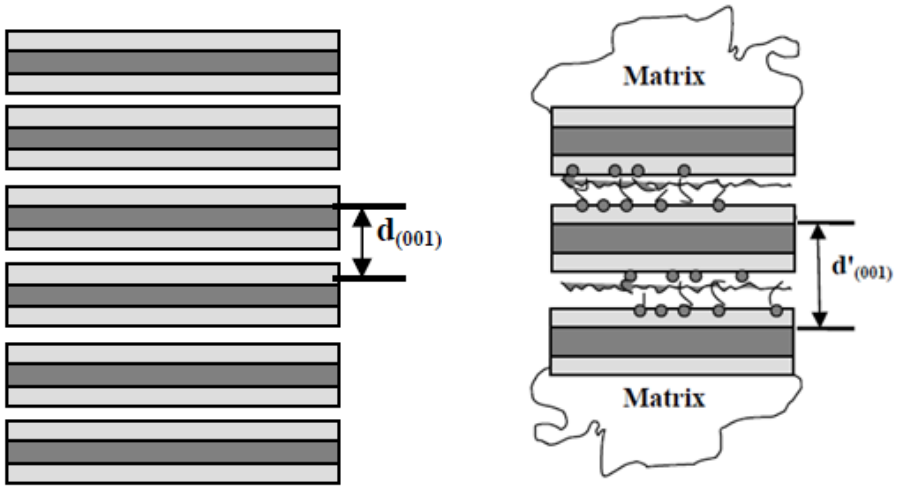

Figure 3.5 Schematic diagram showing the layered graphenes before and after dispersed into a polymer matrix. d (001) and d′(001) denote the d-spacing before and after dispersed into a polymer matrix, respectively.

The effectiveness of those "effective fillers" may be affected by the interlayers in the "intercalated" graphene stacks. The elastic moduli of the layered fillers have been computed in the previous section and are used in this section to estimate the properties of a polymer composite. The polymer system used is the thermosetting epoxy since it is one of the most commonly used polymer systems and its properties are well known: Young's modulus of 4 GPa and Poisson's ratio of 0.3 [19].

Numerous micromechanical models have been proposed to predict the mechanical properties of the fiber/plate composites, including the analytical-based Mori–Tanaka model (exact expressions were provided by Tandon-Weng) and semi-empirical Halpin–Tsai model. Using the effective moduli (E_{L1} and E_{L2}) of the layered graphenes as shown in Figures. 3.2-3.4, the elastic properties of the epoxy-based nanocomposites were estimated. Figures 3.6-3.8 show the elastic moduli of the composites with the aligned layered graphene fillers.

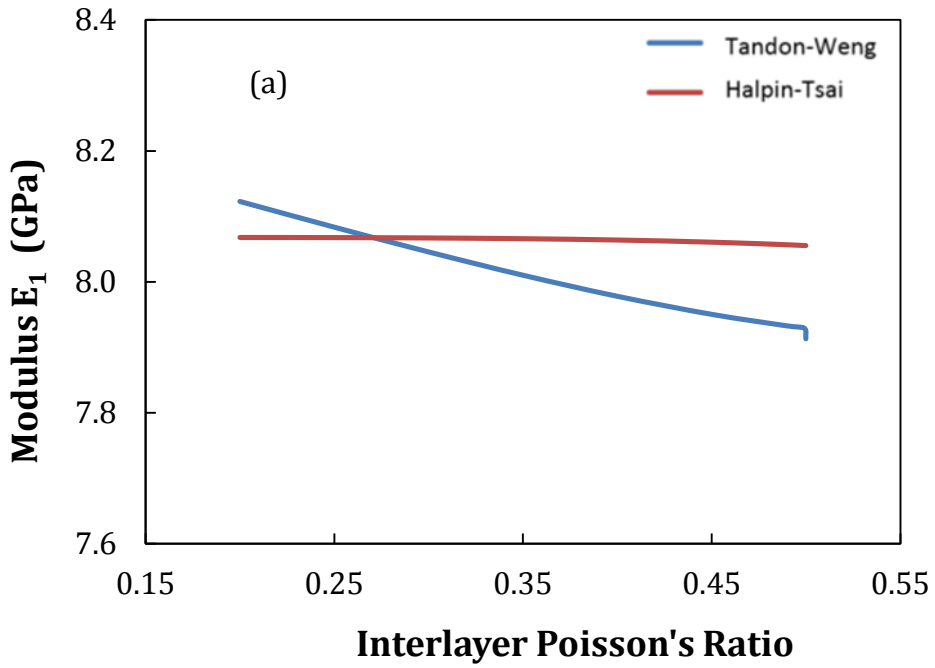

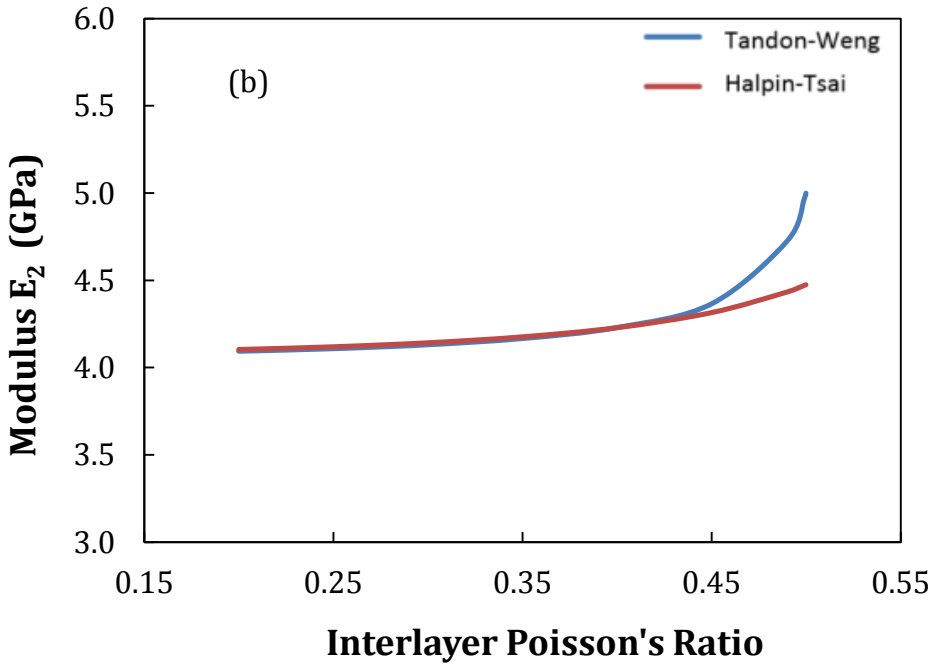

Figure 3.6 Effect of interlayer Poisson's ratio on effective moduli of aligned layered graphene composites, a) longitudinal modulus (E_1) and b) transverse modulus(E_2).

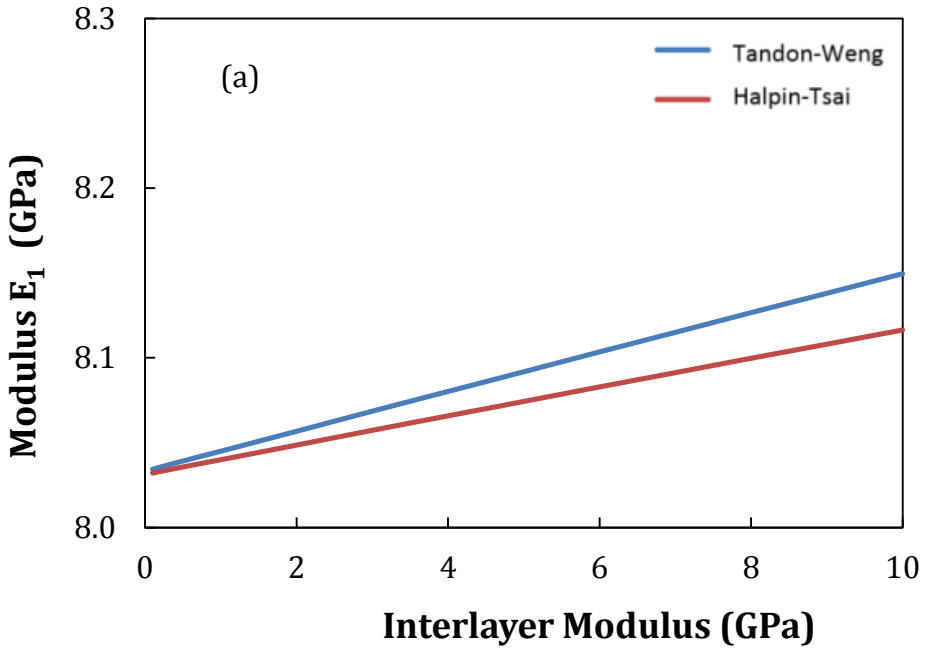

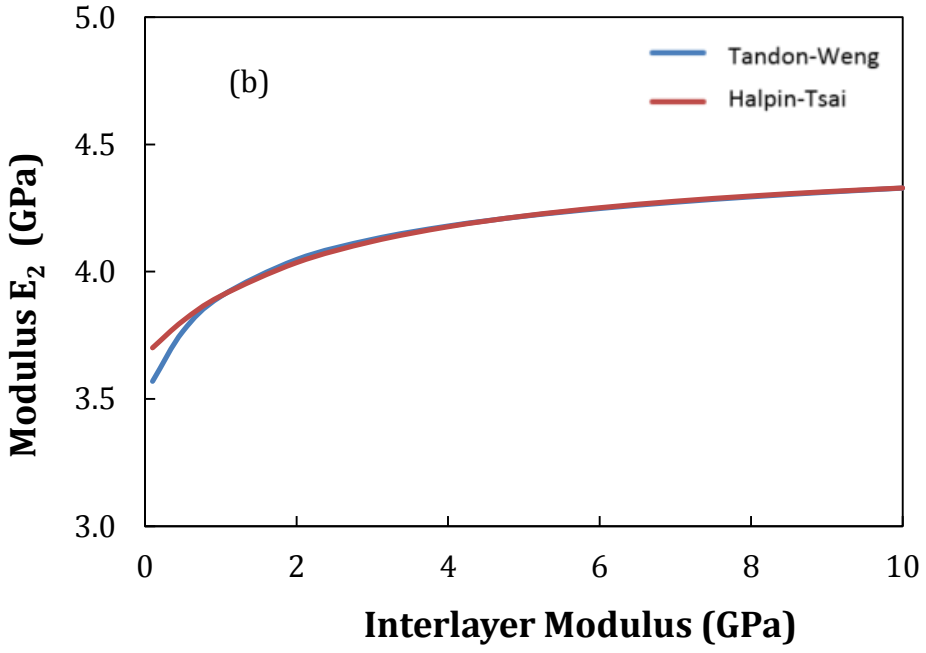

Figure 3.7 Effect of interlayer modulus on effective moduli of aligned layered graphene composites, a) longitudinal modulus (E_1) and b) transverse modulus(E_2).

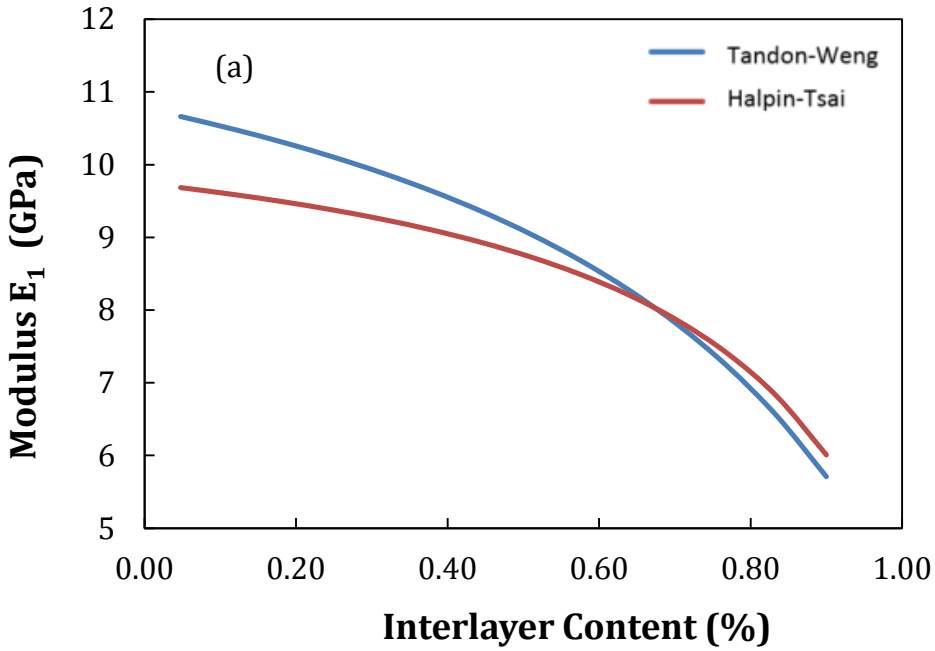

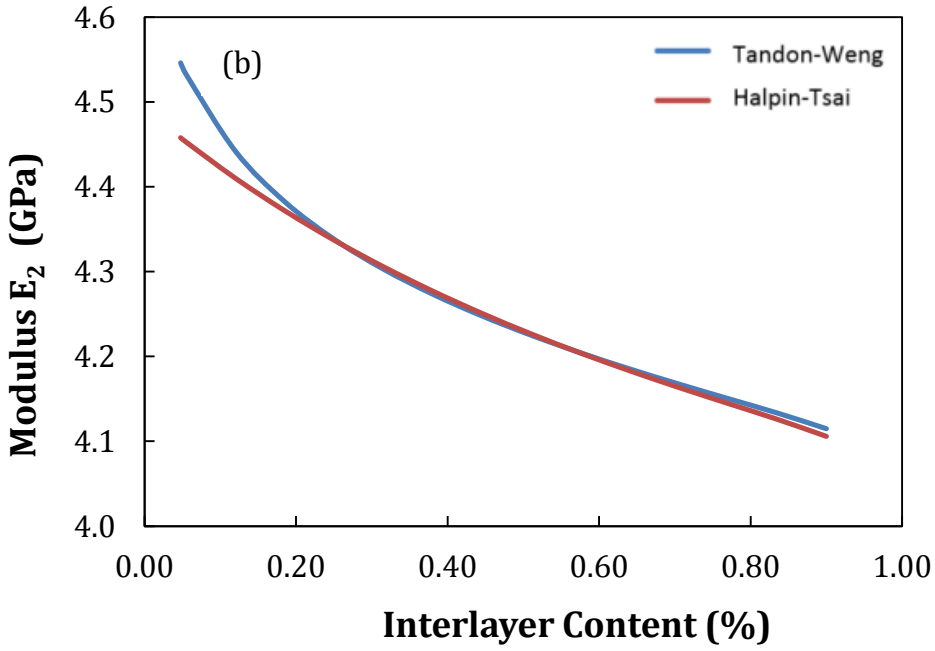

Figure 3.8 Effect of interlayer content on effective moduli of aligned layered graphene composites, a) longitudinal modulus (E_1) and b) transverse modulus (E_2).

It is seen that the results predicted by Tandon-Weng model and Halpin-Tsai model are fairly consistent, except for the case of interlayer Poisson ratio. The Tandon-Weng model predicts that E_1 decreases linearly with ν_i and E_2 increases exponentially with ν_i while the Halpin-Tsai model predicts that both moduli remain almost constant with ν_i. The reason for these discrepancies is that the Halpin-Tsai equations (Eqs. (3.6) and (3.7)) do not consider the lateral deformation (governed by ν) of the reinforcement phases and thus are probably more applicable to one-dimensional fillers, e.g., fiber-type fillers.

Overall, the interlayers in layered graphene fillers are seen to have great influences on the effective moduli of the resultant composites. For longitudinal modulus (E_1), as the Poisson's ratio (ν_i) of the interlayer increases from 0.3 to 0.499, E_1 is reduced by ~5%. When the modulus (E_i) of the interlayer increases from 0.1 GPa to 10 GPa, E_1 is increased by ~5%. If the interlayer spacing is doubled, E_1 can be reduced by more than 30%. For transverse modulus (E_2), as the Poisson's ratio (ν_i) of the interlayer increases from 0.3 to 0.499, E_2 is increased by almost 20%. When the modulus (E_i) of the interlayer increases from 0.1GPa to 10 GPa, E_2 is increased by more than 22%. If the interlayer spacing is doubled, E_2 can be decreased by ~ 5%.

3.3.3 Effective elastic moduli of composite with randomly distributed layered graphene

Figures 3.9-3.11 show the elastic moduli of the composites with randomly distributed layered graphene fillers.

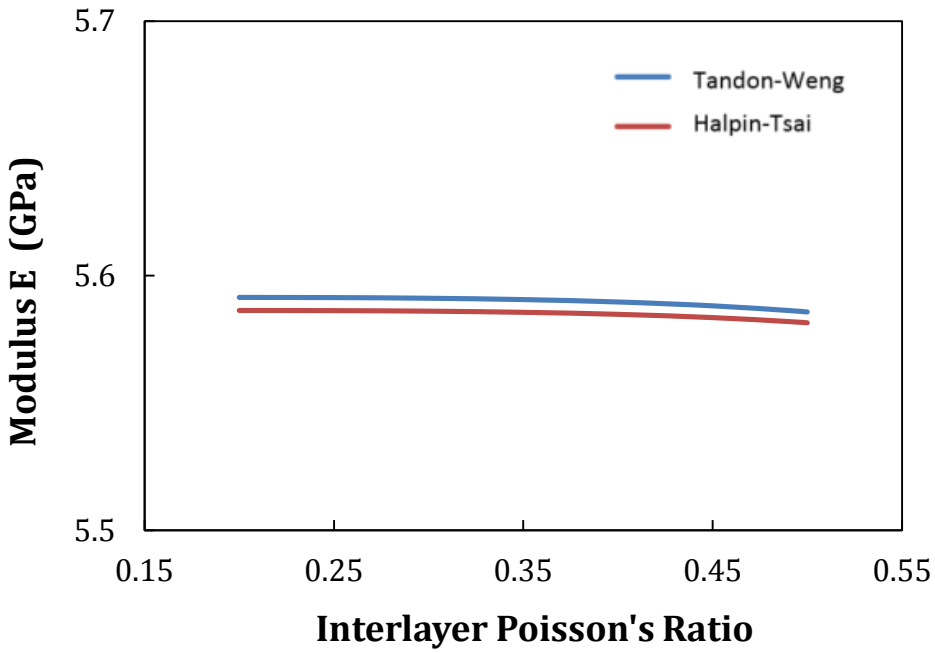

Figure 3.9 Effect of interlayer Poisson's ratio on effective modulus of randomly distributed layered graphene composites.

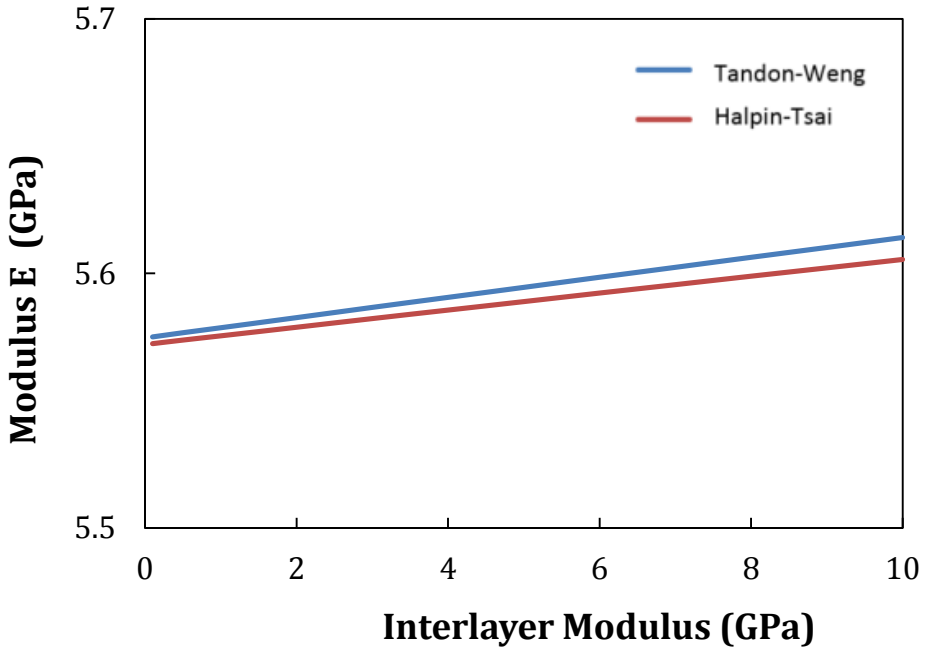

Figure 3.10 Effect of interlayer modulus on effective modulus of randomly distributed layered graphene composites.

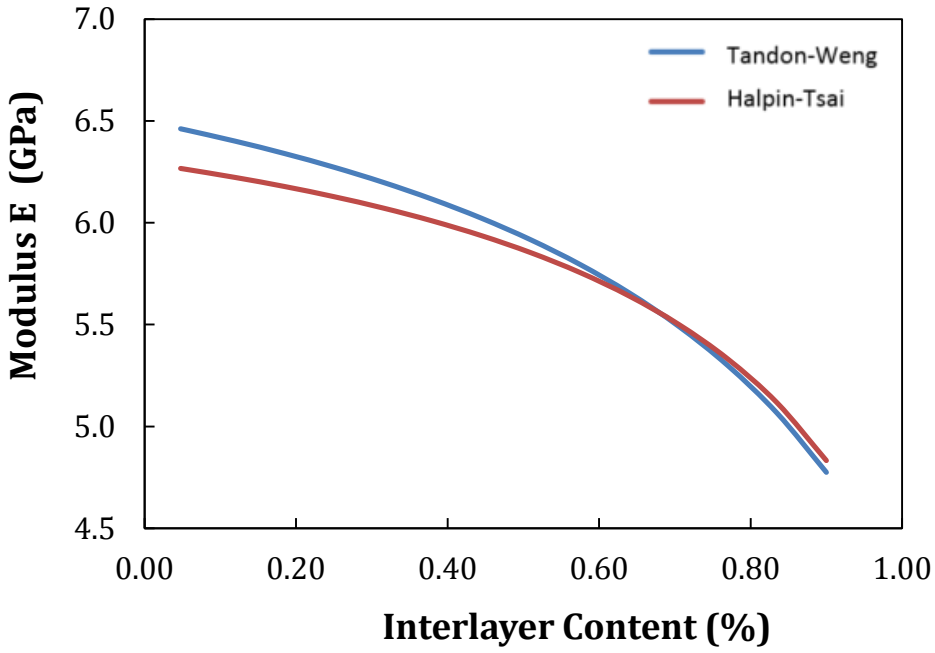

Figure 3.11 Effect of interlayer content on effective modulus of randomly distributed layered graphene composites

In all cases, the Tandon-Weng and the Halpin-Tsai models agree very well. The interlayer properties (modulus and Poisson's ratio) seem to have small or negligible impacts on the property (E) of the composites when the layered graphenes are randomly dispersed into the matrix. However, the interlayer spacing does seem to have a noticeable impact on the modulus of the composites. For example, as the interlayer spacing is doubled, the composite modulus may be reduced by more than 20% (Fig. 3.11).

3.4 Conclusions

Nanocomposites reinforced with two-dimensional, ultra-thin, layered fillers are one of the most important engineering materials that have a wide range of applications. This chapter examines the roles of "interlayers" in the layered fillers on mechanical properties of the composites. The layered graphene fillers and their composites were studied. The effect of interlayers on the effective moduli of layered fillers and their composites were quantified through analytical modeling. As the Poisson's ratio of the interlayer increases, the in-plane

modulus (E_{L1}) of the layered graphenes decreases and the out-of-plane modulus (E_{L2}) of the layered graphenes increases. Both E_{L1} and E_{L2} increase with the increase of the interlayer modulus and decrease with the increase of interlayer content between the graphene layers. For composites with aligned fillers, both the interlayer properties (modulus and Poisson's ratio) and geometry (interlayer spacing) greatly affect the mechanical properties of the composites. For composites with randomly distributed fillers, the interlayer properties (modulus and Poisson's ratio) are seen to have minimum impacts on the properties of the composites. However, the interlayer spacing does have a noticeable impact on the properties of the composites.

CHAPTER 4 - EFFECT OF INTERLAYER ON EFFECTIVE MODULI OF LAYERED GRAPHENE-POLYMER NANOCOMPOSITES

4.1 Introduction

Over the last decade, extensive research has been conducted on graphene and graphene-based nanocomposites. However, there is one important issue that has yet to be fully explored: the roles of interlayers in those two-dimensional, layered graphene fillers. The so-called "interlayer" is the materials that lie between individual graphene sheets. These special materials may be either the chemicals and/or solvents that are used to exfoliate the fillers, or the polymer chains that penetrate into the spaces between graphene layers during preparations of the composites, or a mixture of both [14]. The mechanical properties of the interlayer materials are often unknown and the sizes of the interlayers (interlayer spacing) may be also subjected to continuous changes, depending upon the structures of the specific graphene layer and the polymer chains. In this chapter, the roles of interlayers on mechanical properties of layered graphene polymer composites are examined. First, the effective properties of the layered graphene fillers are computed by using the Arridge's 2D lamellar model. Then, the effects of interlayers on mechanical responses of layered graphene polymer nanocomposites are investigated by using the Tandon-Weng model.

4.2 Analysis of fundamental properties of layered graphene

The layered graphene is made up of stacks of closely spaced graphene sheets. Detailed structure of the layered graphene can be revealed by transmission electron microscopy (TEM) and also characterized quantitatively by various methods, including atomic force microscopy [12, 13], X-ray diffraction [42, 43], and Raman spectroscopy [44-45]. For example, with X-ray diffraction the Bragg reflection of the layered graphene structure may be detected, which is shown as a sharp peak in the intensity-angle plot. This peak (2θ)

would be shifted to a smaller angle and become broadened as the number of layers decreases and it is possible to use the Scherrer formula to estimate the number of layers and the spacing of the interlayer [42, 43]. All studies have shown that the graphene sheet has a constant thickness, ~0.34 nm [42, 46, 12, 43, 44]. However the thickness (spacing) of the interlayer between graphene sheets can be varied, depending up the exfoliation methods of the graphene as well as the dimensions of the polymer coils. It is accepted that the minimum separation of the graphene sheets is larger than the size of the graphene [14, 47]. In this study, the spacing of the interlayer is varied at 0.34 nm, 1 nm, and 2 nm.

The two-dimensional, layered graphene filler consists of alternating layers (graphene sheets and interlayers) having different physical and mechanical properties. Figure 4.1 shows a SEM image of multiply layers of graphene stacked closely together and a model representing the interlayer and graphene interaction in a stack.

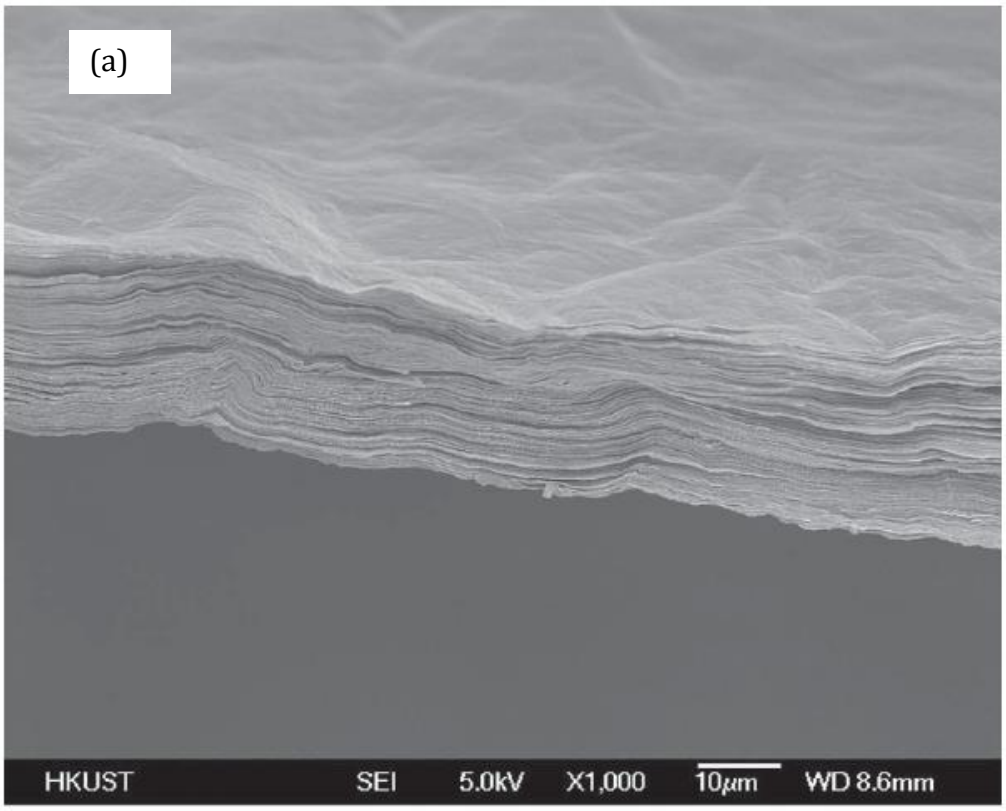

(b)

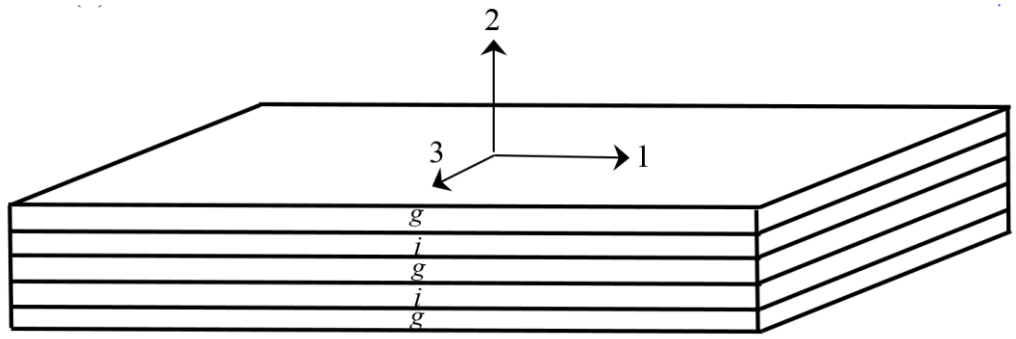

Figure 4.1 (a) SEM image of a layered graphene stack [7] and (b) Model for an effective layered graphene filler.

When those layered fillers are dispersed into a polymer matrix, the polymer coils will intercalate into the interlayers and thus increase the spacing of the interlayers (If the amount of layered graphene fillers is kept to be very small, i.e., <1%, some layered graphene may be partially or completely exfoliated into the polymer matrix [6-9,14, 20]). These layered graphene stacks are considered to be the "effective" reinforcement fillers and the moduli of such structures may be estimated by using the Arridge model, which was originally developed for two-dimensional, layered copolymer lamellas [32].

Take the 1-axis as parallel to the planes of the layered graphene and the 2-axis as perpendicular to the planes of the layered graphene (Figure 4.1). By assuming uniform stress and uniform strain in each layer upon loading, the four fundamental properties of a layered graphene filler can be computed as

$$E_{L1} = V_g E_g + V_i E_i - \frac{V_g V_i E_g E_i (\mu_i - \mu_g)^2}{V_g E_g (\mu_i^2 - 1) + V_i E_i (\mu_g^2 - 1)} \tag{4.1}$$

$$\frac{1}{E_{L2}} = \frac{V_g}{E_g} + \frac{V_i}{E_i} - \frac{2V_g V_i (\mu_g E_i - \mu_i E_g)^2}{E_g E_i [V_g E_g (1-\mu_i) + V_i E_i (1-\mu_g)]} \tag{4.2}$$

$$\frac{1}{G_{L12}} = \frac{V_g}{G_g} + \frac{V_i}{G_i} \tag{4.3}$$

$$\nu_{L12} = -\frac{E_{L1}}{4}\left(\frac{1}{K_L} - S_{33} - 2S_{11} - 2S_{12}\right) \tag{4.4}$$

where E_{L1} is the in-plane Young's modulus, E_{L2} the out-of-plane Young's modulus, G_{L12} the out-of-plane shear modulus, and ν_{L12} the major Poisson ratio. In those equations, "g" stands for graphene layer and "i" stands for interlayer. "V" stands for volume fraction within the layered stack and "μ" stands for Poisson's ratio for the materials within the layered stack. In Eq (4.4), K_L is the bulk modulus and S_{11}, S_{33}, S_{12} are elastic constants whose exact formulas are available in Ref [32].

It is noted that the second terms in Arridge's lamellar model (Eqs (4.1) and (4.2)) are responsible for the lateral deformations in the two-dimensional, layered fillers. For one-dimensional fillers, such as fibers, the lateral deformations can be ignored (μ=0), then the Arridge's model is reduced to the simple "rule-of-mixtures" model [19]: $E_{L1} = V_g E_g + V_i E_i$ and $1/E_{L2} = V_g/E_g + V_i/E_i$.

4.3 Analysis of effective elastic moduli of layered graphene polymer composites

When dispersed into a polymer matrix, the layered stacks remain as the "effective" fillers [48, 49]. The mechanical properties of the layered graphene-polymer composites may be estimated through conventional composite theories. The Tandon-Weng model was chosen in this work because of its effectiveness in predicting stiffness of various types of nanocomposites and their adaptability for "plate-type" filler geometries [10, 34, 50].

The Tandon-Weng equations are a set of analytical solutions to the combined Eshelby's and Mori-Tanaka's theories of inclusion [35-37]. Those expressions allow the predictions of the properties of a composite in terms of properties of polymer matrix and reinforcing fillers together with their proportions and geometry. The elastic moduli of composites with aligned fillers are:

$$E_1 = \frac{E_o}{1 + c(A_1 + 2\nu_o A_2)/A} \tag{4.5}$$

$$E_2 = \frac{E_o}{1 + c[-2\nu_o A_3 + (1-\nu_o)A_4 + (1+\nu_o)A_5 A]/2A} \tag{4.6}$$

$$G_{12} = 1 + \frac{cG_o}{\frac{G_o}{G_{12} - G_o} + 2(1-c)S_{2323}} \tag{4.7}$$

$$K_{23} = \frac{(1+\nu_o)(1-2\nu_o)K_o}{1-\nu_o(1+2\nu_{12}) + c\{2(\nu_{12}-\nu_o)A_3 + [1-\nu_o(1+2\nu_{12})]A_4/A} \tag{4.8}$$

where E_1 and E_2 are the Young's moduli of the composite in 1-axis and 2-axis, respectively. G_{12} is the out-of-plane shear modulus and K_{12} is the plane-strain bulk modulus. c is the volume fraction of the inclusion in the composite. E_0, G_0 and K_0 are Young's modulus, shear modulus, and bulk modulus of the matrix. A and A_1-A_5 are constants that can be directly computed from material and geometrical properties of the filler and the matrix [32].

4.4 Results and discussions

4.4.1 Effective properties of 2D layered graphene fillers

The macroscopic properties of composites are determined by the reinforcement "fillers" and the polymer "matrix". The conventional fillers are mostly one-dimensional structure, isotropic materials with distinctly defined properties (modulus and Poisson's ratio). However, in the case of two-dimensional, ultra-thin, layered fillers, the stiff graphene layers are separated by the soft interlayer materials at varying sizes. As a result, the "layered fillers" are anisotropic and their properties are greatly affected by the properties and geometry of interlayers (Poisson's ratio, modulus, and separation spacing).

Figures 4.2 – 4.5 show the four fundamental properties of layered graphene fillers as a function of the interlayer Poisson's ratio. Those properties were computed by using Arridge's model (Eqs. (4.1)-(4.4)) at three different interlayer spacing: 0.34 nm, 1 nm, and 2 nm.

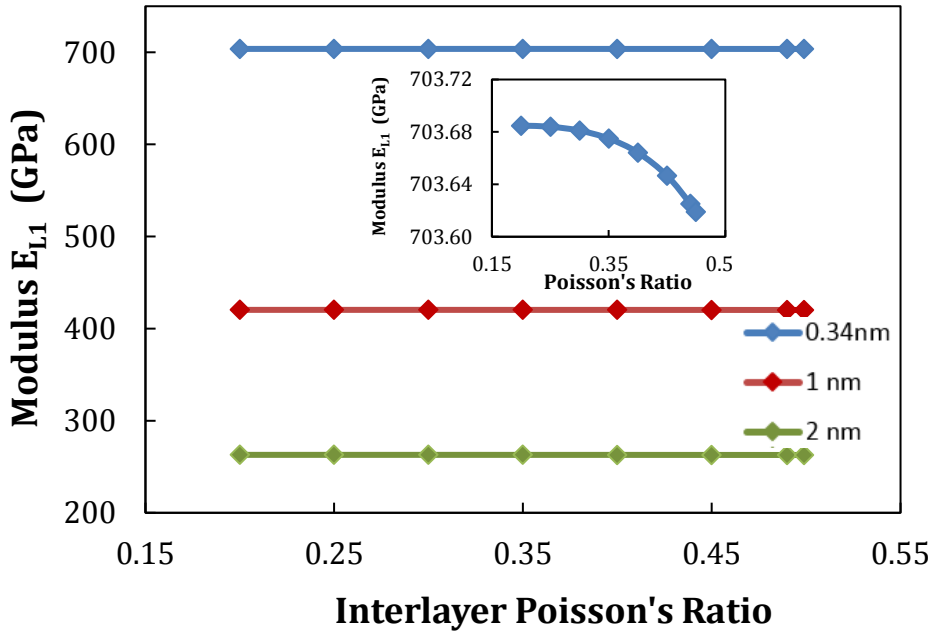

Figure 4.2 Effect of interlayer Poisson's ratio on the modulus of layered graphene filler: In-plane Young's modulus.

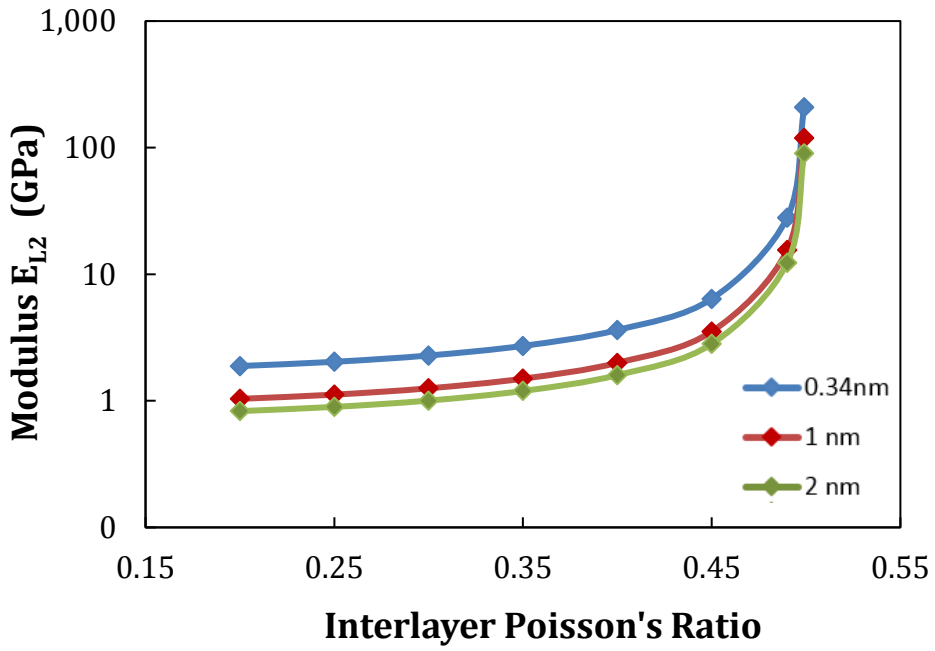

Figure 4.3 Effect of interlayer Poisson's ratio on the modulus of layered graphene filler: Out-of-plane Young's modulus.

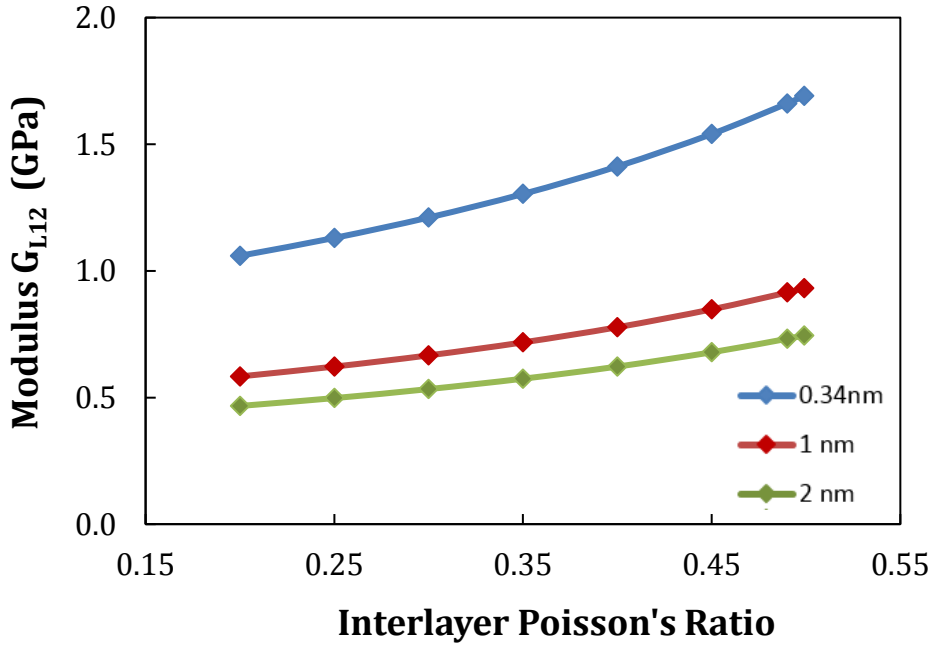

Figure 4.4 Effect of interlayer Poisson's ratio on the modulus of layered graphene filler: Out-of-plane shear modulus.

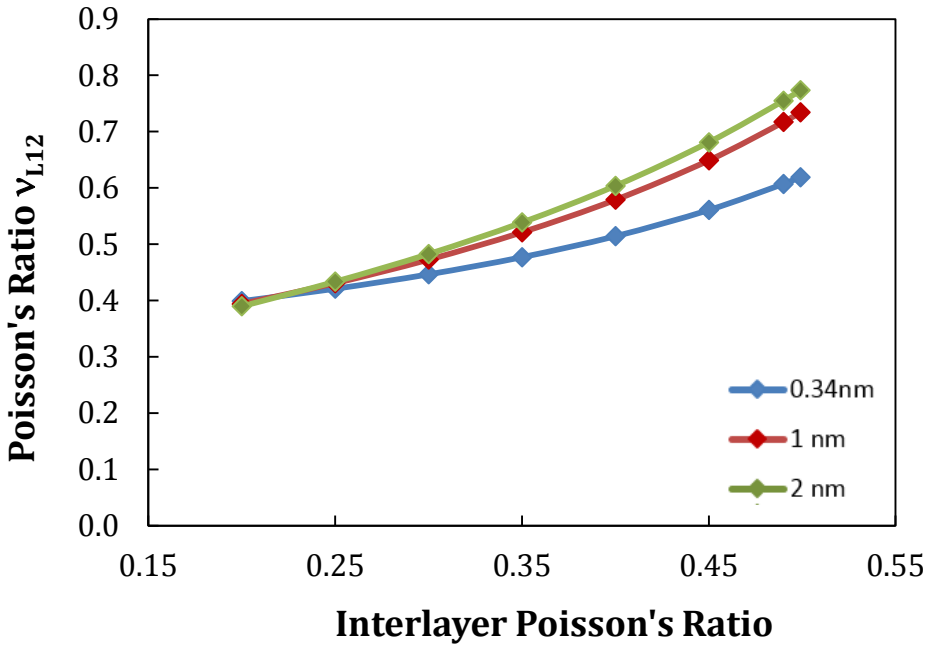

Figure 4.5 Effect of interlayer Poisson's ratio on the modulus of layered graphene filler: Major Poisson's ratio.

It is seen that all properties are affected by the Poisson's ratio of the interlayers. These solutions are derived based on a two-dimensional, thin plate model, as opposed with the one-dimensional "rule-of-mixtures" model which does not take into account of the lateral deflections (as governed by the Poisson's ratio) and thus would predict the constant moduli. According to the Arridge's model, as the Poisson's ratio of the interlayer increases, the out-of-plane modulus (E_{L2}), the out-of-plane shear modulus (G_{L12}), and the major Poisson's ratio (ν_{L12}) of the layered fillers will all increase. The in-plane modulus (E_{L1}) of the fillers does not show significant change by the interlayer Poisson's ratio, since under axial deformation, the loads are predominately carried by the stiff graphene layers.

Figures 4.6-4.9 show the four fundamental properties of the layered graphene filler as a function of interlayer modulus.

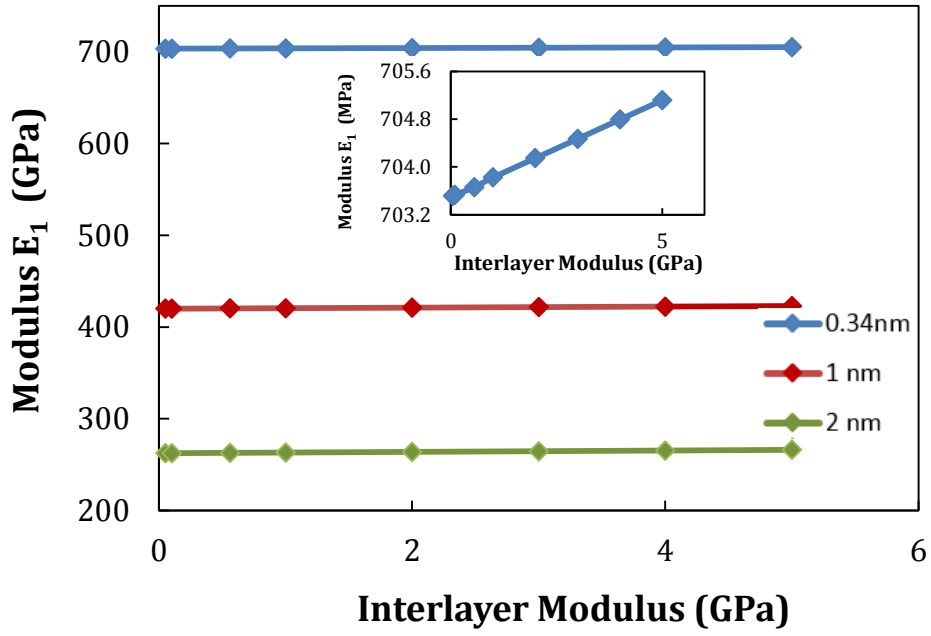

Figure 4.6 Effect of interlayer modulus on the modulus of layered graphene filler: In-plane Young's modulus.

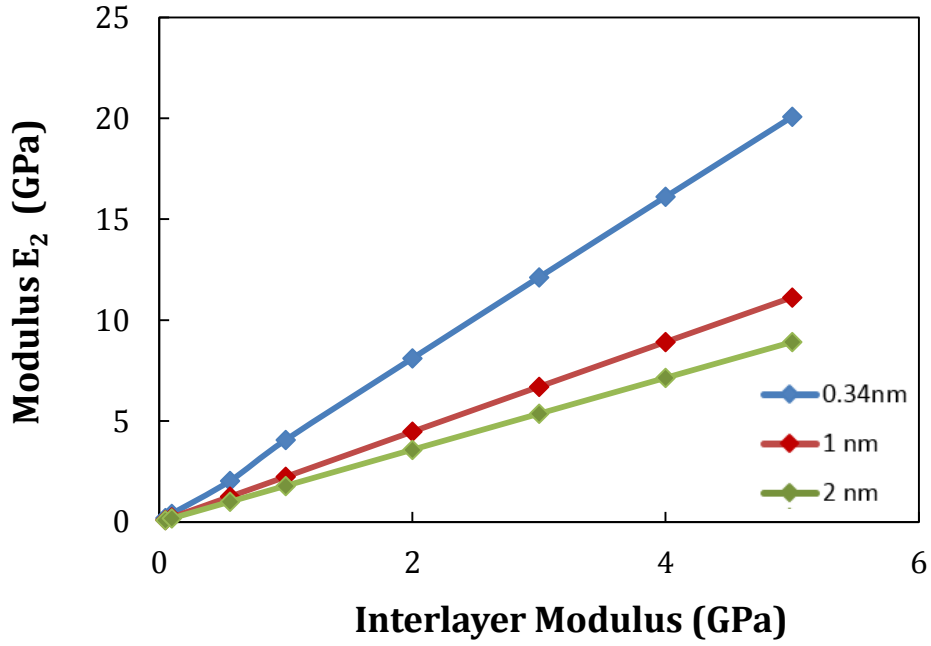

Figure 4.7 Effect of interlayer modulus on the modulus of layered graphene filler: Out-of-plane Young's modulus.

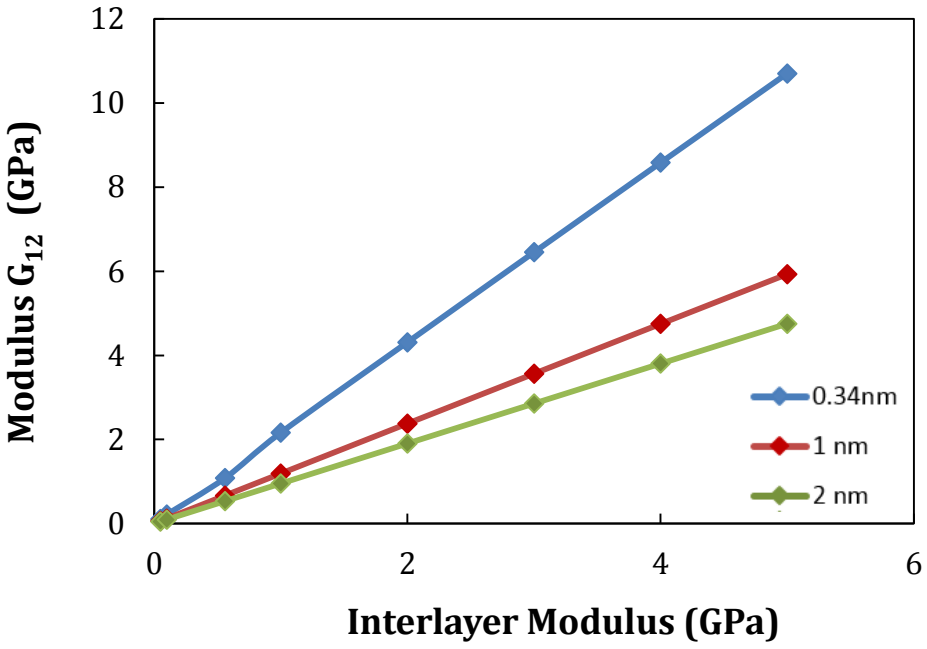

Figure 4.8 Effect of interlayer modulus on the modulus of layered graphene filler: Out-of-plane shear modulus.

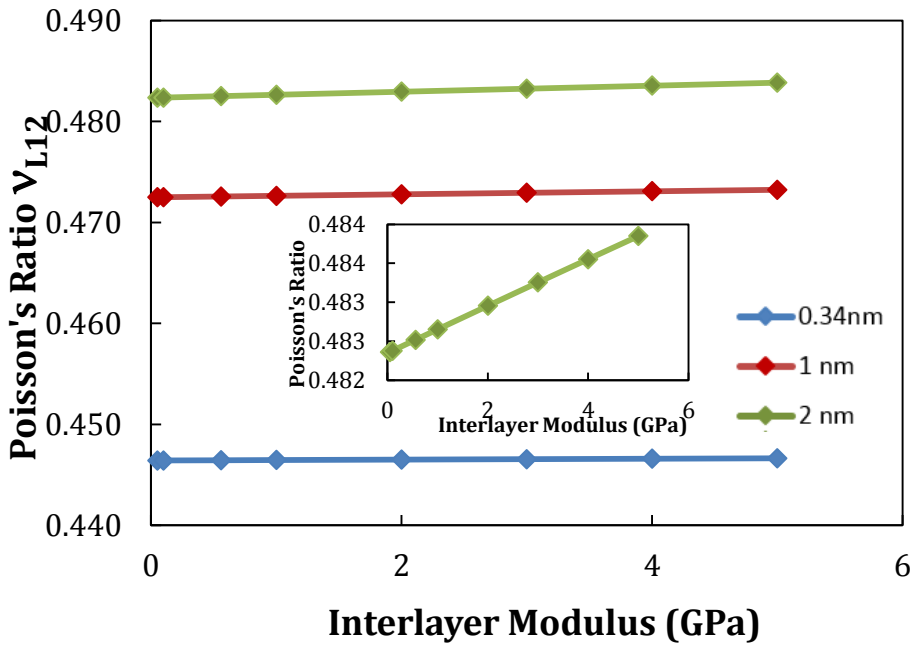

Figure 4.9 Effect of interlayer modulus on the modulus of layered graphene filler: Major Poisson's ratio.

Due to the complex structure (the presences of weak van der Waals bonding and mixture of surfactant modifier molecules and polymer chains), the exact properties of the interlayer are always uncertain. A recent experiment has revealed that the interlayer in the layered graphene structure has a shear modulus in the range of 0.34-0.49 MPa [47]. Based on this, the modulus of the interlayer in this study was varied in the range of 0.01-10 GPa, which represents the modulus of typical polymeric materials. It is seen that as the interlayer modulus increases, all four properties increase, although the changes in in-plane modulus (E_{L1}) and major Poisson's ratio (ν_{L12}) are insignificant. That is again due to the fact that, under axial deformation, the loads are predominately carried by the graphene layers, whose stiffness is almost three orders of magnitude higher than the interlayers.

The above results also reveal that the fundamental properties of the layered filler are greatly affected by the interlayer spacing. As the separation of the interlayer between graphene sheets increases from 0.34 nm to 2 nm, all properties have been decreased significantly. For example, as the interlayer thickness changes from 0.34 nm to 2 nm, all moduli (E_{L1}, E_{L2}, G_{L12}) are reduced by over 60% (Figures 4.2, 4.3, 4.4 and Figures 4.6, 4.7, 4.8). The reduction in modulus is essentially the result of decrease in graphene volume fraction in the layered filler: as the interlayer thickness changes from 0.34 nm to 2 nm, the graphene volume fraction in the effective filler is lowered from 68% to 40%.

4.5 Effective elastic moduli of composite with aligned layered graphene

Due to their nano-scale thickness and large surface areas, the 2D, layered fillers often remain in the "intercalated" form in the polymer matrix during the mixing (Unless the content of the fillers is very low, e.g., <1%, which may result in "fully exfoliated" or "partially exfoliated" morphology [6-9, 14,20]). An intercalated filler is a well-defined spatial volume consisting of both stiff graphene layers and soft interlayers, as seen in the sketch in Figure 4.1. When dispersed into a polymer matrix, these intercalated fillers act as "effective fillers" in reinforcing the polymer matrix. The effectiveness of those "effective

fillers" may be undermined by the presence of weak interlayers in between the graphene layers. The fundamental properties of the "effective fillers" have been computed in the previous section and are used in this section to estimate the properties of the polymer composites. The polymer system used was the thermosetting epoxy since its properties are well known: Young's modulus of 4 GPa and Poisson's ratio of 0.3 [19]. The layered graphene fillers were assumed to be perfectly aligned in the polymer matrix (along 1-axis). The elastic properties of the layered graphene-epoxy nanocomposites were estimated by the Tandon-Weng's composite model, which are solutions to the combined Eshelby's and Mori–Tanaka's inclusion models [32].

Figures 4.10-4.17 show the elastic moduli of the composites as a function of interlayer properties (Poisson's ratio and modulus).

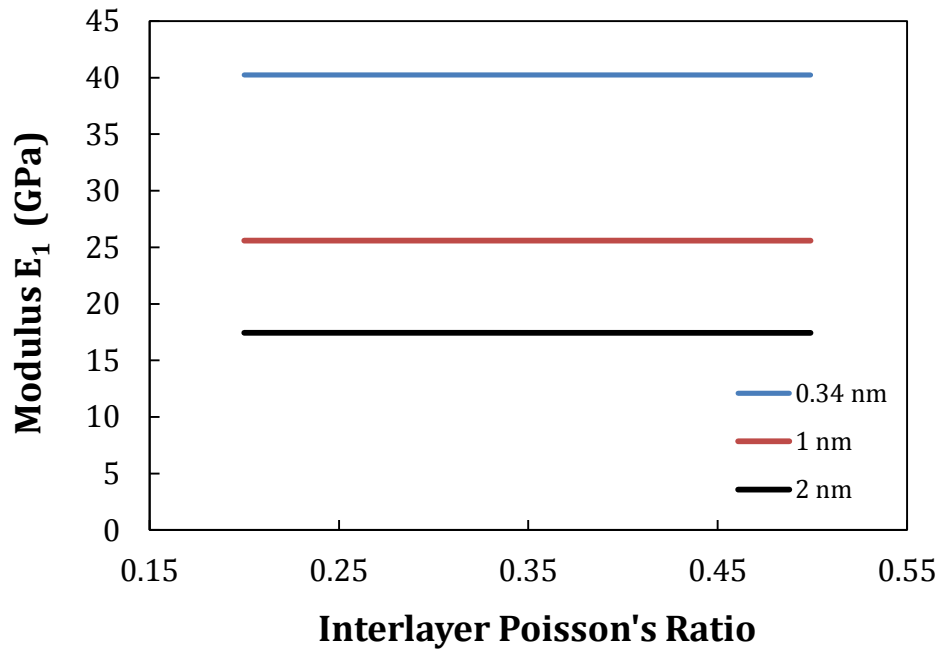

Figure 4.10 Effect of interlayer Poisson's ratio on effective moduli of layer graphene-polymer composites: longitudinal Young's modulus (E_1).

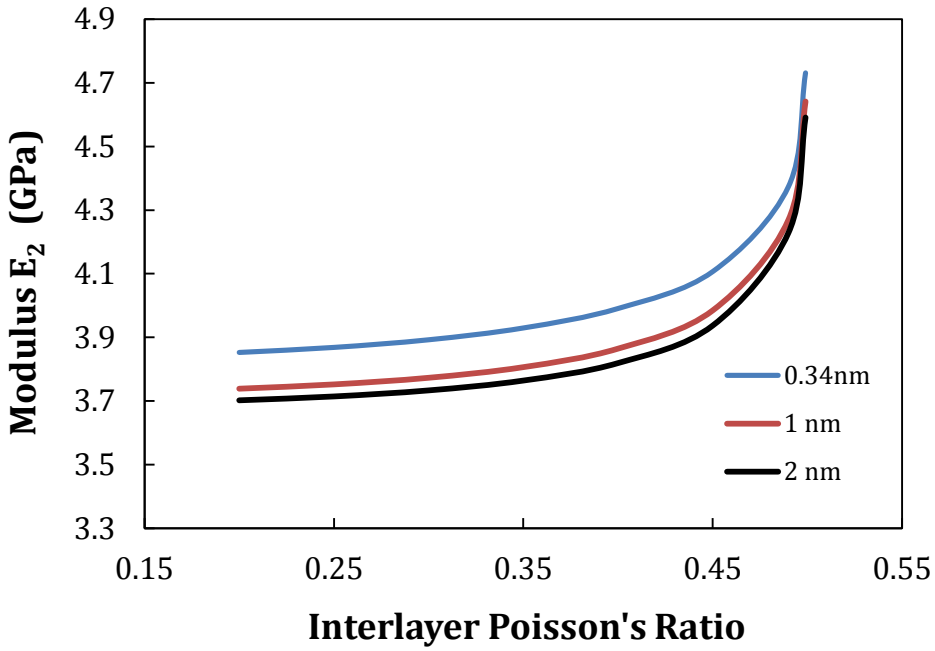

Figure 4.11 Effect of interlayer Poisson's ratio on effective moduli of layer graphene-polymer composites: transverse Young's modulus(E_2).

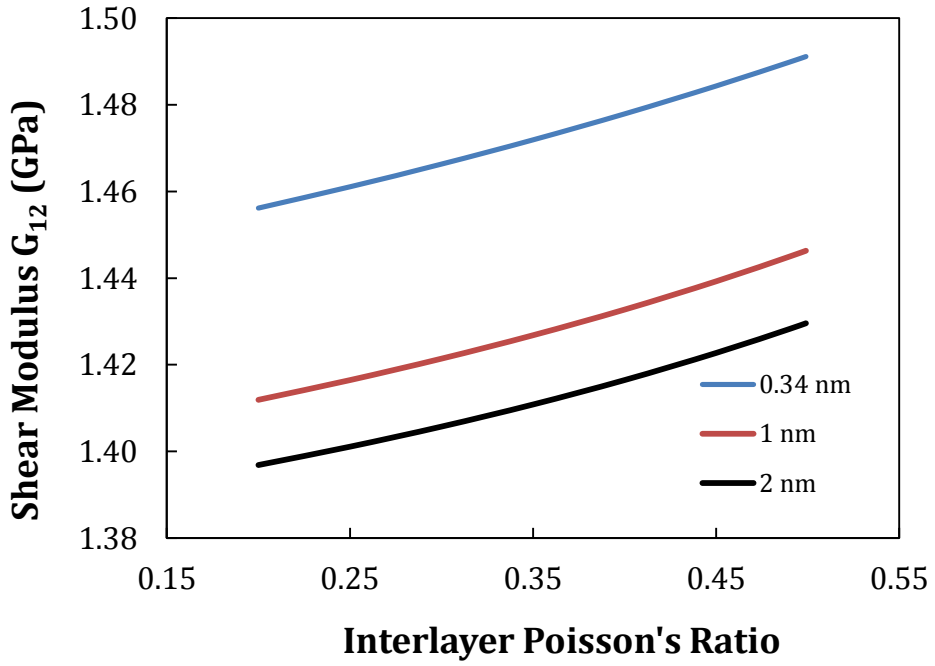

Figure 4.12 Effect of interlayer Poisson's ratio on effective moduli of layer graphene-polymer composites: out-of-plane shear modulus(G_{12}).

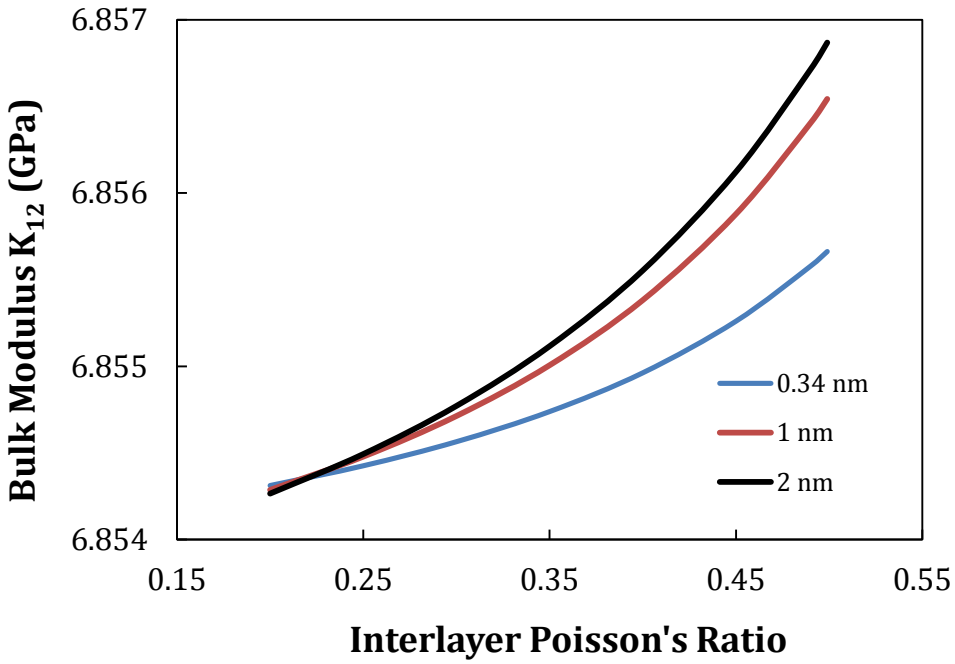

Figure 4.13 Effect of interlayer Poisson's ratio on effective moduli of layer graphene-polymer composites: bulk modulus(K_{12}).

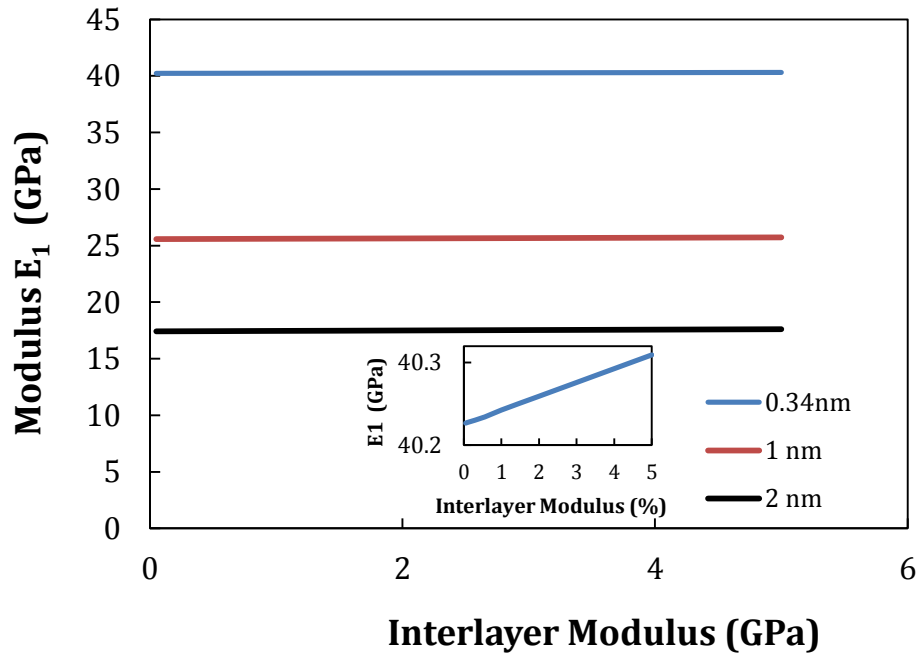

Figure 4.14 Effect of interlayer modulus on effective moduli of layer graphene-polymer composites: longitudinal Young's modulus(E_1).

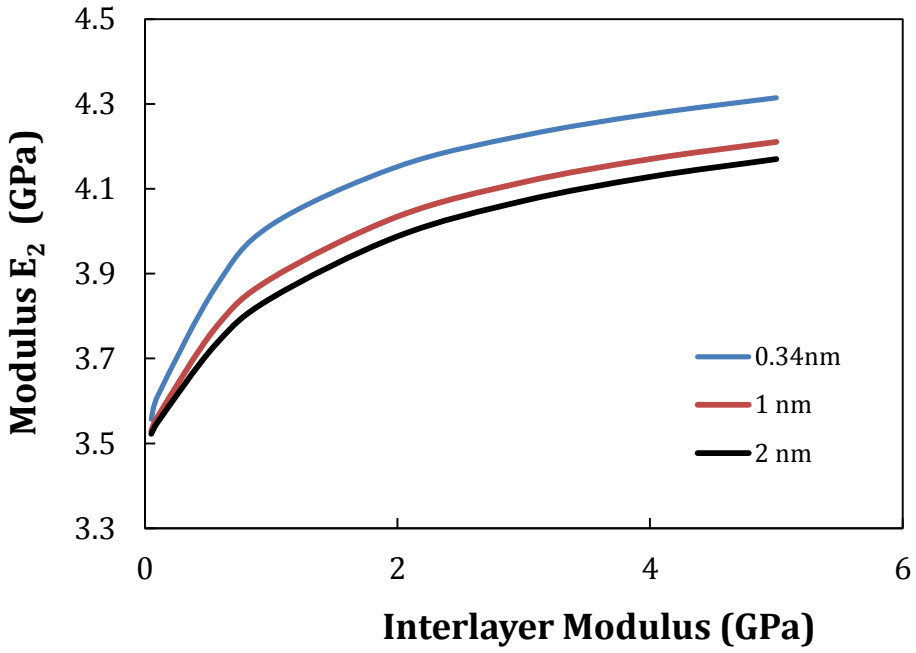

Figure 4.15 Effect of interlayer modulus on effective moduli of layer graphene-polymer composites: transverse Young's modulus(E_2).

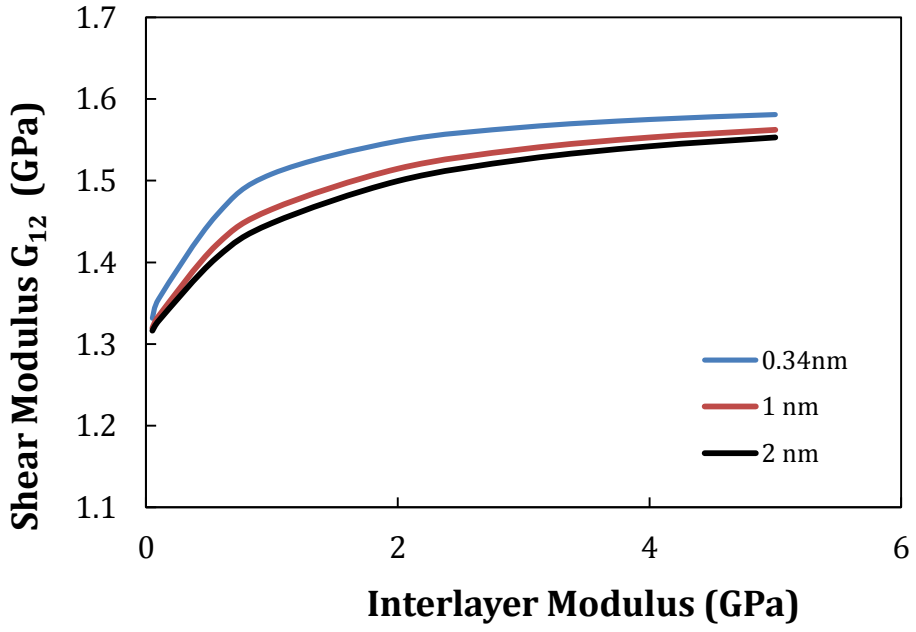

Figure 4.16 Effect of interlayer modulus on effective moduli of layer graphene-polymer composites: out-of-plane shear modulus (G_{12}).

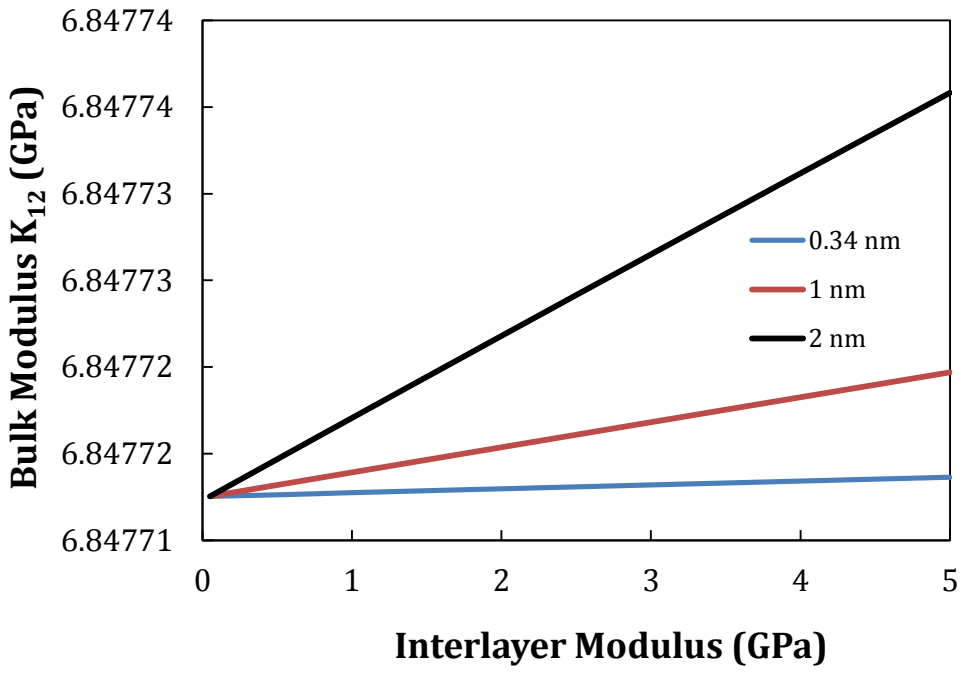

Figure 4.17 Effect of interlayer modulus on effective moduli of layer graphene-polymer composites: bulk modulus (K_{12}).

In all cases, the moduli of the composites are seen to be positively affected by the properties of the interlayers in the layered fillers, particularly the out-of-plane properties (E_2, G_{12}) and the bulk properties (K_{12}). For example, as the interlayer Poisson's ratio increases from 0.2 to 0.499, E_2 and G_{12} are increased by 20% and 5%, respectively (Figures 4.11-4.12). As the interlayer modulus increases from 0.5 GPa to 5 GPa, both E_2 and G_{12} are increased by over 20% (Figures 4.15-4.16). Once again, the in-plane modulus of the composites show minimum changes by the interlayer properties since, when deformed in the axial direction, the stiff graphene layers would carry the majority of the load.

Those results also reveal that the interlayer spacing in layered graphene fillers has great influences on the effective moduli of the polymer composites. As the spacing decreases from 2 nm to 0.34 nm, the longitudinal modulus (E_1) is seen to be increased by up to 52% (Figures 10 and 14) and the out-of-plane modulus (E_2, G_{12}) are increased by over 5% (Figures 4.11, 4.12, 4.15, 4.16).

4.6 Conclusions

Two-dimensional, thin, layered graphene fillers consist of stiff graphene layers and soft interlayers. The mechanical properties of the interlayers are often unknown and the size of the interlayers are dependent upon the molecular structure of polymer matrix and processing conditions of the composites. This chapter has investigated the effect of interlayers on effective moduli of layered graphene polymer composites through analytical modeling. When dispersed into a polymer matrix, the layered graphene stack is treated as an effective filler and the fundamental properties (E_{L1}, E_{L2}, G_{L12}, ν_{L12}) of this effective filler have been computed by Arridge's lamellar model. With the increases of modulus and Poisson's ratio of the interlayer, all four fundamental properties of the filler are increased. The mechanical responses of the layered graphene epoxy composites are further examined by Tandon-Weng's composite model. Results show that the properties of the interlayer affect all elastic properties of the composite, particular the out-of-plane properties (E_2 and G_{12}). Further, the sizes of the interlayer have much greater impact on elastic properties of the composite: with the increase of the interlayer spacing (from 0.34 nm to 2 nm), all properties of the composite have been decreased.

CHAPTER 5 - EFFECT OF INTERLAYER ON INTERFACIAL STRESS TRANSFER OF LAYERED GRAPHENE-POLYMER NANOCOMPOSITES

5.1. Introduction

Nanocomposites reinforced with two-dimensional (2D), thin, layered graphene fillers continue to draw great interest due to their exceptional mechanical and functional properties as well as huge potential applications [6-9,10,14, 20]. However, there is one important issue that has yet to be fully explored: the roles of interlayers in those two-dimensional, layered graphene fillers. The so-called "interlayer" is the materials that lie between individual graphene sheets. These special materials may be either the chemicals and/or solvents that are used to exfoliate the fillers, or the polymer chains that penetrate into the spaces between graphene layers during preparations of the composites, or a mixture of both [14]. The mechanical properties of the interlayer materials are often unknown and the sizes of the interlayers (interlayer spacing) may be also subjected to continuous changes, depending upon the structures of the specific graphene layer and the polymer chains. In this chapter, the roles of interlayers on interfacial stress transfer of layered graphene polymer composites are examined. First, the well-known Shear-Lag theory will produce a bench mark for the finite element model (FEM) procedure. Second, the verified FEM will investigate the effects of interlayers on interfacial stress transfer of layered graphene polymer nanocomposites.

5.2 Analytical shear-lag model for interfacial shear transfer

The Shear-Lag method for composites is a measure of the stress transfer at the interface of a fiber and matrix. The Shear-Lag model is known to be an acceptable approximation for platelet like fibers and is represented in equation 5.1

$$e_f = e_m\left[1-\frac{\cosh\left(ns\frac{x}{l}\right)}{\cosh\left(\frac{ns}{2}\right)}\right] \tag{5.1}$$

Where e_f is the strain in the fiber, e_m is the strain in the matrix, x is the position, l is the length of the fiber, s is the fibers aspect ratio and n represents the reinforcing efficiency shown in equation 5.2.

$$n = \sqrt{\frac{2G_m}{E_f}\left(\frac{t}{T}\right)} \tag{5.2}$$

From equation 5.2 E_f is the Young's modulus for the fiber, G_m is the matrix shear modulus, t is the thickness of the fiber and T is the thickness of the matrix. Equation 5.1 and 5.2 are the last derivations from Shear-Lag's theory of the behavior for a discontinuous filler in a matrix. The behavior of a discontinuous filler in a matrix can be modeled with Shear-Lag theory in which it is assumed that the filler is surrounded by a layer of resin. Figure 5.1 shows the graphene surrounded by resin as modeled for Shear-Lag.

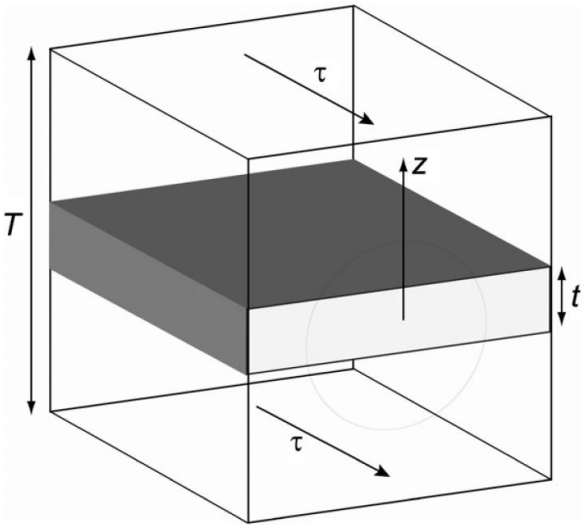

Figure 5.1 Graphene filler surrounded by resin as modeled for shear-lag theory.

From Figure 5.1 T is the total thickness of the composite, Z is the distance from the graphene center to the shear stress τ and t is the thickness of the graphene filler. It is assumed that the filler and the matrix deform elastically and the filler and matrix interface remains intact. For Shear-Lag's theory to work the stress transfer from the matrix to the graphene filler is through shear stress. This allows a relationship between the matrix and the filler to be determined by a force balance of shear forces at the interface. These shear forces help determine the strength of a composite. The product of the reinforcing efficiency n and the aspect ratio s are of great interest when analyzing composites. Figure 5.2 shows the effects of the product of ns as determined by Shear-Lag theory.

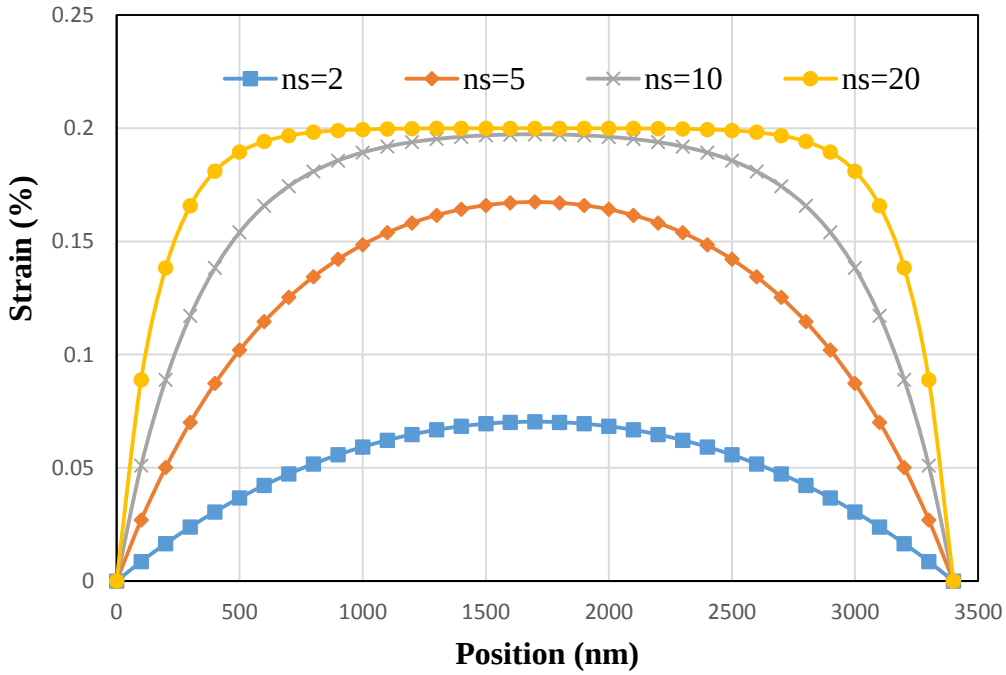

Figure 5.2 Shear-Lag predictions of the importance of the product of ns.

From Figure 5.2 it is shown that the higher the ns value the higher the strain in the composite will be. Having a higher ns value in the shear-lag model shows the dependence of aspect ratio for producing stiffer composites. The higher the aspect ratio in the composite the more effective the fiber carries the load.

5.2.1 Finite element model for interfacial shear transfer

Finite element modeling is a great way to extensively analyze characteristics of various materials as they work together to form a composite regardless of size and shape. Although the typical shape of graphene is rectangular, analytical models for previous filler geometries are not. This makes FEM the best choice for accurately modeling composites composed of graphene fillers for a comparison to conventional analytical theories. The FEM program used to accumulate results for a comparison was ANSYS. In order to accommodate the 2-D Shear-Lag theory for the FEM, shell elements were used for the composite. This allows for more elements across the area while decreasing the computation time and providing accurate results.

5.3. Results and discussions

5.3.1 Comparison of interfacial shear transfer between shear-lag model and FEM: monolayer graphene

The stress transfer between fibers and resin play a major part to how a composite acts under loading conditions. The Shear-Lag model is intended to analyze the stress transfer for one piece or layer of fiber and how it interacts with the resin. The Shear-Lag model is known to make very good approximations under these conditions. However, when fibers are dispersed into a resin the fibers are not always aligned in the same direction and the fibers can stack together. This causes a problem for the Shear-Lag model not accounting for multiple fibers stacked closely together and how that affects the overall composite strength. Knowing that the Shear-Lag model makes very good approximations for monolayer fibers, a base model was created using ANSYS. The model used had graphene fiber properties of 1050 Gpa for the Youngs modulus, .19 as the Poisson's ratio and an aspect ratio of 10,000. The resin material properties were 2.1 Gpa for the Young's modulus and .35 for the Poisson's ratio. The volume fraction of the composite is 10%. Figure 5.3 shows the comparison between the shear-lag model and the FEM.

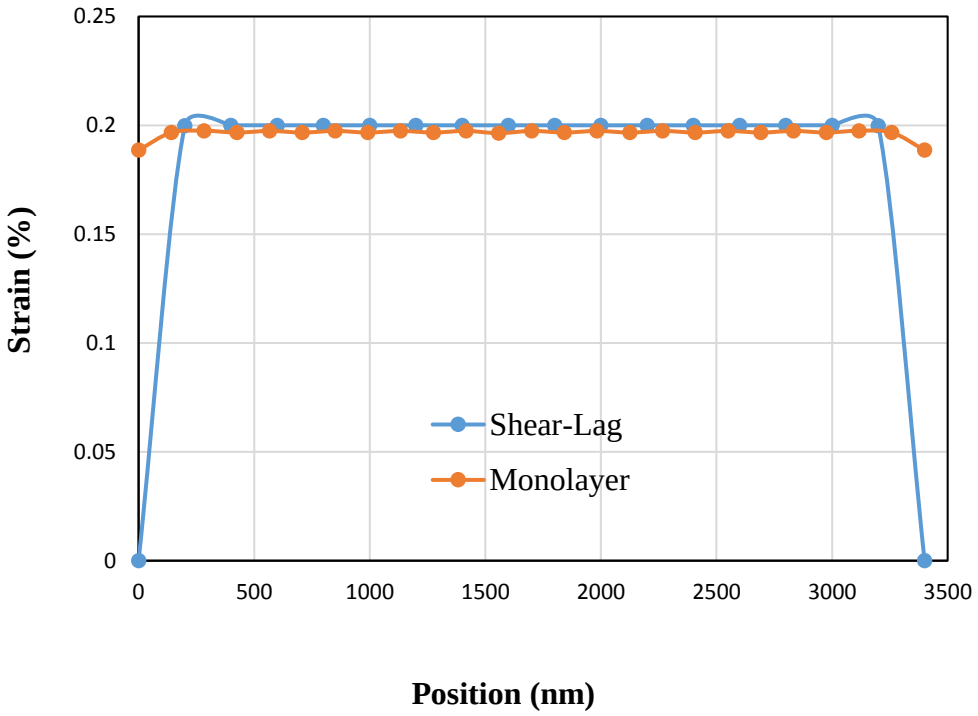

Figure 5.3 Comparison of Monolayer Shear-Lag theory and FEM graphene composite.

The FEM was strained to .2%. The stress from the interlayer section of the FEM was then converted to strain for the comparison to the Shear-Lag model. From figure 5.3 the Shear-Lag model goes to .2% strain while the FEM is just below that at .19% strain. Figure 5.3 shows that the FEM modeling procedure is in good agreement with the well-known Shear-Lag model when producing results. This comparison verifies the preceding procedures for modeling multi-layered graphene stacks in a composite.

5.3.2 Interfacial stress transfer of composite with aligned layered graphene

5.3.2.1 Effect of interlayer modulus

Accurately predicting the characteristics of a composite is an ongoing investigation. There are several ways that a fiber and resin interact to make up the overall strength of a composite. With Shear-Lag and FEM in good agreement for monolayer graphene composites the remaining models will be multi-layered graphene composites. Figure 5.4 shows the FEM with a three-layer stack of graphene and the stress transfer across the center of the graphene filler.

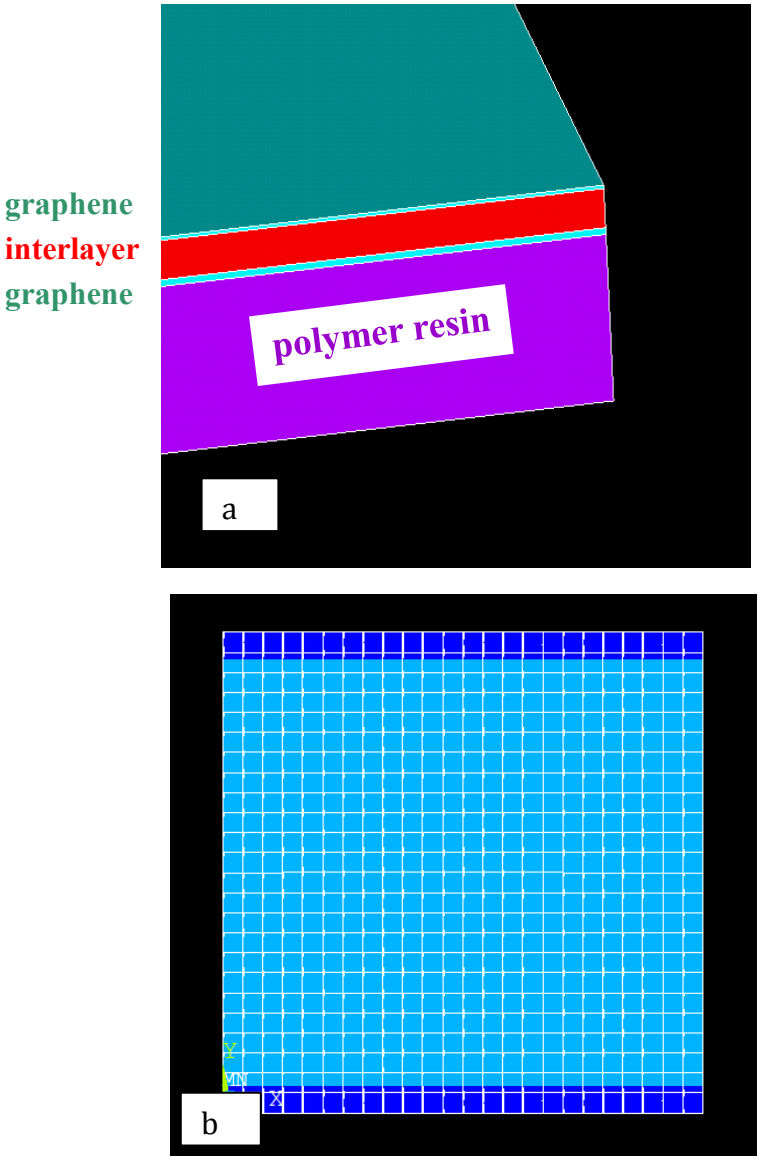

Figure 5.4 Finite element model for a three-layer stack of graphene, a) represents the full model, b) represents the strain results as indicated from ANSYS.

Figure 5.4 a) shows the three-layer stack of graphene as modeled in ANSYS. The reason figure 5.4 a) only shows two fillers of graphene and one layer of interlayer is first, to cut down on computation time and second, to account for the limitations for boundary conditions for wanting to look at interlayer stress transfer regions. The models produced in ANSYS are symmetric models from a full stack of graphene. Like most finite element modeling programs Figure 5.4 b) show the darker regions for less amounts of stress and lighter regions more stress. The following figures show the results for various interlayer material changes. Figures 5.5-5.7 focus on the interaction from the interlayer modulus of elasticity with a varying thickness for a three-layer stack of graphene. The selected modulus of elasticity between each layer of graphene is .01 GPa, .1 GPa, 2.1 GPa and 10 Gpa while the thicknesses are .34 nm, 1 nm and 2 nm. The aspect ratio of graphene is 10,000 with a composite volume fraction of 10%.

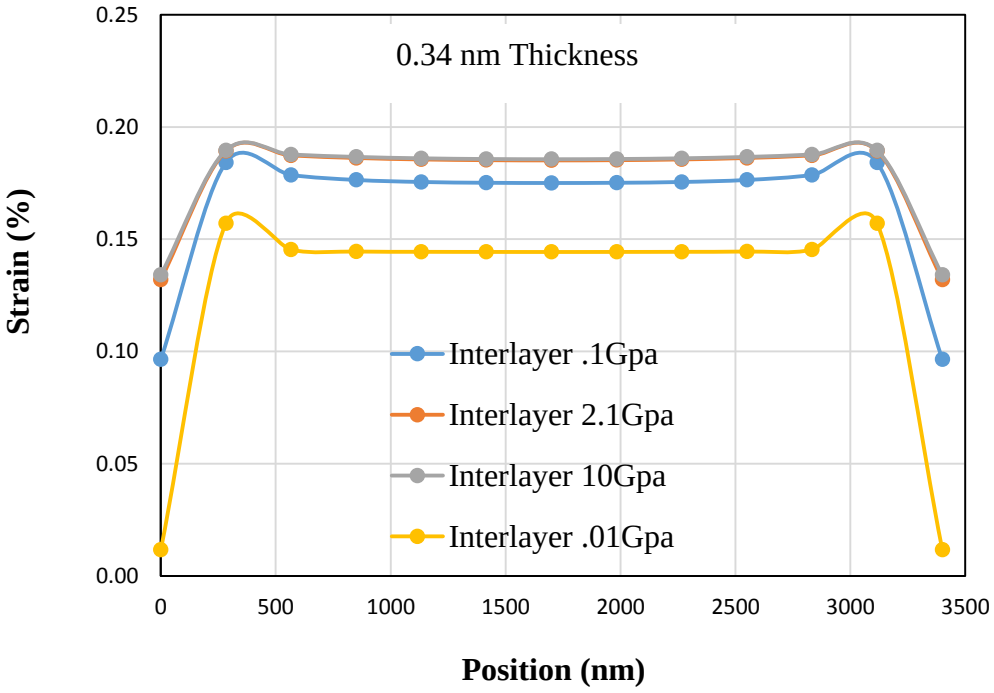

Figure 5.5 FEM with varying interlayer modulus, a .34 nm thickness and graphene aspect ratio of 10,000.

From Figure 5.5 it is seen that lowering the interlayer modulus decreases the overall strain in the composite. The higher interlayer moduli of 10 GPa and 2.1 GPa do not have a large difference at lower strains, but if the modulus continues to drop the overall strength of the composite is reduced. Figure 5.6 shows the effects of increasing the interlayer thickness from .34 nm to 1 nm.

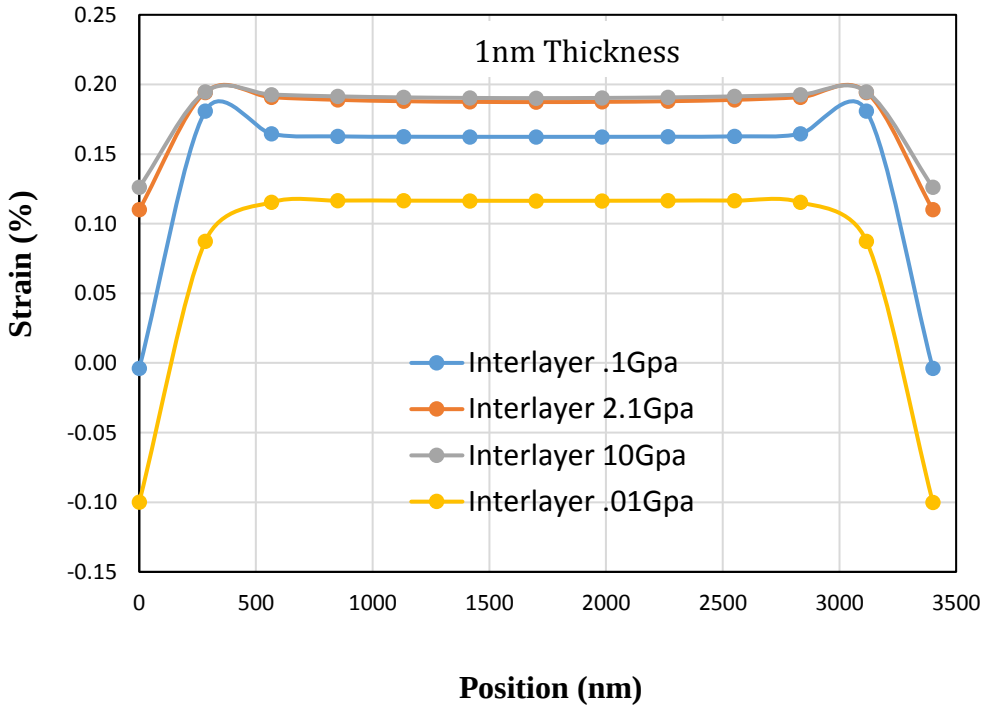

Figure 5.6 FEM with varying interlayer modulus, a 1 nm thickness and a graphene aspect ratio of 10,000.

Increasing the interlayer modulus of the three-layer graphene stack produces different results for a higher modulus and a lower modulus. The higher modulus when increased in interlayer thickness produces higher strains in the composite which produces a weaker overall strength. The lower modulus of .01GPa dropped in strain meaning that the composite has become stronger overall. This is not the case, the .01 GPa interlayer modulus has reached its failure point. This means that the bond between the graphene and the interlayer is now slipping or the delamination effect. One other important note from figure 5.6 is that the lower modulus interlayer is producing negative strains for the composite. This is due to the limited loading

conditions when using shell elements in ANSYS. Figure 5.7 shows the effects of increasing the interlayer thickness to 2 nm with the same interlayer range of modulus.

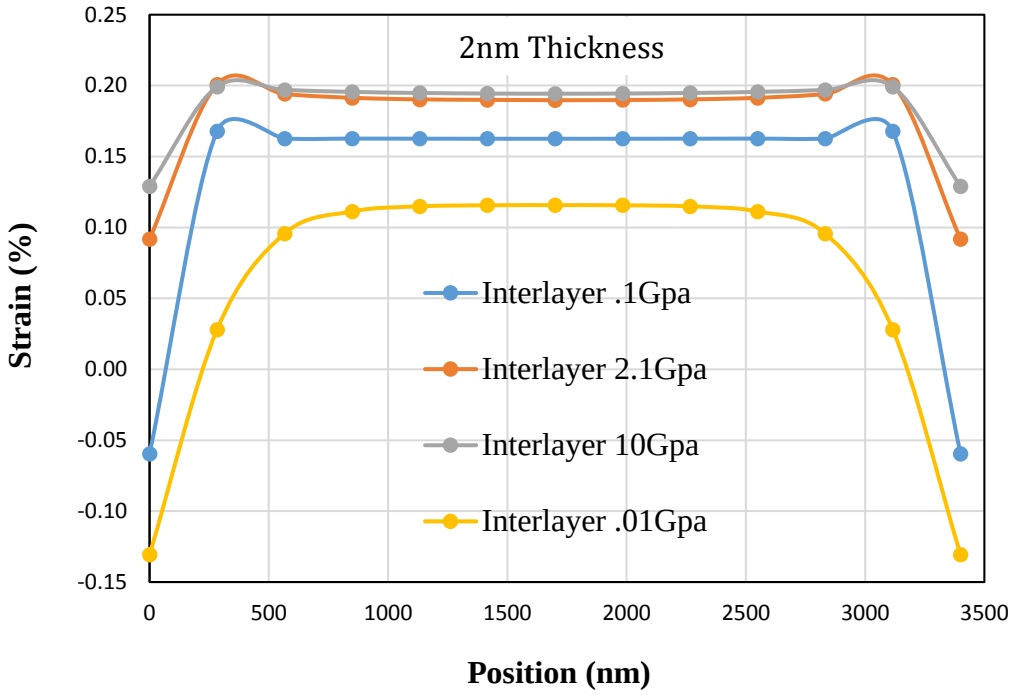

Figure 5.7 FEM with varying interlayer modulus a 2 nm thickness and a graphene aspect ratio of 10,000.

From figure 5.7 the same trend is still present for the high modulus ratios and the lower modulus ratios found in figure 5.6. The 2.1 Gpa interlayer modulus is seen to start reaching its failure limits as it interacts with the graphene fiber.

Graphene is well known to have exceptional ranges of aspect ratios and figures 5.8-5.10 will have a graphene aspect ratio of 35,000 while keeping the volume fraction at 10%. Figures 5.8-5.10 investigates the trend of increasing the interlayer thickness while decreasing the interlayer modulus will produce a weaker composite with a graphene aspect ratio of 35,000. Figure 5.8 shows the effects of a varying interlayer modulus with an interlayer thickness of .34 nm.

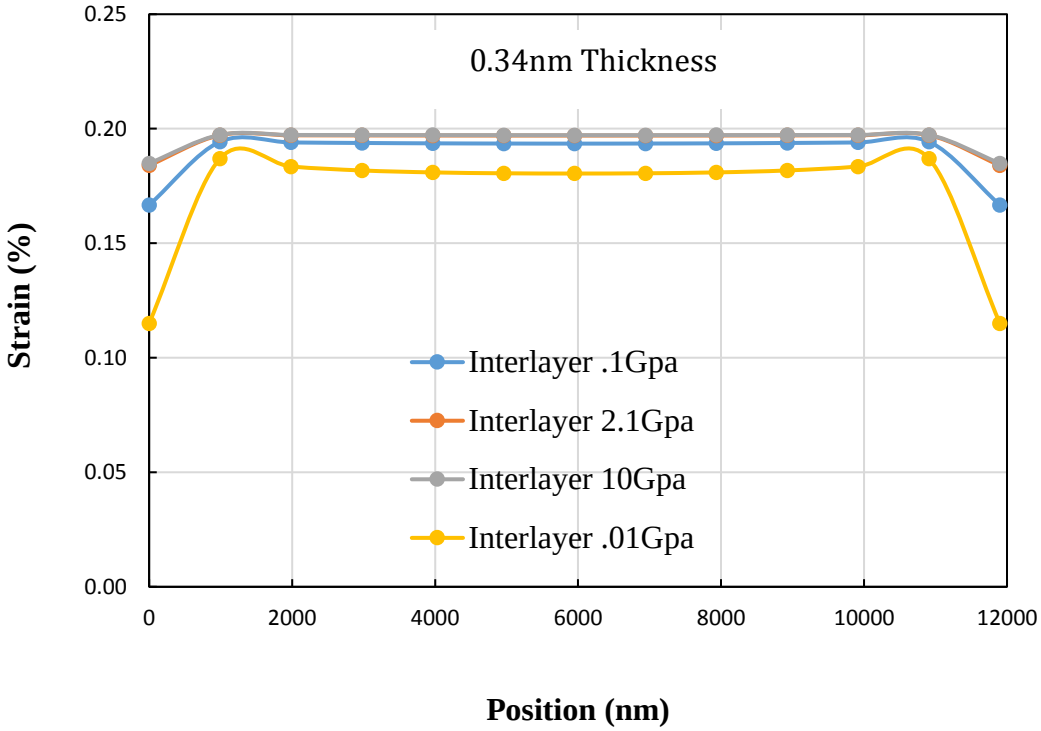

Figure 5.8 FEM with varying interlayer modulus a .34 nm thickness and a graphene aspect ratio of 35,000.

Figure 5.8 shows that increasing the aspect ratio increases the strain in the composite, what is unclear from just figure 5.8 is that the increase in interlayer thickness will decrease the strength in the composite. The FEM for the increased aspect ratio of 35,000 was forced to be larger than the FEM of 10,000. Figure 5.8 will be the starting base for the investigation for the trend as seen in figures 5.5-5.7. Figure 5.9 shows the three layer stack of graphene while increasing the interlayer thickness to 1 nm.

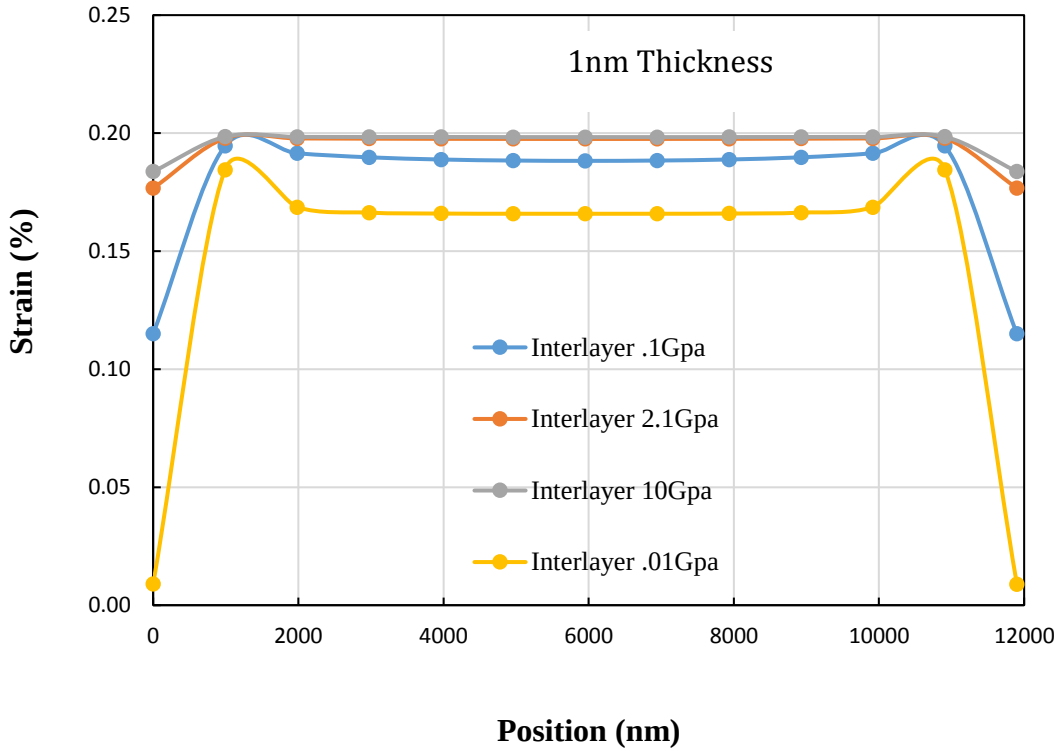

Figure 5.9 FEM with varying interlayer modulus a 1 nm thickness and a graphene aspect ratio of 35,000.

Figure 5.9 starts to show the same trends as figures 5.5-5.7 where the limitations to the FEM loading conditions affect the results based on the delamination between the graphene filler and the interlayer. Increasing the graphene aspect ratio has helped produce a stiffer composite as compared to the graphene aspect ratio of 10,000. The drastic drop in stain from lower interlayer modulus is not as convincing with a higher aspect ratio. Figure 5.10 further increases the interlayer thickness to 2 nm.

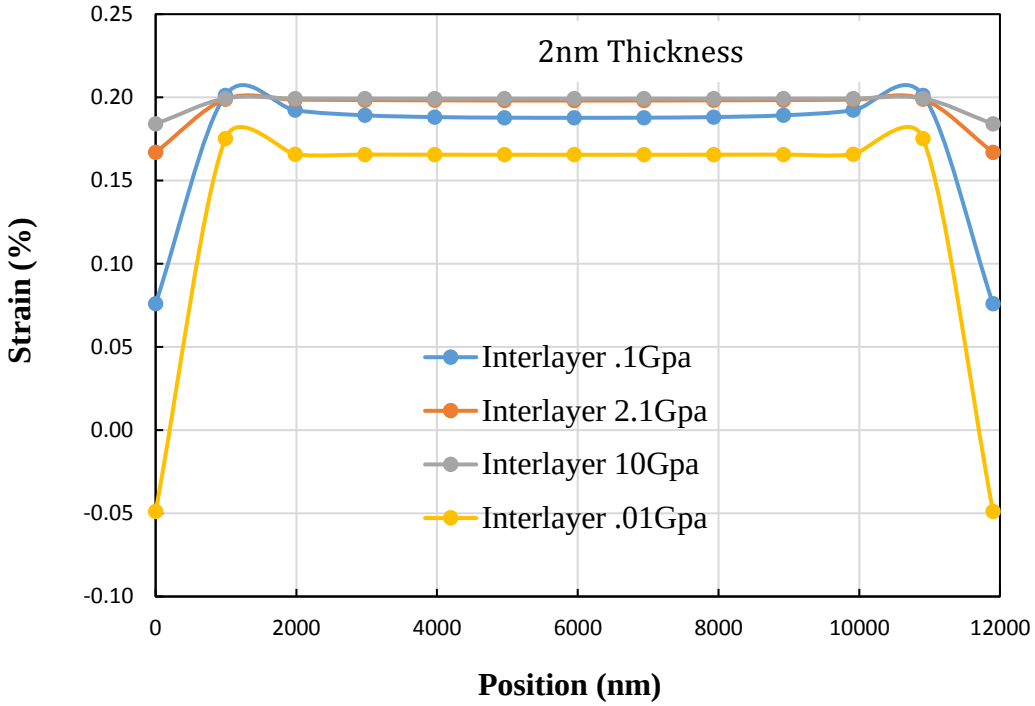

Figure 5.10 FEM with varying interlayer modulus a 2 nm thickness and a graphene aspect ratio of 35,000.

Figure 5.10 confirms the trend of a composite for increasing the interlayer thickness and decreasing the interlayer modulus weakens the composite. Like the trends from figures 5.5-5.7 figures 5.8-5.10 show the same results, however, the larger aspect ratio composite seems to carry the loads better at a lower interlayer modulus.

5.3.2.2 Effect of interlayer Poisson's ratio

The interaction between the fiber and the interlayer can also be affected by the Poisson's ratio. Poisson's ratio is another material characteristic that can affect the overall composite strength. Figures 5.11-5.13 show the effects of varying the interlayer Poisson's ratio while increasing the interlayer thickness. The interlayer Poisson's ratios will be .2, .3 and .49. The thicknesses will vary from .34 nm, 1 nm and 2 nm while keeping the volume fraction and aspect ratio for the composite at 10% and 10,000 respectively.

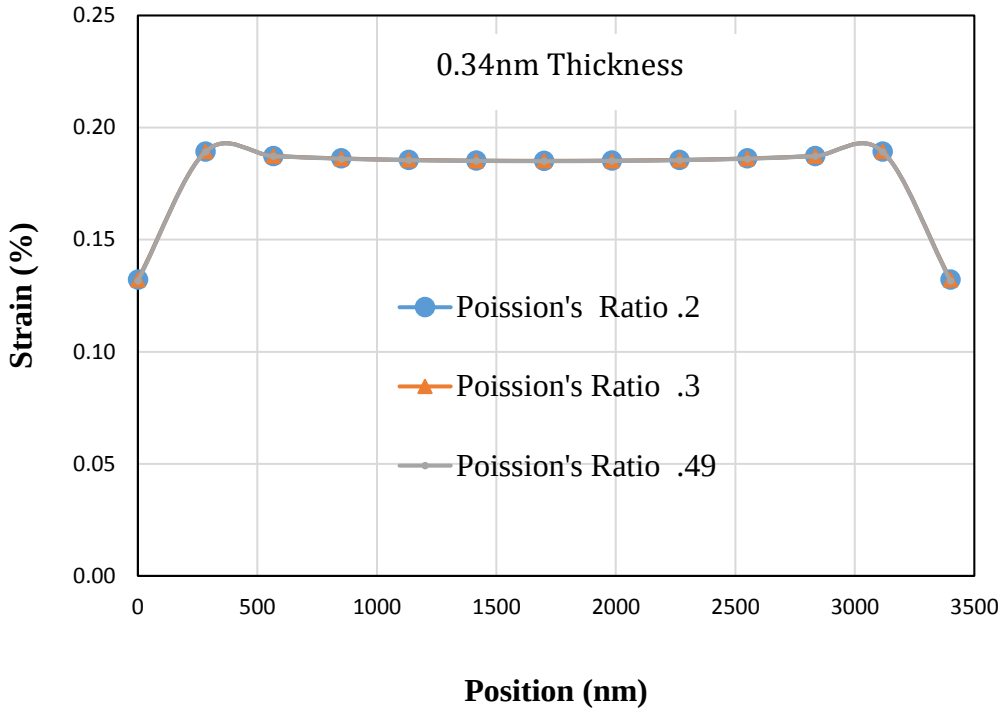

Figure 5.11 FEM with varying interlayer Poisson's ratios an interlayer thickness of .34 nm and a graphene aspect ratio of 10,000.

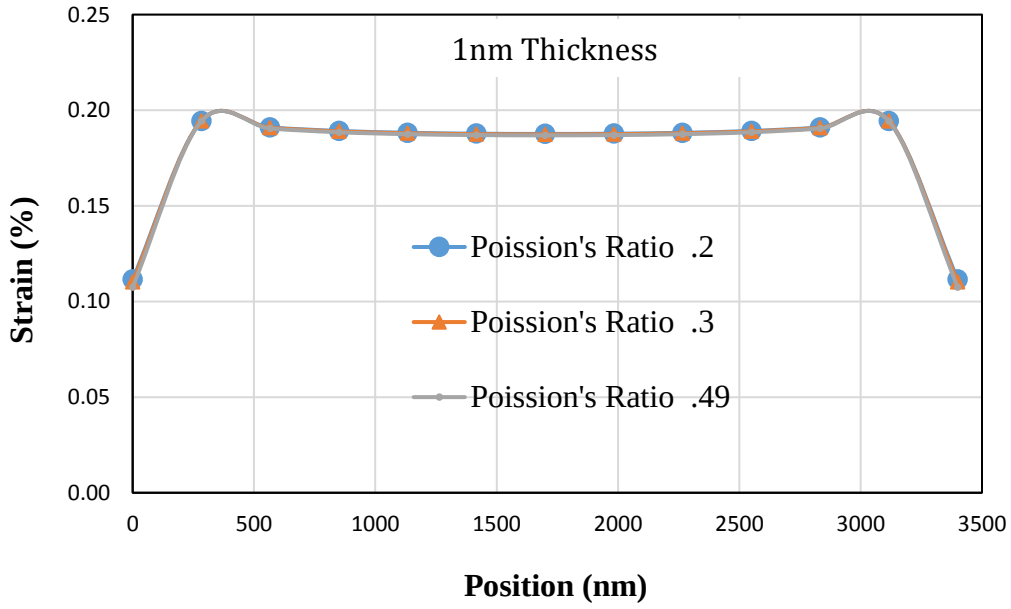

Figure 5.12 FEM with varying interlayer Poisson's ratios an interlayer thickness of 1 nm and a graphene aspect ratio of 10,000.

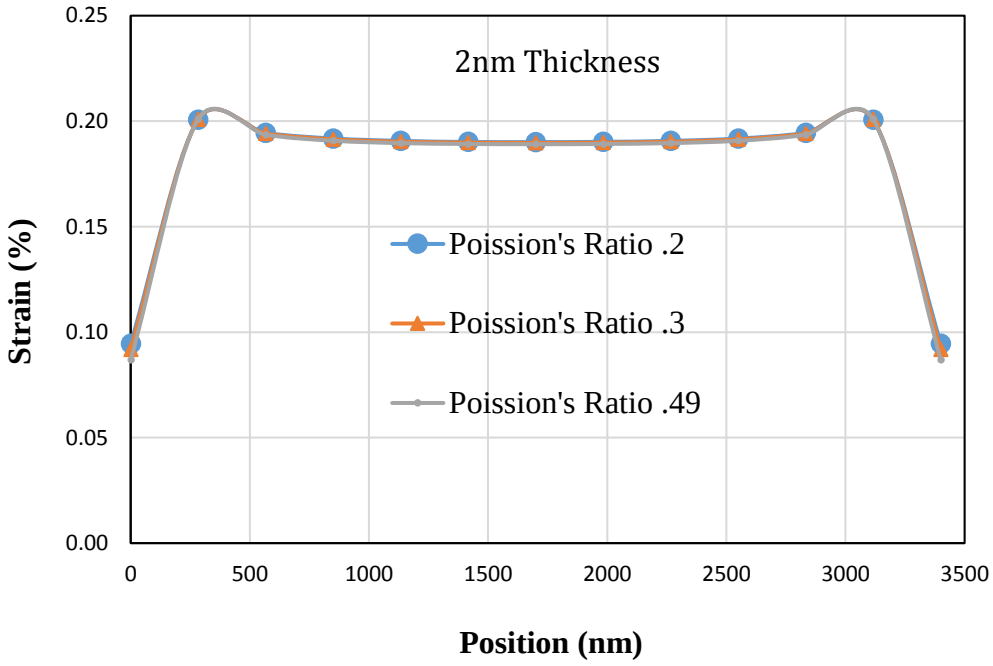

Figure 5.13 FEM with varying interlayer Poisson's ratios an interlayer thickness of 2 nm and a graphene aspect ratio of 10,000.

From figures 5.11-5.13 the interlayer Poisson's ratio does not have a large effect to the overall strength of the composite. What is noticed from the FEM is increasing the interlayer thickness does increase the composite strain for each value of the Poisson's ratio. Due to the increase in strain the composite is weakened for the increased interlayer thickness.

Figures 5.14-5.16 have the same comparison as figures 5.11-5.13, however, the graphene aspect ratio is now increased to 35,000.

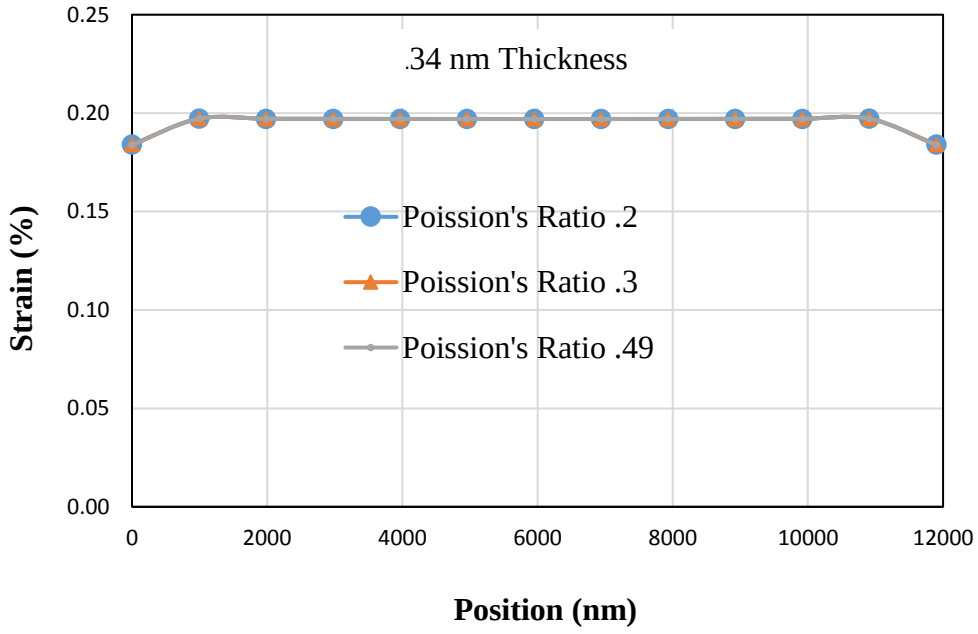

Figure 5.14 FEM with varying interlayer Poisson's ratios with an interlayer thickness of .34 nm and a graphene aspect ratio of 35,000.

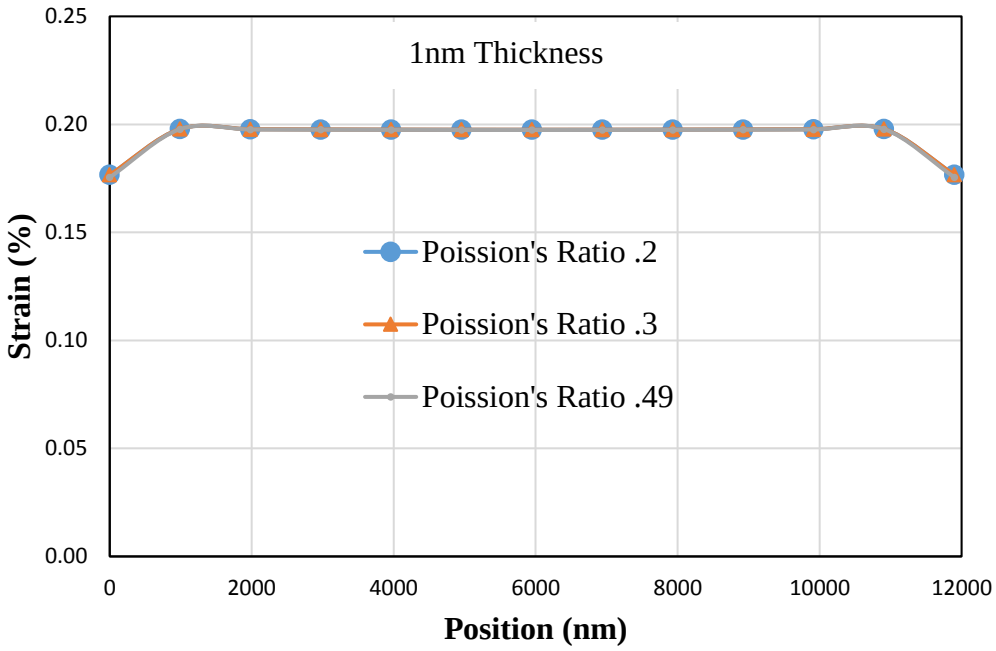

Figure 5.15 FEM with varying interlayer Poisson's ratios with an interlayer thickness of 1 nm and a graphene aspect ratio of 35,000.

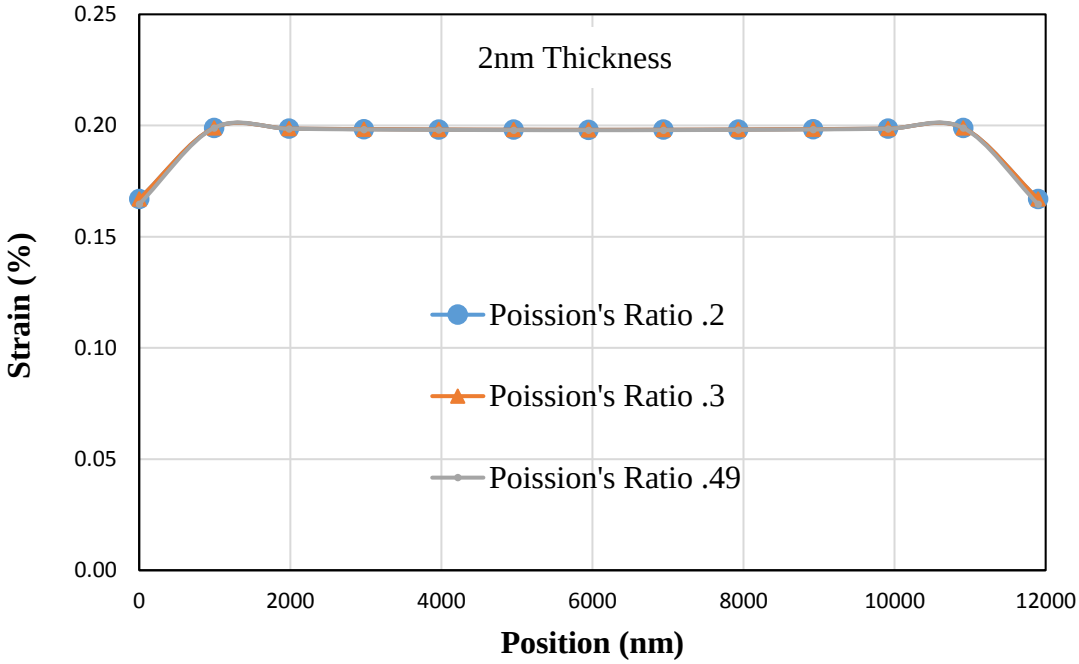

Figure 5.16 FEM with varying interlayer Poisson's ratios with an interlayer thickness of 2 nm and a graphene aspect ratio of 35,000.

Like figures 5.11-5.13 figures 5.14-5.16 show that the interlayer Poisson's ratio has little effect on the overall composite strength. Also, from figures 5.14-5.16 the increase in interlayer thickness decreases the overall composite strength, however, from the figures it is not as easily seen.

5.3.3 Effect of interlayer spacing

The interlayer material characteristics have shown changes in the composite strain. Previous figures have shown increasing or decreasing the interlayer modulus has a large effect to the composite strain. Where as, increasing or decreasing the interlayer Poisson's ratio did not have a large effect. What is noticed from previous figures is increasing the interlayer thickness increases the composite strain. Figure 5.17 shows the FEM prediction

of increasing the interlayer thickness while the aspect ratio of the graphene filler is 10,000 and a volume fraction of 10%.

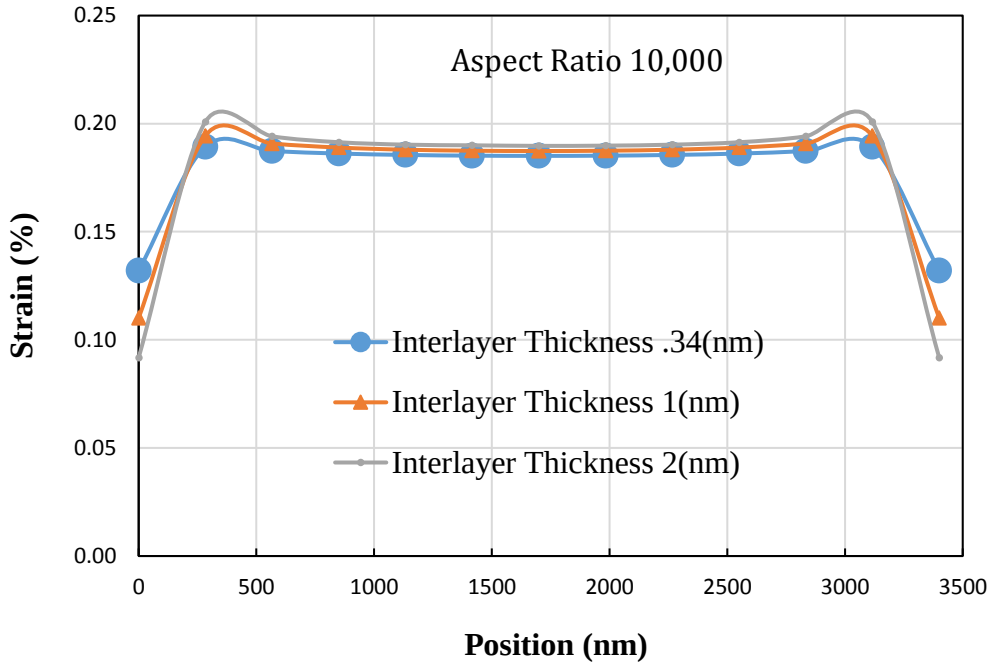

Figure 5.17 FEM predictions with increasing interlayer thickness with a Graphene aspect ratio of 10,000.

Figure 5.17 shows that increasing the interlayer thickness with a lower graphene aspect ratio produces a large effect to the composite strain. The larger the interlayer thickness the larger the strain in the composite. Figure 5.18 shows the same FEM, however, the aspect ratio for the graphene fill has increased to 35,000.

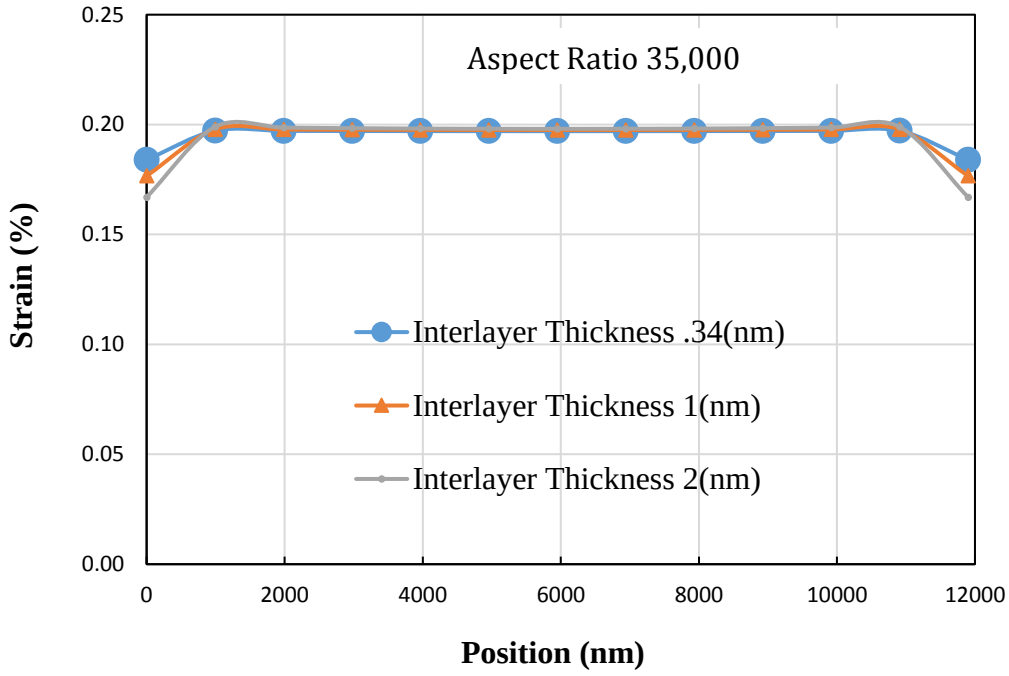

Figure 5.18 FEM predictions with increasing interlayer thickness with a Graphene aspect ratio of 35000.

Figure 5.18 shows that increasing the aspect ratio for the filler reduces the significance of the increase to the strain in the composite. However, increasing the aspect ratio does not eliminate the increase in composite strain so the same trend is still present.

5.3.4 Effect of number of layers

The previous representative graphs have displayed the effects of interlayer material characteristics and interlayer spacing. Another aspect to the interlayer effects of a graphene stack in a composite would be the number of interlayers there are in the stack. This means adding more layers of graphene and increasing the number of interlayers. Previously, increasing the interlayer spacing has decreased the strength of the composite, however, the effects of multiple layers with a thickness of .34 nm is unknown. Figure 5.19 and figure 5.20 show the effects of adding interlayers to the composite.

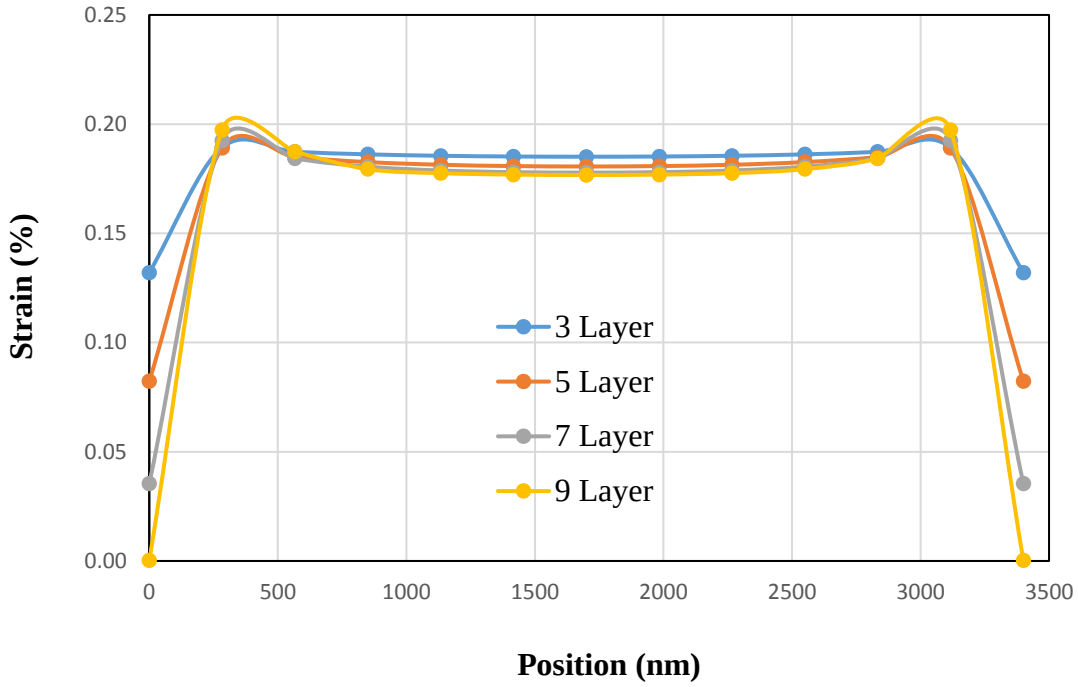

Figure 5.19 Multiple interlayers with a graphene aspect ratio of 10,000.

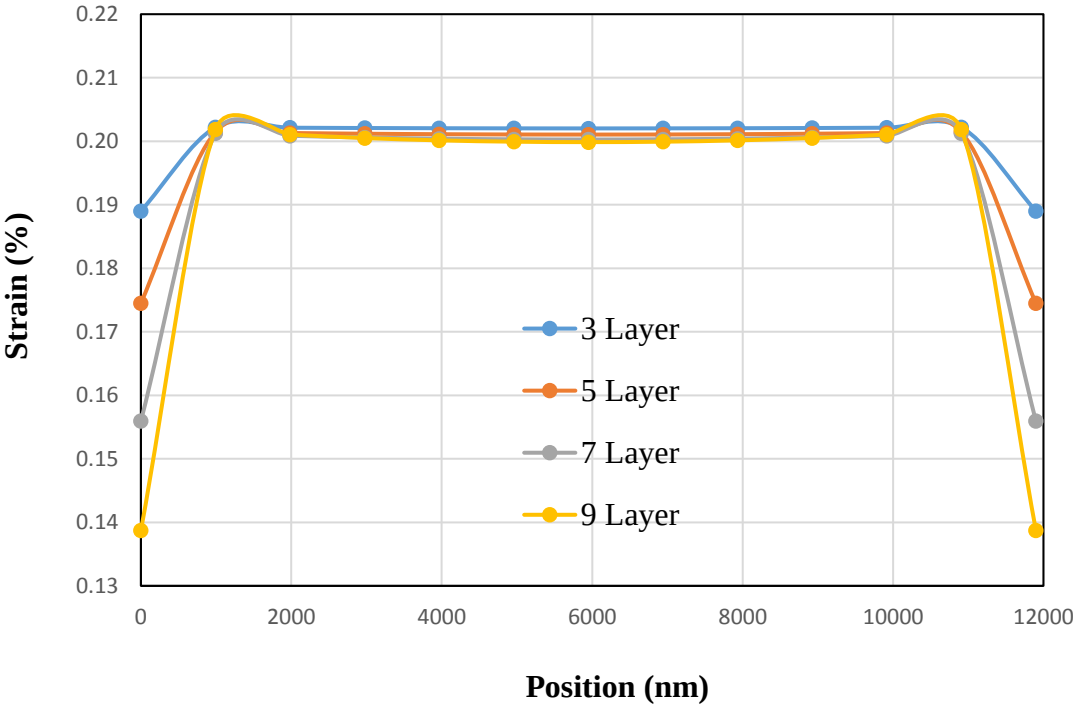

Figure 5.20 Multiple interlayers with a graphene aspect ratio of 35,000.

Figures 5.19 and 5.20 show similar trends for the overall strain in the composite. Increasing the number of interlayers increases the strain in the composite. This will produce a weaker composite as it relates to strength. The effects of increasing the number of interlayers is very similar to increasing the interlayer spacing in the composite. Figure 5.19 shows more of the trend due to the aspect ratio only being 10,000.

5.4 Conclusions

The mechanism of reinforcement by a multilayer graphene filler is investigated in this chapter. Understanding the roles of interlayers on reinforcement efficiencies is very important when producing stronger and lighter graphene based composites. The conventional Shear-Lag theory is accurate for predicting the reinforcement efficiency of monolayer graphene nanocomposites. However, the Shear-Lag theory is somewhat limited when a filler has multiple layers. The finite element method has been used to model the reinforcement mechanism of 2D, layered graphene fillers. The criterion set by the Shear-Lag theory was important as this theory is known to predict very accurate results when compared to experimental results. This criterion set the standard for the finite element models. The procedures for the finite element models were accurate within a certain range of parameters. This was evident when analyzing figures of interlayer affects to composite strength. The trend of increasing the interlayer thickness produces weaker overall composite strength is a trend not achieved from Shear-Lag theory. Also, FEM showed that the interlayer Poisson's ratio has little effect to the composite and the interlayer modulus ratio has a large effect to the composite and could be an important design parameter when designing novel graphene based nanocomposites.

CHAPTER 6 – GENERAL CONCLUSIONS AND FUTURE WORK

6.1 General Conclusions

The use of 2D, ultra-thin graphene as reinforcement fillers has shown great potential for producing strong composites when used with high aspect ratios and moderate volume fractions. The design of a novel composite requires the use of accurate, robust models. Although several theoretical models have been developed for predicting properties of composite materials reinforced with one-dimensional (1D) fillers, they have yet been proven to be suitable for 2D, ultra-thin, high aspect graphene fillers. In this work, two existing composite models (Halpin-Tsai model and the Tandon-Weng model) have been comprehensively examined in the modeling of graphene-polymer composites. The composites have been considered for the cases of both aligned fillers and randomly distributed fillers. Due to the limitations and the lack of consideration for the contributions of large aspect ratios and Poisson's ratios from graphene fillers, Halipn-Tsai's theory is not adequate for predicting nanocomposites reinforced with 2D, ultra-thin graphene. Tandon-Weng's theory produces more consistent predictions with varying aspect ratios, volume fractions, modular ratios, and graphene orientations (aligned and randomly distributed). Selecting which method to analyze the composite should be determined based on the aspect ratio and volume fraction of the filler for the composite. In the instance of graphene having exceptionally high aspect ratios Tandon-Weng models should be used.

The study of interlayers for composites is very important when achieving the overall strength a nanocomposite can produce. The reason this is so important is to do the dispersion process for creating nanocomposites which is one of the common ways of doing so. When a filler such as graphene is dispersed in to a matrix to form a composite the over lapping of graphene is present as well as forming tightly packed stacks. The interlayer material between the sheets of graphene affects the overall strength. Analyzing the material characteristics in these interlayers as well as the spacing then becomes an important

modeling parameter. In order to accurately predict the roles of these interlayers the Arridge's 2D lamellar model was used to compute the fundamental properties of the effective filler (the graphene layered stack as one filler). This fundamental effective filler was then used in Tandon-Weng's theory to further investigate the roles of interlayers. Tandon-Weng's prediction for aligned fillers show that the material properties of the interlayer effect all elastic properties of the composite. When analyzing the interlayer effects of a random oriented graphene composite the modulus and the Poisson's ratio seem to have little effect to the overall composite strength. When the fibers are aligned the Poisson's ratio and the modulus do have a noticeable impact to the overall composite strength. The interlayer spacing content has a noticeable impact for both the random and aligned orientations for the fiber. When the interlayer spacing is increased, the overall composite strength is decreased.

The mechanism of reinforcement by layer graphene fillers has been investigated using the finite element method. Understanding the roles of interlayers on reinforcement efficiencies is very important when producing stronger and lighter graphene based composites. The conventional Shear-Lag theory is accurate for predicting the reinforcement efficiency of monolayer graphene nanocomposites, but is not applicable to the case of a filler with multiple layers. The FEM predicts that the interlayer material characteristics play a major role for the strength of a composite. Increasing the interlayer spacing between each graphene sheet weakens the overall strength of the composite and validating the predictions of the align Tandon-Weng theory. This prediction is also valid for the interlayer modulus. The interlayer Poisson's ratio did not show a large effect to the overall composite strength from the FEM and at this time is unclear as to how much the composite would be affected.

6.2 Future Work

The current study shows that there are still some areas for nanocomposites that can be improved upon. The adequacy of Tandon-Weng model still requires further validation from other sources, such as the finite element modeling of composites reinforced with 2D

graphene at various conditions (aspect ratio, volume fraction, modular ratio, and graphene orientations (aligned and randomly distributed)). The roles of interlayers should be further investigated for more material aspects that have the ability to weaken the composite. Further, new analytical models should be made in order to account for the "effective moduli" effects form interlayers. For more current studies there should be experiments for the effects of multiple layer stacks of graphene so these theoretical frameworks can be validated or disproven.

References

1. Giannelis EP (1996) Polymer layered graphene nanocomposites. Adv Mater 8:29–35.
2. LeBaron PC, Wang Z, Pinnavaia TJ (1999) Polymer-layered graphene nanocomposites: an overview. Appl Clay Sci 15: 11–29.
3. Biswas M, Sinha Ray S (2001) Recent progress in synthesis and evaluation of polymer–montmorillonite nanocomposites. Adv Polym Sci 155:167–221.
4. Ray SS and Okamoto M (2003) Polymer/layered graphene nanocomposites: a review from preparation to processing. Prog. Polym. Sci. 28: 1539–1641.
5. Pavlidou S and Papaspyrides CD (2008) A review on polymer–layered graphene nanocomposites. Progress in Polymer Science 33: 1119–1198.
6. Kim H, Abdala AA, Macosko CW. (2010) Graphene/polymer nanocomposites. Macromolecules 43 :6515-30.
7. Verdejo R, Bernal MM, Romansanta LJ, Lopez-Manchado MA. (2011) Graphene filled polymer nanocomposites. J Mater Chem 21: 3301-10.
8. Singh V, Joung D, Zhai L, Das S, Khondaker SI, Seal S. (2011) Graphene based materials: past, present and future. Prog Mater Sci 56: 1178-271.
9. Potts a, J.R., Dreyer, D.R., Bielawski, C.W., Ruoff, R.S. (2011) Graphene-based polymer nanocomposites. Polymer 52: 5-25.
10. King, J.A., Klimek, D.R., Miskioglu, I., Odegard, G.W. (2013) Mechanical Properties of Graphene Nanoplatelet/Epoxy Composites. J. Appl. Polym. Sci 128: 4217-4223.
11. Terrones, M. et al. "Interphases in Graphene Polymer-based Nanocomposites: Achievements and Challenges." Advanced Materials (2011) 1-9].
12. C. Lee, X. Wei, J.W. Kysar, J. Hone. Science. 321(2008):385–8.
13. C. Lee, X. Wei, Q.Y. Li, R. Carpick, J.W. Kysar, J. Hone. J. Phys Status Solidi B – Basic Solid State Phys. 246 (2009) 2562.
14. Young, R.J., Kinloch, I.A., Cong, L., Novoselov, K.S. (2012) The mechanics of graphene nanocomposites: A review. Composites Science and Technology 72: 1459-1476.

15. S. Ghosh, I. Calizo, D. Teweldebrhan, E.P. Pokatilov, D.L. Nika, A.A. Balandin, et al. Appl Phys Lett. 92 (2008) 151911.
16. J.H. Seol, I. Jo, A.L. Moore, L. Lindsay, Z.H. Aitken, M.T. Pettes, et al. Science. 328 (2010) 213.
17. R.R. Nair, P. Blake, A.N. Grigorenko, K.S. Novoselov, T.J. Booth, T. Stauber, et al. Science. 320 (2008) 1308.
18. Alexandre, M. and Dubois, P., (2000) Polymer-layered Graphene Nanocomposites: Preparation, Properties and Uses of a New Class of Materials. Materials. Science and. Engineering Reports 28: 1–63
19. Daniel, I.M., and Ishai, O. (2006). Engineering Mechanics of Composite Materials, Oxford University Press, New York.
20. Hussain, F., Hojjati, M., Okamoto, M., Gorga, R.E. (2006) Polymer-matrix Nanocomposites, Processing, Manufacturing, and Application: An Overview Journal of Composite Materials, 40 (17): 1151-1175.
21. Jesson, D.A., and Watts, J.F. (2012). The Interface and Interphase in Polymer Matrix Composites: Effect of Mechanical Properties and Method for Identification. Polymer Reviews, 52:321-354.
22. Skandan, G., and Singhal, A. (2006). Perspectives on the Science and Technology of Nanoparticle Synthesis. In: Nanomaterials Handbook, Edited by Gogotsi, Y., CRC Press, Bpca Raton, FL, USA.
23. Charles l. Tucker III, Erwin Liang (1998) Stiffness predictions for unidirectional short-fiber composites: review and evaluation. Composites science and technology
24. G.P. Tandon,G.J. Weng (1986) Average Stress in the matrix and effective moduli of randomly oriented composites. Composites science and technology 0266-3538
25. J. C. Halpin, J. L. Kardos, (1976) The Halpin-Tsai Equations: a review. Polymer engineering and science, vol. 16 no. 5
26. Potts a, J.R., Dreyer, D.R., Bielawski, C.W., Ruoff, R.S. (2011) Graphene-based polymer nanocomposites. Polymer 52: 5-25.
27. Kim H, Abdala AA, Macosko CW. (2010) Graphene/polymer nanocomposites. Macromolecules 43 :6515-30.

28. Verdejo R, Bernal MM, Romansanta LJ, Lopez-Manchado MA. (2011) Graphene filled polymer nanocomposites. J Mater Chem 21: 3301-10.
29. Singh V, Joung D, Zhai L, Das S, Khondaker SI, Seal S. (2011) Graphene based materials: past, present and future. Prog Mater Sci 56: 1178-271.
30. Potts a, J.R., Dreyer, D.R., Bielawski, C.W., Ruoff, R.S. (2011) Graphene-based polymer nanocomposites. Polymer 52: 5-25.
31. Pavlidou S and Papaspyrides CD (2008) A review on polymer–layered graphene nanocomposites. Progress in Polymer Science 33: 1119–1198.
32. Arridge, R. G. C. (1975) Stresses and displacements in lamellar composites: Part I. J. Phys. D: Appl. Phys., 8: 34-52.
33. Young, R.J., Kinloch, I.A., Cong, L., Novoselov, K.S. (2012) The mechanics of graphene nanocomposites: A review. Composites Science and Technology 72: 1459-1476.
34. Fornes, T.D., Paul, D.R. (2003) Modeling properties of nylon 6/clay nanocomposites using composite theories. Polymer 44: 4993–5013.
35. Mori T, Tanaka K. (1973) Average stress in matrix and average elastic energy of materials with misfitting inclusions. Acta Metallurgica 21(5):571-4.
36. Eshelby JD. (1957) The Determination of the Elastic Field of an Ellipsoidal Inclusion, and Related Problems. Proceedings of the Royal Society of London. Series A. Mathematical and Physical Sciences 241(1226):376-396.
37. Tandon GP, Weng GJ. (1984) The effect of aspect ratio of inclusions on the elastic properties of unidirectional aligned composites. Polym Compos 5:327–33.
38. Tandon GP, Weng GJ. (1986) Average stress in the matrix and effective moduli of randomly oriented composites. Composites Sci. Technol, 27, 111.
39. Halpin JC.(1969) Stiffness and Expansion Estimates for Oriented Short Fiber Composites. J Compos Mater 3:732–4.
40. Halpin JC, Kardos JL. (1976) The Halpin-Tsai equations: a review. Polym Engng Sci 16(5):344–52.
41. Ashton JE, Halpin JC, Petit PH. (1969) Primer on composite materials: analysis. Stamford, Conn: Techomic Pub. Co.

42. V. Singh, D. Joung, L. Zhai, S. Das, S.I. Khondaker, S. Seal. Prog Mater Sci. 56 (2011) 1178-271.
43. C.N. R. Rao, K. Biswas, K.S. Subrahmanyam, A. Govindaraj. J Mater Chem. 19 (2009) 2457-69.
44. A.C. Ferrari, J.C. Meyer, V. Scardaci, C. Casiraghi, M. Lazzeri, F. Mauri, et al. Phys Rev Lett. 97 (2006) 187401.
45. P. Ponchiral, A. Ayari, T. Michel, J.L. Siuvajo. Phys Rev B. 78 (2008) 113407.
46. K.I. Bolotin, K.J. Sikes, Z. Jiang, M. Klima, G. Fudenberg, J. Hone. Solid State Commun. 146 (2008) 351.
47. L. Gong, R.J. Young, I.A. Kinloch, I. Riaz, R. Jalil, K.S. Novoselov. ACS Nano. 6 (2012) 2086-2095.
48. Sheng, N.; Boyce, M. C.; Parks, D. M.; Rutledge, G. C.; Abes, J. I. and Cohen, R. E. (2004) Multiscale micromechanical modeling of polymer/clay nanocomposites and the effective clay particle. Polymer, 45: 487–506.
49. Y. Fan, Y.C. Lu, J. Lou, C.C. Tang, D.M. Shinozaki. J. Appl. Polym. Sci. 127 (2015): 1387–1393.
50. K. S. Kim, Y. Zhao, H. Jang, S. Y. Lee, J. M. Kim, K. S. Kim, J.-H. Ahn, P. Kim, J.-Y. Choi, B. H. Hong. Nature. 457 (2009) 706 .

Vita

COLTON CHASE ROACH

EDUCATION

MS, Mechanical Engineering, University of Kentucky (UK), Lexington, KY (May 2017)

BS, Cum Laude, Mechanical Engineering, University of Kentucky, Paducah, KY (May 2015)

AS, High Distinction, West Kentucky Community and Technical College, Paducah, KY (May 2013)

PROFESSIONAL EXPERIENCE

Graduate Research Assistant – 05/2015-05/2017
- University of Kentucky – College of Engineering, Lexington, KY

Consulting Engineer – 01/2017-Present
- Harper Industries Inc., Paducah, KY

AWARDS AND AFFILIATIONS

- Kentucky NASA Space Grant
    - Graduate Fellowship – Spring 2016/Fall 2016

PUBLICATIONS/PRESENTATIONS

Journals:

C.C. Roach, Y.C. Lu, Analytical modeling of the effect of interlayer on effective moduli of layered graphene-polymer nanocomposites, Journal of Materials Science & Technology (2017), in press.

C.C. Roach, Y. Fan, Y.C. Lu, Effect of interlayer on effective moduli of polymer nanocomposites reinforced with 2D layered fillers: layered silicates, SAE International Journal of Materials and Manufacturing (2017), submitted.

Conference Presentations:

C.C. Roach, Y.C. Lu, Effects of Interlayers on Effective Moduli and Interfacial Stress Transfers of Graphene-Polymer Nanocomposites, 2nd Global Nanotechnology Congress and Expo, Las Vegas, NA, USA, December 1-3, 2016.

C.C. Roach, H.E. Whitlock, Y.C. Lu, Numerical and Analytical Analysis of Graphene Nanocomposites, 11th Annual Dayton Engineering Sciences Symposium (DESS 2015), Dayton, OH, November, 2015.

T. Stoffel, J. Garcia, C.C. Roach, Y.C. Lu, Effects of interlayers on effective moduli and interfacial stress transfers of graphene-polymer nanocomposites, 31st Annual National Conference on Undergraduate Research, University of Memphis, TN, April 6-8, 2017